

Alma Mater Studiorum – Università di Bologna

DOTTORATO DI RICERCA IN

CHIMICA

Ciclo XXXIV

Settore Concorsuale: 03/A1- CHIMICA ANALITICA

Settore Scientifico Disciplinare: CHIM/01-CHIMICA ANALITICA

**Development of Thermochemiluminescence-based
Sensitive Probes: Synthesis, Optimization, and
Characterization of C2- and C7-Substituted
Acridine-containing 1,2-Dioxetanes**

Presentata da: Giada Moroni

Coordinatore Dottorato

Luca Prodi

Supervisore

Mara Mirasoli

Co-supervisore

Antimo Gioiello

Esame finale anno 2022

TABLE OF CONTENTS

List of Abbreviations	1
Acknowledgments	4
Abstract	5
1. Chapter 1. Introduction	7
1.1 Overview on luminescent detection techniques	7
1.2 Thermochemiluminescence as ultrasensitive detection method	11
1.3 Development of acridine-based 1,2-dioxetanes for thermochemiluminescence applications	14
1.4 Synthetic methods to prepare 1,2-dioxetanes	22
1.5 Decomposition mechanisms of 1,2-dioxetanes	34
Aims of the Work	42
2. Chapter 2. Results and Discussion	44
2.1 Design of novel <i>N</i> -acridine containing 1,2-dioxetanes	44
2.2 Synthesis	46
2.2.1 <i>Synthesis and photophysical properties of acridone intermediates</i>	46
2.2.2 <i>Synthesis of acridine containing 1,2-dioxetanes</i>	51
2.2.3 <i>Chemometric analyses and computational prediction of the photooxygenation step reactivity</i>	56
2.3 Optimization of photooxygenation step by continuous flow technology	60
2.4 Characterization	70
2.4.1 <i>TCL measurements of the final products</i>	70
2.4.2 <i>TCL imaging of the unsubstituted probe model: proof of concept</i>	86
2.5 Development of new bioconjugated probes based on TCL phenomenon	87

2.5.1	<i>Directly conjugated probes</i>	89
2.5.2	<i>Biotinylated probe</i>	94
2.5.3	<i>Sulfonated probes</i>	98
	Concluding Remarks and Future Perspectives	100
3.	Chapter 3. Experimental Section	102
3.1	Synthesis	102
3.2	Computational details	132
3.3	Analytical measurements	132
	References and Notes	138

List of Abbreviations

Ab	Antibody
Acr ⁺ -Mes	9-Mesityl-10-methylacridinium ion
Ag	Antigen
AlN	Aluminium nitride
AUC	Area under the curve
(±)-BINAP	(±)-2,2'-Bis(diphenylphosphino)-1,1'-binaphthalene
Boc ₂ O	Di-tert-butyl dicarbonate
BPEA	9,10-Bis(phenylethynyl)anthracene
BPR	Back pressure regulator
BSA	Bovine serum albumin
bt	Biotin
CAN	Cerium (IV) ammonium nitrate
CASSCF	Complete active space self-consistent field
CCD	Charge-coupled device
CEA	Carcinoembryonic antigen
CIEEL	Chemically initiated electron exchange luminescence
CL	Chemical luminescence
CL/BL	Chemi- and Bioluminescence
CN-PPV	Cyano-polyphenylene vinylene
COMU	(1-Cyano-2-ethoxy-2-oxoethylideneaminoxy)dimethylamino-morpholino-carbenium hexafluorophosphate
COVID-19	Coronavirus disease 2019
DBDMH	1,3-Dibromo-5,5-dimethylhydantoin
DCC	<i>N,N'</i> -Dicyclohexylcarbodiimide
DFT	Density-functional theory
DIH	1,3-Diiodo-5,5-dimethylhydantoin
DIPEA	<i>N,N</i> -Diisopropylethylamine
DLS	Dynamic light scattering
DMAP	4-(Dimethylamino)pyridine
DME	Dimethoxyethane
DMF	<i>N,N</i> -Dimethylformamide
DMSO	Dimethyl sulfoxide
DPA	9,10-Diphenylanthracene
DSC	<i>N,N'</i> -Disuccinimidyl carbonate
E_a	Activation energy
EA	Energy acceptor
ECL	Electrogenerated chemiluminescence
EDC	<i>N</i> -(3-dimethylaminopropyl)- <i>N'</i> -ethylcarbodiimide hydrochloride
EDG	Electron donating group
EMCCD	Electron-multiplying charge-coupled device
EMR	Electromagnetic radiation
ESP	Electrostatic potential
EWG	Electron withdrawing group

FITS	Flexible image transport system
HaCaT	Human aneuploid immortal keratinocyte cell line
<i>hCG</i>	Human chorionic gonadotropin
<i>hIgG</i>	Human immunoglobulin G
H ₂ TPP	Tetraphenylporphyrin
HOBt	1-Hydroxybenzotriazole
HOMO	Highest occupied molecular orbital
HPLC	High-performance liquid chromatography
HRP	Horseradish peroxidase
IC	Internal conversion
ISC	Intersystem crossing
K _d	Dissociation constant
LDA	Linear discriminant analysis
LED	Light-emitting diode
ln <i>A</i>	Pre-exponential factor
LOD	Limit of detection
LogP	Partition coefficient
LUMO	Lowest unoccupied molecular orbital
MB	Methylene blue
MBs	Magnetic beads
MCL	Mechanoluminescence
MEP	Minimal energy path
MFC	Mass flow controller
MM	Molecular mechanics
MVP	1-(2'-Methoxyvinyl)pyrene
NHS	<i>N</i> -hydroxysuccinimide
NMR	Nuclear magnetic resonance
NOA	Norland optical adhesive
NP	Nanoparticle
ORMOSIL	Organically modified silica
PCA	Principal component analysis
PDI	Polydispersity index
Pdots	Polymer dots
PEG	Polyethylene glycol
PEOE	Partial equalization of orbital electronegativity
PES	Potential energy surface
PG	Protecting group
pH	Potential of hydrogen
PL	Photoluminescence
PluS	Pluronic silica
POC	Point-of-care
PPO	Polypropylene oxide
PS	Polystyrene
RB	Rose bengal
RLU	Relative light unit
r.t.	Room temperature
SA	Streptavidin

SCF	Self-consistent field
SD	Standard deviation
SET	Single electron transfer
SM	Starting material
SOC	Spin-orbit coupling
STP	4-Sulfo-2,3,5,6-tetrafluorophenol sodium salt
TBTU	2-(1 <i>H</i> -Benzotriazole-1-yl)-1,1,3,3-tetramethylaminium tetrafluoroborate
TCL	Thermochemiluminescence
TEM	Transmission electron microscopy
TEOS	Tetraethyl ortosilicate
TFA	Trifluoroacetic acid
THF	Tetrahydrofuran
TLC	Thin layer chromatography
TMSCl	Trimethylsilyl chloride
TPhP	Triphenyl phosphate
TPP	Triphenyl phosphite
TPPO	Triphenylphosphite ozonide
UV-Vis	Ultraviolet-visible
VFIA	Vertical flow immunoassay
VPA	Valproic acid
ZnH ₂ TTP	Zinc tetraphenylporphyrin

Acknowledgments

This PhD Thesis is the result of the dedication and the support of several people to whom I would like to express my sincere gratitude. First of all, I am deeply grateful to my Supervisors Prof. Mara Mirasoli (University of Bologna) and Prof. Antimo Gioiello (University of Perugia) for the possibility to have taken part in the Doctorate path always supported by their guidance and professional experience.

I want also to thank Prof. Aldo Roda for his precious advice, for believing in the potential of the project, and for having confidence in me all along.

I am grateful to Prof. Marco Lombardo and Dr. Arianna Quintavalla (University of Bologna) for the computational calculations, Prof. Massimo Guardigli and Dr. Donato Calabria (University of Bologna) for the spectroscopic and thermochemiluminescent analyses, and Prof. Luca Prodi (University of Bologna) for the results in photophysical characterization and nanomaterials fields.

A special thank goes to Prof Jean-Christophe Monbaliu (University of Liege, Belgium) and “CiTOS” group that welcomed me during my period abroad revealing treasured flow photochemical secrets.

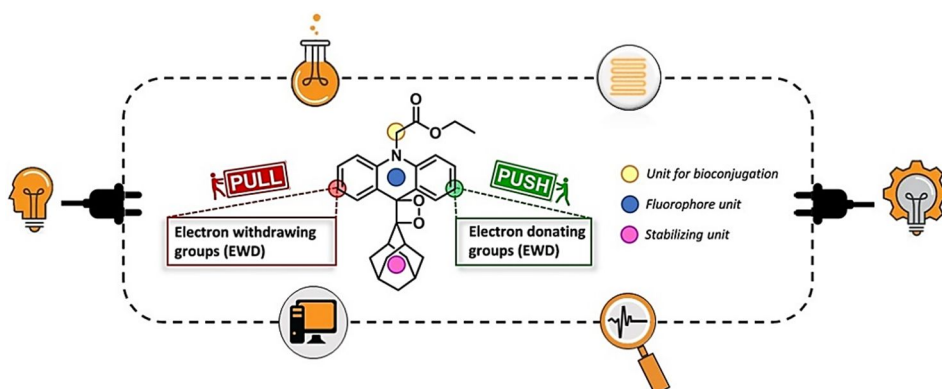
I want to thank my “second” family composed of all my colleagues for sharing with me joys and sorrows of this hard work. Not less important, I would like to thank my family and Riccardo for always being there and supporting me every single moment.

Abstract

After initial efforts in the late 1980s, the interest in thermochemiluminescence (TCL) as an effective detection technique has gradually faded due to some drawbacks, such as the high temperatures required to trigger the light emission and the relatively low intensities, which determined a poor sensitivity. Recent advances made with the adoption of variably functionalized 1,2-dioxetanes as innovative luminophores, have proved to be a promising approach for the development of reagentless and ultrasensitive detection methods exploitable in biosensors by using TCL compounds as labels, as either single molecules or included in modified nanoparticles.

In this PhD Thesis, a novel class of *N*-substituted acridine-containing 1,2-dioxetanes was designed, synthesized, and characterized as universal TCL probes endowed with optimal emission-triggering temperatures and higher detectability particularly useful in bioanalytical assays. The different decorations introduced by the insertion of both electron donating (EDGs) and electron withdrawing groups (EWGs) at the 2- and 7-positions of acridine fluorophore was found to profoundly affect the photophysical properties and the activation parameters of the final 1,2-dioxetane products. Challenges in the synthesis of 1,2-dioxetanes were tackled with the recourse to continuous flow photochemistry to achieve the

target parent compound in high yields, short reaction time, and easy scalability. Computational studies were also carried out to predict the olefins reactivity in the crucial photooxygenation reaction as well as the final products stability. The preliminary application of TCL prototype molecule has been performed in HaCaT cell lines showing the ability of these molecules to be detected in real biological samples and cell-based assays. Finally, attempts on the characterization of 1,2-dioxetanes in different environments (solid state, optical glue and nanosystems) and the development of bioconjugated TCL probes will be also presented and discussed.



Chapter 1. Introduction

1.1 Overview on luminescent detection techniques

The luminescence-based detection techniques are particularly attractive for bioanalytical applications and biosensors development as they combine a high detectability with simple instrumentations.^{1,2} Such technologies are particularly relevant for the implementation of miniaturized devices and compact analytical formats that need smaller, faster, and still accurate analytical tools for sensing and imaging methods.

The term luminescence was coined by Eilhardt Wiedemann at the end of XIX century to describe physical phenomena based on the photon emission of specific materials when submitted to different nature processes (i.e., absorption of light, chemical or electrochemical reactions, decomposition of thermally sensitive precursors).³ Concerning the features of the triggering phenomenon, an electronically excited molecule can embrace a similar fate. As consequence of the trigger (e.g., absorption of light quantum energy as photon from the external environment when photoluminescence is involved), electrons of the molecule are promoted from the ground state (S_0) to a singlet excited one (S_n , $n \geq 1$) based on the energy absorbed. Electrons stand in that excited state for a short time, and

1.1 Overview on luminescent detection techniques

then gradually decay relaxing to the ground state following two different intramolecular pathways, as depicted by the Jablonski diagram (**Figure 1**). Finally, the excess of energy is released as an electromagnetic radiation (EMR) after the vibrational relaxation of an electronically excited molecule to its electronic S_0 corresponding to the energy gap between the electronic levels (HOMO-LUMO) involved in the transition.^{2c}

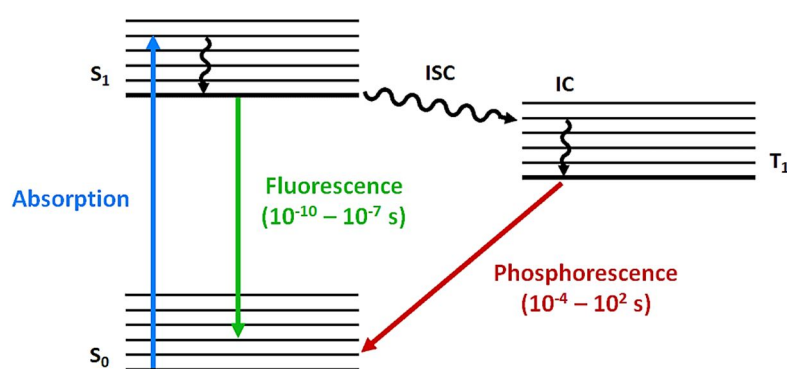


Figure 1. The Jablonski energy diagram. The radiative (i.e., fluorescence and phosphorescence) and non-radiative (i.e., IC and ISC) processes are represented by solid and wavy lines, respectively.

Based on the mode of decay, two different processes can occur, including the radiative and non-radiative relaxations. The latter describes a pathway in which the excess of energy is dissipated as thermal energy, such as the internal conversion (IC) and the intersystem crossing (ISC). Although the direct excitation of the molecule at triplet states (T_n , $n \geq 1$) by the absorption of a radiation from the ground state is not tolerated because of the forbidden spin transition, the population of triplet states is allowed as the result of the overlapping between the vibrational levels of the two excited states *via* the ISC.⁴ Consequently, both processes lead the excited molecule to its lower excited state, S_1 or T_1 , respectively. On the other hand, when the excited molecule decays to its

ground state emitting a photon, the relaxation is named radiative and generally involves fluorescence ($S_1 \rightarrow S_0$ transition) and/or phosphorescence ($T_1 \rightarrow S_0$ transition).

The luminescence process can be distinguished in two main categories according to the different ways of the excited state generation: photoluminescence (PL) and chemical luminescence (CL). PL is certainly the most employed luminescence detection technique as it has been exploited for a wide range of applications, including clinical diagnostics, environmental monitoring and bioimaging.⁵ The light emission is produced as a consequence of EMR absorption through a physical process (i.e., photoexcitation of emissive species). In fact, common fluorescent or phosphorescent substrates require the energy absorption and the consequent excitation from optics and external light sources, such as UV-Vis lamps, lasers, etc.⁶ The production of photons without photoexcitation sources has prompted the search of CL-based approaches to solve issues associated with the light scattering, background signal interference, and relatively complex instrumentation.⁷

Superior analytical performance can be achieved by using CL detection techniques, such as chemi- and bioluminescence (CL/BL),^{1b,8,9} electrogenerated chemiluminescence (ECL),¹⁰ and thermochemiluminescence (TCL).¹¹ All these phenomena consist in the photon emission from chemically excited species promoted by a chemical reaction, in dark conditions, where catalysts, enzymes, redox systems, and/or thermally induced decomposition of unstable molecules are involved (**Figure 2**).¹²



Figure 2. Representative luminescence based-detection techniques: photo-, chemi-, bio-, electrochemi-, and thermochemiluminescence.

Generally, CL techniques produce less intense light emission than PL since the light arises from the molecules *via* a chemical reaction, while in the photoexcitation the light emission depends on the excitation light intensity. Although being fairly weak, the chemical luminescence light signal is characterized by minimal nonspecific background interferences, thus resulting in a very high signal-to-noise ratio. Moreover, the weak intensity of light signal is now easily measurable thanks to the advanced analytical instrumentation (i.e., photomultiplier tubes or charge coupled devices) able to provide accurate measurements of few photons.^{1a,12} Therefore, CL measurements can be realized using simple and economical equipment as the excitation source is not required. Moreover, CL detections have shown wide dynamic ranges facilitating analysis of samples at diverse analyte concentrations.¹³ The main pitfall of this approach is the potential effect of sample matrix constituents that can interfere and affect the light generated during the process. Indeed, the matrix interferences could contribute to artefacts and irreproducible results in an unpredictable way.^{1b,13} On the other hand, BL applications often require chemicals and expensive enzyme labels that need to be carefully manipulated to preserve the enzyme activity at the investigated experimental conditions.¹⁴

In this context, TCL has emerged as an alternative and sensitive technique to overcome such limitations. In this case, relatively unstable molecules, i.e., 1,2-dioxetanes, undergo a thermal decomposition above a threshold temperature

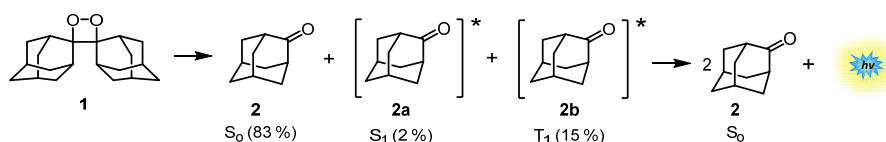
generating light. TCL combines a potential high sensitivity similar to other more common chemical luminescence methods (CL/BL/ECL) with a great simplification of measurement procedures being a “reagentless” approach since the light emission is simply triggered by the heat. The implementation of TCL performance through the design and synthesis of novel TCL labels characterized by a high stability at room temperature and a reasonably low emission triggering, could open new and unexplored perspectives in the bioassay field. Recently, a renewed interest in TCL has prompted several research groups to reinvestigate this poorly exploited detection technique. The main TCL principles and analytical applications involving the use of 1,2-dioxetanes in various luminescence assays will be extensively discussed in the next sections.

1.2 Thermochemiluminescence as ultrasensitive detection method

Among the luminescence methods based on the decomposition of relatively unstable molecules, thermochemiluminescence represents the less investigated one.¹⁵ TCL was described for the first time in 1963, but only in the late ‘80s it was suggested as an alternative analytical approach for immunoassays, though with limited practical applications. After the pioneering works on the Fluorescent Amplified Thermochemiluminescence IMmunoAssay (FATIMA) and adamantylidene adamantane-1,2-dioxetane (**1**, **Scheme 1**), this technique was completely abandoned because of the high temperatures required to promote the decomposition of the 1,2-dioxetane **1** (more than 200 °C) and the poor detectability in comparison to other labels.

Compound **1** was synthesized by Wieringa and co-workers as the most stable 1,2-dioxetane known nowadays.¹⁶ Indeed, the adamantyl unit is a rigid and sterically demanding framework able to significantly stabilize the 1,2-dioxetane scaffold. The presence of two hindered groups protects the endoperoxide from

the ring opening by conferring a high stability in comparison to other 1,2-dioxetanes.¹⁷ For this reason, **1** is essentially used as the standard reference for TCL emission measurements.¹⁸ The white and crystalline compound can be stored at room temperature for years ($t_{1/2} = 1.2 \times 10^4$ years at 25 °C) decomposing slowly in two corresponding 2-adamantanones (**2**).¹⁹ The endoperoxide unit can undergo a fast thermal decomposition above 200-250 °C generating identical carbonyl fragments (**2**, **2a**, **2b**) at different energetic states (S_0 , S_1 , T_1) (**Scheme 1**). When the singlet excited one (**2a**) relaxes to its ground state, an emission of a high energy photon with a wavelength at 425 nm is observed.^{19b,20}



Scheme 1. TCL decomposition of adamantylidene adamantane-1,2-dioxetane (**1**).

Overall, this approach has evidenced some drawbacks. The high triggering temperatures (ranging from 200-250 °C) require the use of expensive heat-resistant materials for the biosensing detection device thus limiting the field of application, especially in water environment. Moreover, 2-adamantanone (**2**) is a weak fluorophore ($\Phi_F = 0.015$) with a very poor light emission efficiency requesting the use of an energy acceptor (EA) of fluorescence. Consequently, the TCL quantum yield (Φ_{TCL}) of the above-described system is quite low since the carbonyl fragment shows almost no singlet decay.²¹

Nevertheless, several research groups have employed dioxetane-based immunological analysis for the detection of common biomolecules of interest. For instance, in 1986 Luider and co-workers used an adamantyl dioxetane derivative to develop a TCL immunoassay for human chorionic gonadotropin (*hCG*).²² The assay was realized by functionalizing the monoclonal anti-*hCG* with the 1,2-dioxetane scaffold alone or in the presence of the EA (9,10-

diphenylanthracene, DPA). In the first case, a larger dynamic range than the classical enzyme-based assays was measured despite a lower precision and detection limit. The response was increased by conjugating several EA molecules to the monoclonal anti-*h*CG. The electronic energy of the singlet excited ketone produced by 1,2-dioxetane decomposition can be transferred in a non-radiative way to an acceptor molecule. This phenomenon can be used to amplify the TCL signal from 1,2-dioxetane labels and labelled compounds.

Improvements of TCL-based immunoassays have reached by Hummelen and collaborators. They described the FATIMA system for the detection of human immunoglobulin G (*h*IgG) and carcinoembryonic antigen (CEA).^{15c,23} The antibodies were labelled with “lightbulbs” constituted by a dual conjugate of bovine serum albumin (BSA) with up to 25 molecules of adamantylidene adamantane-1,2-dioxetane (**1**) and the energy acceptor DPA. The dioxetane moiety was then engaged into a cyclodextrin to improve both reproducibility and linearity of TCL signal (**Figure 3**).

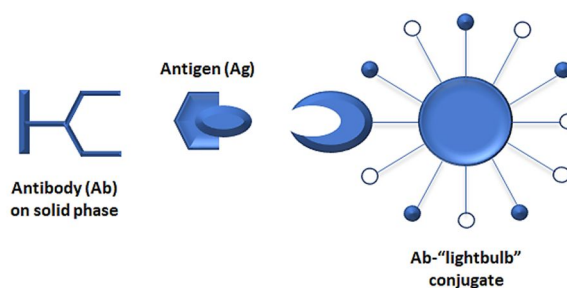


Figure 3. Basic principles of FATIMA assay.

Despite these advances, the interest in TCL technique was gradually abated because of the poor analytical performance. Recently, the advantages shared with the other CL techniques combined with the possibility to work in a complete reagentless approach, are encouraging the development of novel and efficient TCL labels.

1.3 Development of acridine-based 1,2-dioxetanes for thermochemiluminescence applications

1,2-Dioxetanes represent an uncommon class of fluorescent organic molecules. The structure is characterized by a four-membered endoperoxide ring whose inherent instability can lead to the energy release in form of light upon thermal or chemical decomposition (**Figure 4**).²⁴ This peculiar feature of 1,2-dioxetanes has been exploited to discover molecules with improved TCL properties in terms of emission efficiency and stability at room temperature for bioanalytical applications. Despite the progress made, there is still room for effective and stable 1,2-dioxetanes for translational innovation.

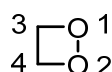


Figure 4. General structure of 1,2-dioxetane.

Recently, Roda and his team have reinvestigated the TCL principle proposing a new class of TCL probes characterized by *N*-substituted acridine 1,2-dioxetane derivatives (**Figure 5**).²⁵ The spiro-bonded adamantyl moiety ensures stability to the dioxetane preventing the spontaneous decomposition at room temperature, while the acridine framework is the unit involved in the generation of the electronically excited product. In addition, the insertion of an ester group to the nitrogen of acridine system provides higher stability to the molecule by folding above the ring. At the same time, the *N*-side chain offers a potential binding site for bioconjugation. Not less important, the acridone moiety is a much more efficient fluorophore than 2-adamantanone (**2**) with a significantly higher fluorescence quantum yield (Φ_F) (0.1 vs 0.015, respectively).

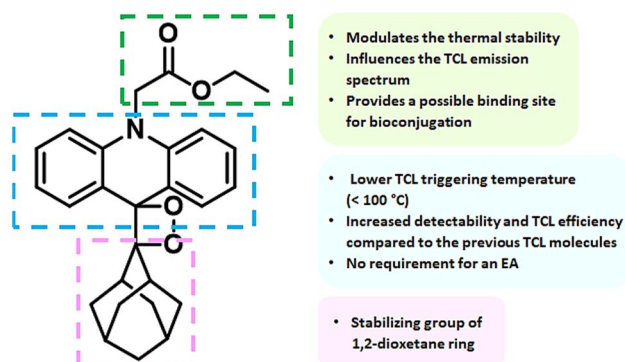
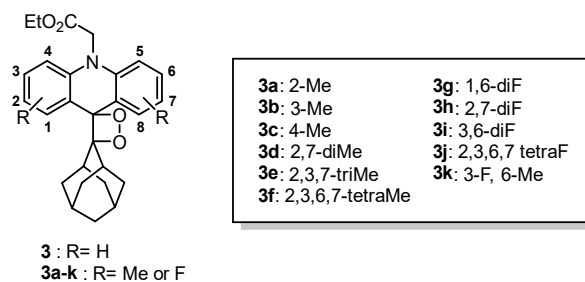


Figure 5. General structure and features of the 1,2-dioxetane parent compound (**3**) containing *N*-substituted acridine and adamantyl moieties.

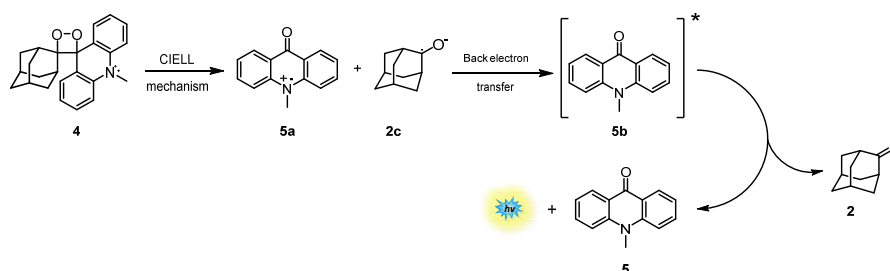
A series of variably functionalized derivatives endowed with different photochemical properties was synthesized and analyzed in terms of TCL efficiency. (**Scheme 2**). In particular, a set of methyl and/or fluorine-substituted 1,2-dioxetane derivatives (**3a-k**, **Scheme 2**) was prepared to investigate the effect of weak electron donating groups (EDGs) as the methyl group and/or electron withdrawing groups (EWGs) as the fluorine at different positions of the acridine system.^{25a-b}



Scheme 2. Structure of ethyl 2-(9-((5*r*,7*r*)-adamantan-2-ylidene)acridin-10(9*H*)-yl)acetate (**3**) and of the corresponding methyl and/or fluorine-substituted derivatives (**3a-k**).

Methyl substituents in proximity to the double bond we found to inhibit the photooxygenation reaction for steric reasons. Tri- and tetramethyl-substituted 1,2-dioxetanes (**3e** and **3f**, **Scheme 2**) gave limit of detection (LOD) values more than ten times lower in comparison to the not-decorated derivative **3** in TCL imaging experiments showing a good inverse correlation with the Φ_F of the corresponding acridone derivatives (0.52 and 0.48, respectively).^{25b} Moreover, the presence of fluorine atoms on the acridine ring remarkably stabilized the corresponding 1,2-dioxetanes, especially when they were placed at the C3- and/or C6-positions (**3g** and **3i**, **Scheme 2**), while 2,7-difluorinated derivative (**3h**, **Scheme 2**) has shown an improved Φ_F in comparison to the parent dioxetane **3** (0.65 vs 0.11, respectively).^{25a} The fluorine substituent basically displays a double nature, being a strong EWG *via* inductive effect due to its high electronegativity, but also being able to donate a lone pair to the aromatic ring by resonance. Thus, the ED character mitigates the inductive effect leaving a greater negative charge density on the ortho- and para-positions, while the inductive effect fades with the distance.

All the acridine-based 1,2-dioxetanes are subjected to a decomposition mechanism named Chemically Initiated Electron Exchange Luminescence (CIEEL) (**Scheme 3**).^{17a,c} The lone pair of the endocyclic nitrogen plays a crucial role in the O-O bond rupture. The first step consists in an electron transfer from the nitrogen to the endoperoxide system of the acridine derivative (**4**) and the simultaneous formation of products **5a** and **2c** derived from the ring fragmentation. Then, a back-electron transfer occurs leading to the formation of the electronically excited 10(9*H*)-acridone (**5b**) that relaxes affording the corresponding compound **5** and 2-adamantanone **2** at the ground state (**Scheme 3**) (*see also* Paragraph 1.5).



Scheme 3. CIEEL mechanism for the decomposition of acridine-based 1,2-dioxetanes.

In order to obtain detectability comparable to those of classical CL methods, TCL-based nanometric probes, including functionalized silica nanoparticles and semiconductive polymer dots, have been developed and applied in immunoassays.^{26,27} A new class of TCL organically modified silica nanoparticles (TCL-ORMOSIL NPs) was realized by inserting different acridine-based 1,2-dioxetanes and an EA (9,10-bis(phenylethynyl)anthracene, BPEA) into the nanometric system (**Figure 6A**).^{26,28} The doped ORMOSIL NPs were further amino-functionalized with biotin (bt) for binding to streptavidin-conjugated (bt-SA) biospecific probes to obtain an universal detection instrument for immunoassays (**Figure 6A**). Despite the enhanced emission efficiency and the simple (bio)functionalization, TCL-ORMOSIL NPs have shown some stability issues that caused a slow degradation of acridine/dioxetane system in the reaction media, and consequent loss in TCL signal.^{29,30} Alternative nanomaterials such as semiconductive polymer dots (Pdots) were also evaluated as ultrabright labels in a model non-competitive immunoassay for IgG detection (**Figure 6B**).²⁷

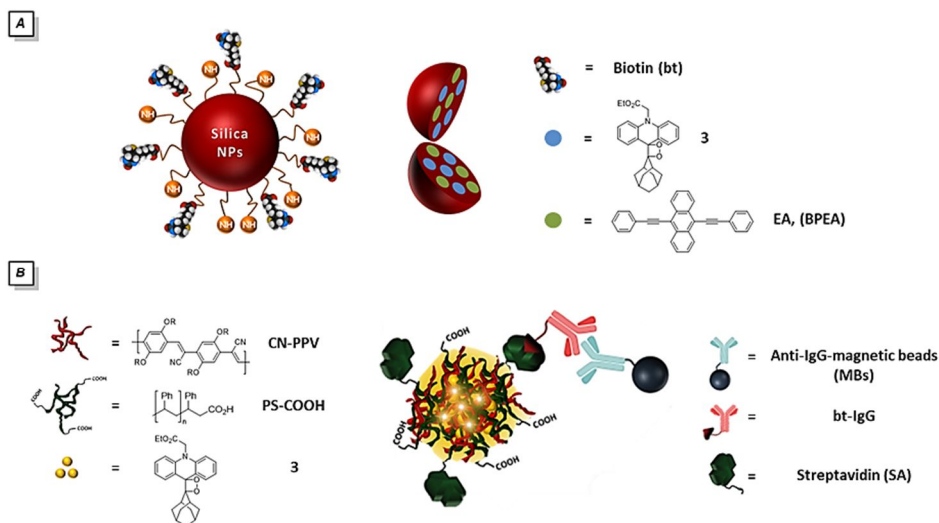


Figure 6. TCL-based probes immunoassays. A) TCL-ORMOSIL NPs and B) bt-IgG/Anti-IgG-MBs/TCL-Pdot-SA complex.

Silica NPs doped TCL molecules were integrated into the smartphone technology to realize a home-made portable device for valproic acid (VPA) detection in blood and saliva through a one-step competitive immunoassay based on vertical flow immunoassay (VFIA) format (**Figure 7**).³¹

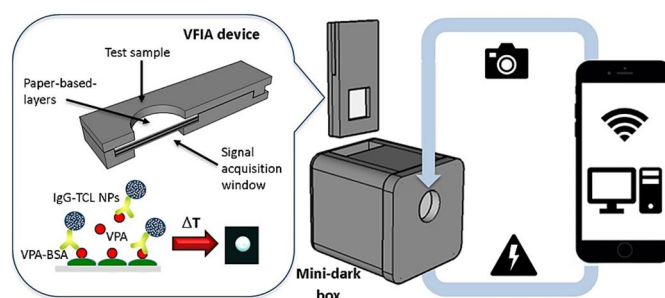
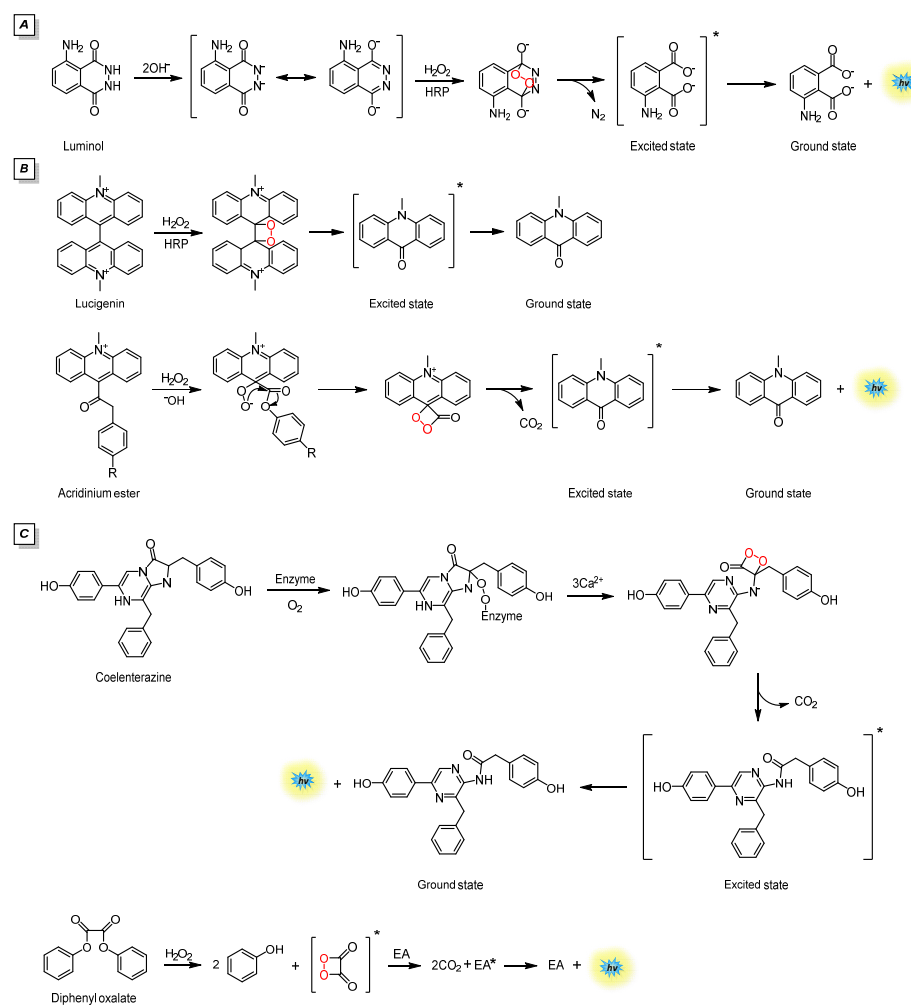


Figure 7. Smartphone-based TCL immunosensor for VPA detection. Reprinted with the permission from ³¹.

Through the implementation of simple and compact 3D-printers that allow to design smartphone accessories, any mobile device can effectively become a portable mini-luminometer for point-of-care (POC) testing, exploiting the additional features of direct signal elaboration, data handling and storage, connectivity, and cloud servicing for remote sensing.

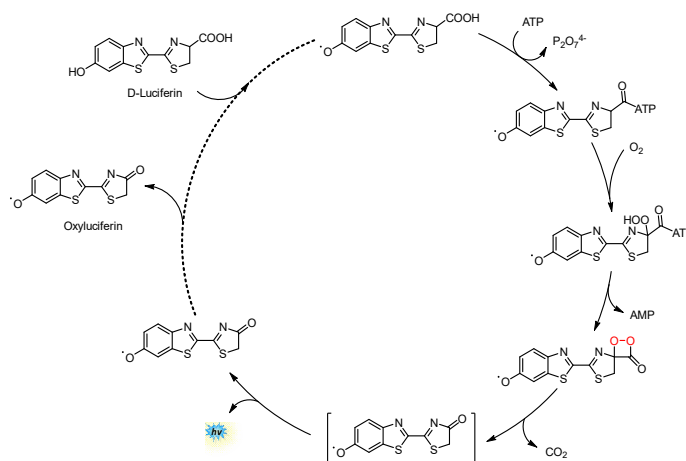
Box 1. The role of 1,2-dioxetane framework in luminescent processes

1,2-dioxetane derivatives have played an important role in luminescence oxidation processes acting as reactive reagents or intermediates. Since the advent of synthetic CL molecules, such as luminol and its derivatives (**Scheme 4A**),³² lucigenin and acridinium esters (**Scheme 4B**),³³ coelenterazine and oxalate esters (**Scheme 4C**),³⁴ the endoperoxide unit has emerged as a functional framework in the decomposition mechanism of these substrates and in the consequent light emission.



Scheme 4. The role of 1,2-dioxetane compounds in CL processes. A) Mechanism for the CL reaction of luminol.³⁵ B) Mechanism for the CL reaction of lucigenin and acridinium esters.³⁶ C) Mechanism for the CL decomposition of coelenterazine and diphenyl oxalate.³⁷

Nature-inspired chemistry prompted the researchers to mimic biological processes by generating new synthetic entities able to decompose unstable intermediates (i.e., dioxetanes and/or dioxetanones) in the singlet excited state. Luciferin-luciferase pair undoubtedly represent the substrate/enzyme couple of reference in view of its involvement in BL reactions and applications (**Scheme 5**).^{91, 38}



Scheme 5. Mechanism for the BL reaction from firefly (*Photinus pyralis* species).³⁹

Recently, adamantylidene adamantane-1,2-dioxetane (**1**) was combined with polymers technology developing a rubber-like poly methyl acrilate system able to produce a bright light. An intense emission was observed by submitting the adduct to mechanical force (sonication) upon the polymer chains (**Figure 8**).⁴⁰

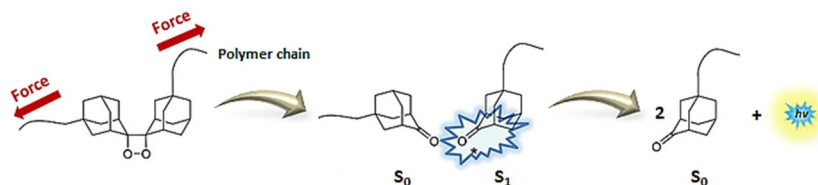
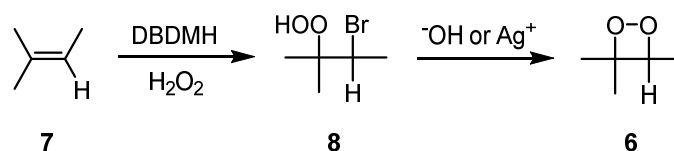


Figure 8. Representation of mechanoluminescence (MCL) process involving 1,2-dioxetane-containing polymers.

1.4 Synthetic methods to prepare 1,2-dioxetanes

Since 1,2-dioxetanes are thermally labile compounds and prone to respond to redox mechanism, synthetic methods for their preparation are rather limited. Significant efforts in the synthesis of 1,2-dioxetanes were conducted during the 1970s by different research groups.⁴¹ In this Thesis, the attention has been directed towards synthetic approaches based on the employment of olefin systems.

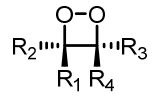
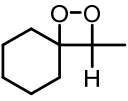
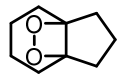
The first synthesis of the 1,2-dioxetane scaffold was described in 1969 by Kopecky and Mumford.^{42,43} It concerned the preparation of 3,3,4-trimethyl-1,2-dioxetane (**6**) as yellow solution in benzene. The reaction of 2-methyl-2-butene (**7**) with hydrogen peroxide (H_2O_2) and 1,3-dibromo-5,5-dimethylhydantoin (DBDMH) at $-78\text{ }^\circ\text{C}$ formed the β -bromo hydroperoxide **8** that underwent to cyclization by means of alkali or silver salts (**Scheme 6**). The final product **6** showed an unexpected kinetic stability ($t_{1/2}$ = several days at $20\text{ }^\circ\text{C}$) generating a pale blue glow.



Scheme 6. General conditions for the synthesis of 3,3,4-trimethyl-1,2-dioxetane (**6**) according to the Kopecky method. *Step a*) formation of β -halo hydroperoxide. *Step b*) dehydrohalogenation and consecutive cyclization.

Since then, the Kopecky approach has been adopted for the synthesis of diverse 1,2-dioxetane derivatives (**Table 1**).

Table 1. Examples of 1,2-dioxetanes synthesized by Kopecky method.

Entry		Reaction conditions ^a	Yield (%)	Ref
1	Me Me Me Me	a) 2,3-dimethyl-2-butene, DBDMH or DIH, H ₂ O ₂ (98%), Et ₂ O, -40 °C; b) AgO ₂ CCH ₃ , CH ₂ Cl ₂ , 25 °C	30	[42]
2	Me Me Me H	a) 2-methyl-2-butene, DBDMH, H ₂ O ₂ (98%), Et ₂ O, -78 °C; b) NaOH, H ₂ O/MeOH 1:1, (v/v), -10 °C	30	[42]
3	Me Me H H	a) 2-methyl-1-propene, DBDMH, H ₂ O ₂ (98%), Et ₂ O, -78 °C; b) NaOH, H ₂ O/MeOH 1:1, (v/v), -10 °C	26	[44]
4	Me H Me H	a) (<i>E</i>)-2-butene, DBDMH, H ₂ O ₂ (98%), Et ₂ O, -78 °C; b) NaOH, H ₂ O/MeOH 1:1, (v/v), -10 °C	27	[44]
5	Me H H Me	a) (<i>Z</i>)-2-butene, DBDMH, H ₂ O ₂ (85%), Et ₂ O, -40 °C; b) KOH, H ₂ O/CH ₂ Cl ₂ 1:1, (v/v), -20 °C	39	[45]
6	Me H H H	a) 1-propene, DBDMH, H ₂ O ₂ (85%), Et ₂ O, -40 °C; b) KOH, H ₂ O/CH ₂ Cl ₂ 1:1, (v/v), -20 °C	3	[45]
7	H H H H	a) ethene, DBDMH, H ₂ O ₂ (85%), Et ₂ O, -40 °C; b) KOH, H ₂ O/CH ₂ Cl ₂ 1:1, (v/v), -20 °C	1	[45]
8	Bn Bn H H	a) 2-benzyl-3-phenyl-1-propene, DBDMH, H ₂ O ₂ (98%), Et ₂ O, -40 °C; b) NaOCH ₃ , MeOH, -30 °C	38	[46]
9	Ph Ph H H	a) 1,1-diphenylethylene, DBDMH, H ₂ O ₂ (98%), DME, -40 °C; b) NaOCH ₃ , MeOH, -30 °C	21	[46]
10		a) ethylidenecyclohexane, DBDMH, H ₂ O ₂ (98%), Et ₂ O, -40 °C; b) NaOH, H ₂ O/MeOH 1:1, (v/v), 0 °C	12	[42]
11		a) 2,3,4,5,6,7-hexahydro-1 <i>H</i> -indene, DBDMH, H ₂ O ₂ (98%), Et ₂ O, -5 °C; b) AgO ₂ CCH ₃ , CH ₂ Cl ₂ , 0 °C	11	[47]

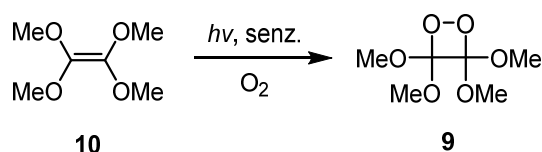
^a General reagents and conditions: Step a) olefin, halogenation reagent (DBDMH or 1,3-diiodo-5,5-dimethylhydantoin, DIH), H₂O₂ (85-98%), anhydrous solvent (Et₂O, CH₂Cl₂, DME). Step b) base (NaOH, KOH, NaOCH₃) or silver salts (AgO₂CCH₃), solvent (MeOH, CH₂Cl₂ or mixture with H₂O 1:1, v/v).

1.4 Synthetic methods to prepare 1,2-dioxetanes

It is worth noting that four-membered ring peroxides, as well as several hydroperoxides, are highly explosive and should be therefore handled with caution and prepared preferentially in small quantities.^{45,48} Moreover, silver catalysts (oxide, acetate, or more conveniently succinimide) must be freshly prepared to prevent the degradation of the final 1,2-dioxetane promoted by metallic silver under light exposure.^{24e} Consequently, in the last years novel and more sustainable methodologies have been developed as discussed below.

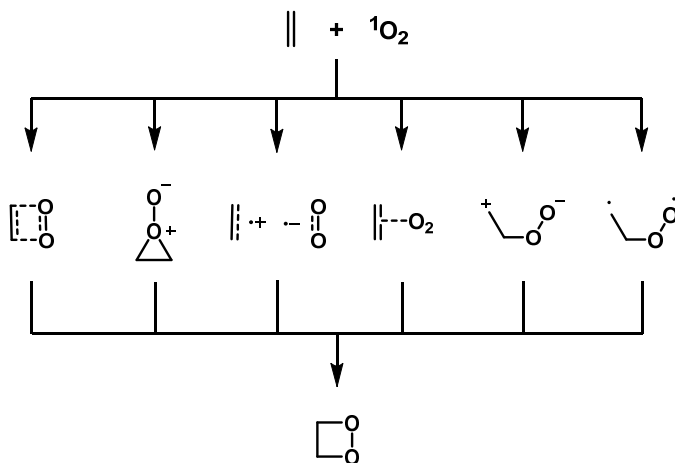
The cycloaddition of the singlet oxygen ($^1\text{O}_2$) to electron rich alkenes represents the prevalent method used for the construction of functionalized 1,2-dioxetanes.⁴⁹ Dye-sensitized photooxygenations *via* the generation of $^1\text{O}_2$ specie are sought to provide sustainable oxidative processes. $^1\text{O}_2$ is conveniently generated *in situ* by photosensitization of the triplet molecular oxygen ($^3\text{O}_2$) in its ground state, upon the exposure to light irradiation in the presence of catalytic amounts of an organic sensitizer (dye). Classical photosensitizers, such as the methylene blue (MB), rose bengal (RB) and tetraphenylporphyrin (H_2TPP), absorb the EMRs in the visible range and transfer the energy to the molecular oxygen *via* a radiationless transition. $^1\text{O}_2$ generated is then added to the substrate.⁵⁰

Footo and Mazur illustrated another method to prepare 3,3,4,4-tetramethoxy-1,2-dioxetane (**9**) under photooxygenation conditions (**Scheme 7**).⁵¹ The reaction was carried out at $-70\text{ }^\circ\text{C}$ by adding zinc tetraphenylporphyrin (ZnH_2TPP) or 1,8-dinaphthalenethiophene as sensitizers to an ether solution of the corresponding olefin (1,1,2,2-tetramethoxyethene, **10**) using a water-cooled immersion irradiation apparatus under oxygen atmosphere.^{52,53} A pale-yellow liquid was obtained in almost quantitative yield (94%) after solvent evaporation at $-78\text{ }^\circ\text{C}$ and distillation at $25\text{ }^\circ\text{C}$. The pure product resulted quite stable ($t_{1/2} = 102\text{ min}$ at $56\text{ }^\circ\text{C}$), although it was partially decomposed by the photosensitizer.



Scheme 7. Synthesis of 3,3,4,4-tetramethoxy-1,2-dioxetane (**9**) via photooxygenation reaction involving the generation of 1O_2 from light irradiation.

Several reaction mechanisms have been proposed for this transformation as illustrated in **Scheme 8**. 1O_2 addition seems to depend on variable factors that determine the success of the photooxygenation reaction. Since the classical [2+2]-cycloaddition of 1O_2 occurs in electron rich systems, the nature of olefin substituents (ED ability, presence of hydrogen-bond acceptors and/or donors, geometry, and steric hindrance) strongly influences the reactivity and the reaction pathway. In addition, the solvation energy and the sensitizer used play a pivotal role in the mechanism of this process.⁵⁴



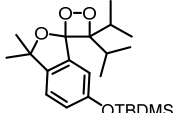
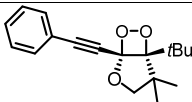
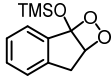
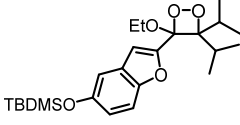
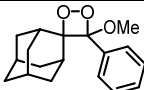
Scheme 8. A representation of the various hypothesized mechanisms for the formation of 1,2-dioxetane through 1O_2 addition to olefin.

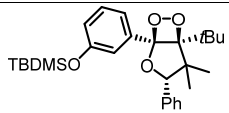
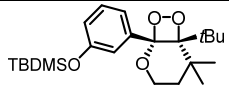
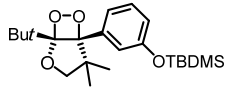
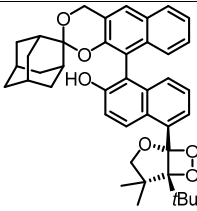
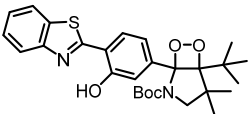
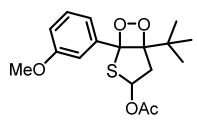
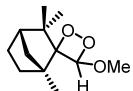
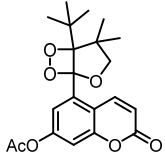
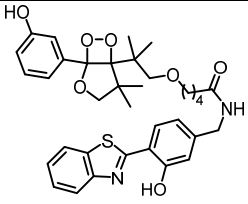
1.4 Synthetic methods to prepare 1,2-dioxetanes

The lifetime of $^1\text{O}_2$ in solutions is generally in the microsecond range because of the fast deactivation through electronic-to-vibrational coupling with solvent molecules. Both the solvent and temperature are known to influence the photooxidation process.⁵⁵ Chlorinated solvents, especially deuterated, and low temperatures enhance $^1\text{O}_2$ lifetime and prevent the thermal decomposition of the 1,2-dioxetane scaffold.⁵⁶

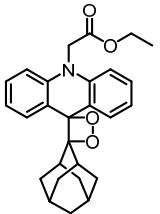
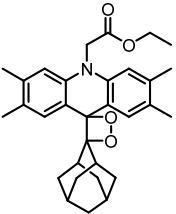
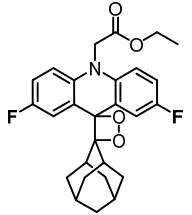
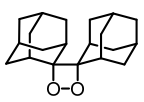
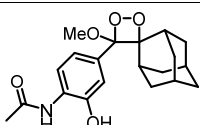
Diverse examples of 1,2-dioxetanes synthesized *via* [2+2]-cycloaddition reaction of $^1\text{O}_2$ to olefin substrates have been described favouring a rapid access to forbidden structures compared to the classical Kopecky method with significantly higher reaction yields (**Table 2**).

Table 2. Examples of variably functionalized 1,2-dioxetanes prepared under photooxygenation conditions.

Entry	1,2-Dioxetane	Reaction conditions ^a	Yield (%)	Ref
1		H ₂ TPP, 940 W Na lamp, CH ₂ Cl ₂ , -78 °C, O ₂	89	[57]
2		RB, Na lamp, CH ₂ Cl ₂ , -78 °C, O ₂	80	[58]
3		H ₂ TPP, 500 W high-pressure Hg lamp, CH ₂ Cl ₂ , 0 °C, O ₂	95	[59]
4		H ₂ TPP, 940 W Na lamp, CH ₂ Cl ₂ , -78 °C, O ₂	72	[60]
5		MB, 400 W medium pressure Hg lamp, CH ₂ Cl ₂ , 25 °C, O ₂	93	[61]

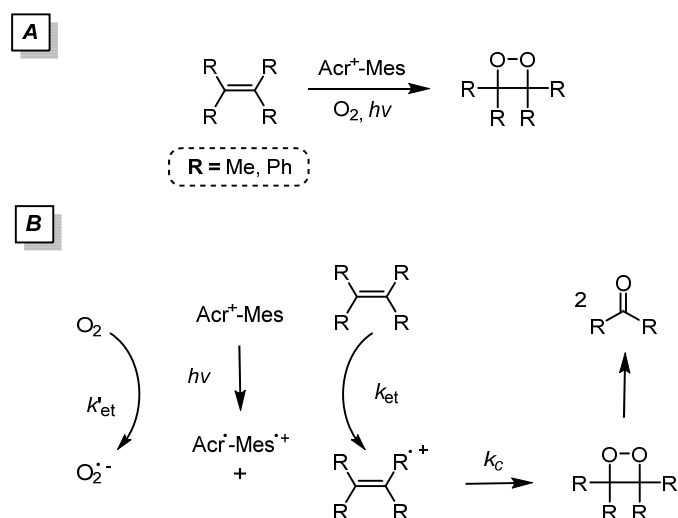
6		H ₂ TPP, 940 W Na lamp, CH ₂ Cl ₂ , 0 °C, O ₂	95	[62]
7		H ₂ TPP, 940 W Na lamp, CH ₂ Cl ₂ , 0 °C, O ₂	74	[63]
8		H ₂ TPP, 940 W Na lamp, CH ₂ Cl ₂ , -78 °C, O ₂	83	[64]
9		H ₂ TPP, 940 W Na lamp, CH ₂ Cl ₂ 0 °C, O ₂	88	[65]
10		H ₂ TPP, 940 W Na lamp, CH ₂ Cl ₂ 0 °C, O ₂	100	[66]
11		MB, 940 W Na lamp, CH ₂ Cl ₂ , 0 °C, O ₂	88	[67]
12		H ₂ TPP, 2 × 500W halogen lamps, CDCl ₃ , -20 °C, O ₂	98	[68]
13		MB, 300 W halogen lamp, CDCl ₃ , 0 °C, O ₂	63	[69]
14		H ₂ TPP, 940 W Na lamp, CH ₂ Cl ₂ , 0 °C, O ₂	100	[70]

1.4 Synthetic methods to prepare 1,2-dioxetanes

15		RB, 400 W halogen lamp, CH ₂ Cl ₂ , -78 °C, O ₂	64	[25c]
16		RB or MB, 500 W halogen lamp, CH ₂ Cl ₂ , 0 °C, O ₂	84	[25b]
17		MB, 500 W halogen lamp, CH ₂ Cl ₂ , -20 °C, O ₂	89	[25a]
18		MB, LEDs (650 nm), CH ₂ Cl ₂ , 0 °C, O ₂	77	[71]
19		MB, 500W halogen lamp, CH ₂ Cl ₂ , 0 °C, O ₂	80	[72]

^a General reagents and conditions: olefin, photosensitizer (H₂TPP, RB, MB), lamp (Na, pressure Hg, halogen, LED), solvent (CH₂Cl₂, CDCl₃), O₂ atmosphere.

An interesting although not-well explored method for the preparation of 1,2-dioxetanes is the photocatalytic oxygenation of olefins in the presence of O₂ via the selective radical coupling using 9-mesityl-10-methylacridinium ion (Acr⁺-Mes) as the electron-transfer photocatalysis (**Scheme 9**).⁷³



Scheme 9. A) Synthesis of 1,2-dioxetanes *via* radical coupling using Acr⁺-Mes and B) reaction mechanism.

¹O₂ can be generated either by photo or chemical reactions. The latter approach does not involve the use of light, consequently the generation of ¹O₂ occurs in “dark” conditions.⁷⁴ Storable ¹O₂ could be generated from triphenylphosphite ozonide (TPPO),^{17c,75} trialkylsilyl hydrotrioxide,^{76,77} calcium peroxide diperoxohydrate (CaO₂·2H₂O₂),^{78,79} molybdate ion with hydrogen peroxide (MoO₄²⁻/H₂O₂ system), and many other sources (**Figure 9**).^{80,81}

1.4 Synthetic methods to prepare 1,2-dioxetanes

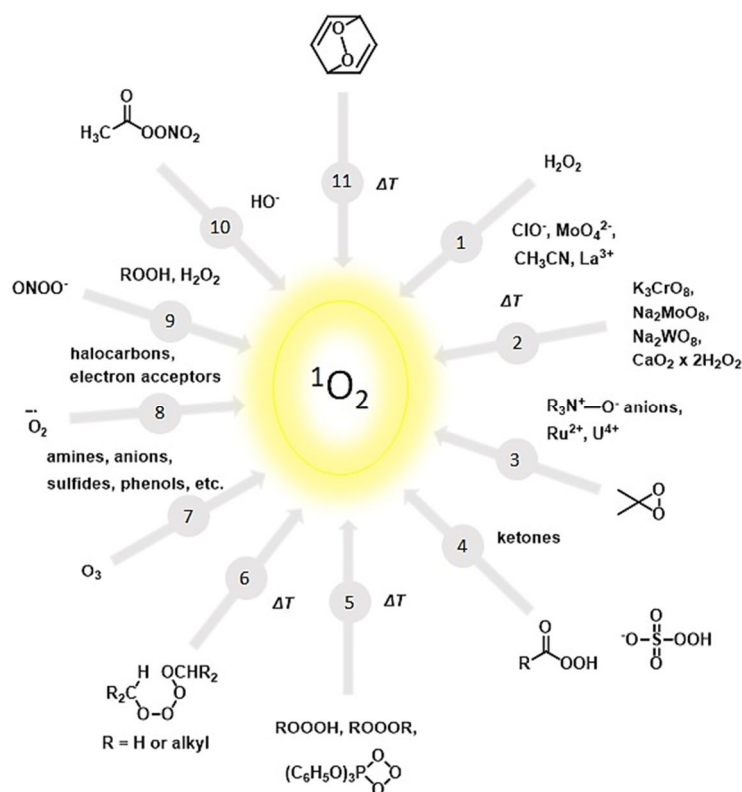
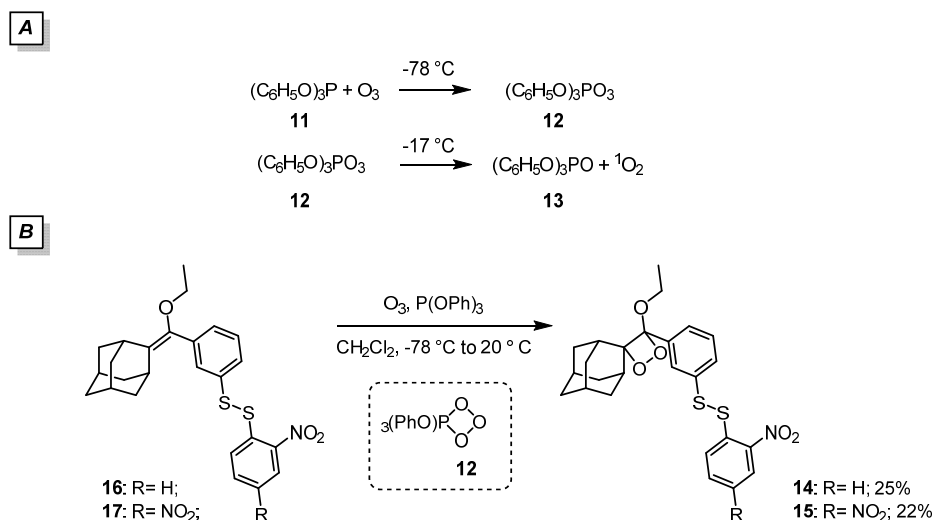


Figure 9. Generation of dark $^1\text{O}_2$ in CL peroxide reactions.⁷⁴

[2+2]-cycloadditions of $^1\text{O}_2$ with enol ethers were successfully conducted by ozone (O_3) reduction with triphenyl phosphite (TPP) (**11**, Scheme 10A).^{75d,82} This approach is particularly recommended in the presence of functional groups susceptible to oxidative conditions as the delivery of $^1\text{O}_2$ can be constantly monitored to avoid the formation of overoxidation side-products.⁸³ TPPO (**12**) is formed at $-78\text{ }^\circ\text{C}$ as the result of the oxidation of TPP (**11**) by O_3 . Then, the pentacoordinated phosphorane **12** is spontaneously decomposed leading to the formation of triphenyl phosphate (TPhP, **13**) and $^1\text{O}_2$ (Scheme 10A).

Sabelle and colleagues adopted this strategy for the synthesis of **14** and **15**, 1,2-dioxetanes particularly sensitive to oxygenated species because of the presence of disulfide bonds.⁸⁴ Accordingly, both compounds were prepared starting from

the corresponding enol ethers (**16** and **17**) in moderate yields under mild conditions and controlled $^1\text{O}_2$ generation (**Scheme 10B**).

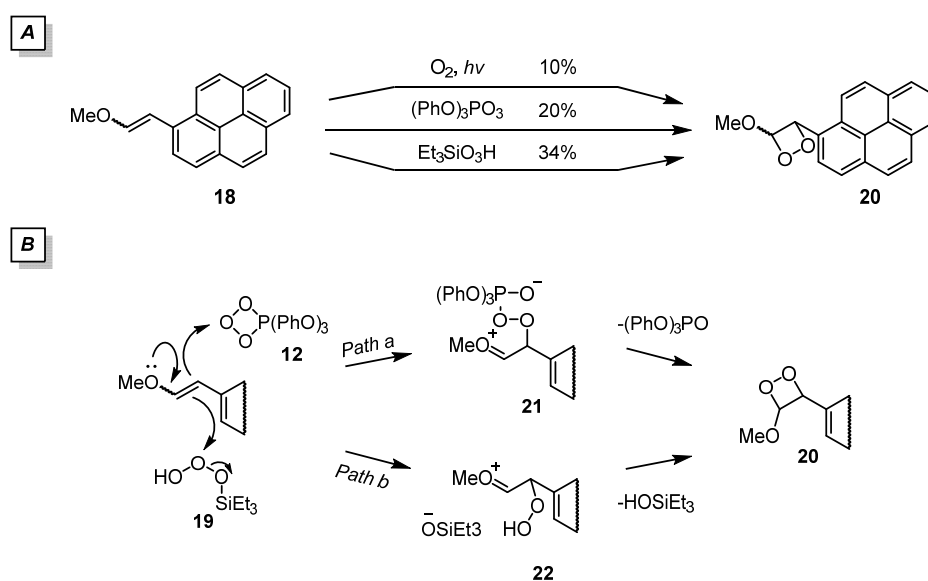


Scheme 10. A) Preparation of TPPO (**12**) from TPP (**11**) and O₃. B) [2+2]-cycloaddition for the synthesis of 1,2-dioxetanes **14** and **15** involving TPPO (**12**) as $^1\text{O}_2$ source.

Trialkylsilanes undergo a similar reaction with O₃ to form trialkylsilanols through a pathway that may involve trialkylsilyl hydrotrioxides as intermediates. The employment of low temperatures facilitates the synthesis of unstable endoperoxides increasing the lifetime of $^1\text{O}_2$.⁸⁵ By this method, Posner and co-workers reported the [2+2]-cycloaddition of 1-(2'-methoxyvinyl)pyrene (MVP, **18**) in the presence of TPPO (**12**) and triethylsilyl hydrotrioxide (**19**) produced *in situ* from O₃.^{75a} The results clearly indicated the superior performance of TPPO (**12**) and triethylsilyl hydrotrioxide (**19**) for the preparation of aryl 1,2-dioxetanes (pyrenyldioxetane, **20**) affording the desired product in low to moderate yields (20-34%) in comparison to the photooxygenation procedure (10%) (**Scheme 11A**). The proposed mechanism consists in the nucleophilic attack by the electron rich methoxyvinyl group of MVP (**18**) to the central oxygen atom of TPPO (**12**)

1.4 Synthetic methods to prepare 1,2-dioxetanes

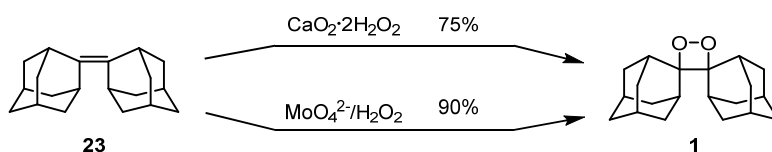
and triethylsilyl hydrotrioxide (**19**) generating the oxonium intermediates as the zwitterion **21** (Scheme 11B, path a)⁸⁶ and as the ion pair **22** (Scheme 11B, path b), respectively. The fragmentation of zwitterion **21** and the acid-base reaction of ion pair **22** followed by ring closure lead then to the 1,2-dioxetane **20** (Scheme 11B).



Scheme 11. A) Synthesis of pyrenyldioxetane (**20**) through photo- and chemically generated $^1\text{O}_2$. B) Proposed mechanisms for the formation of 1,2-dioxetanes involving TPPO (**12**) (*path a*) and triethylsilyl hydrotrioxide (**19**) (*path b*).

A promising alternative to photochemical methods for the generation of ‘dark’ $^1\text{O}_2$ is represented by the molybdate-catalyzed disproportionation of H_2O_2 .^{81,87} Although, this process is well-studied and uses economic reagents,^{88,89} its application in organic synthesis is rather limited. The procedure requires long reaction times,⁹⁰ the only use of methanol and ethanol as system solvents ($^1\text{O}_2$ lifetime is 10 μs and 14 μs , respectively), and excess of surfactants that renders the product recovery from the reaction mixture quite tedious. Alternatively,

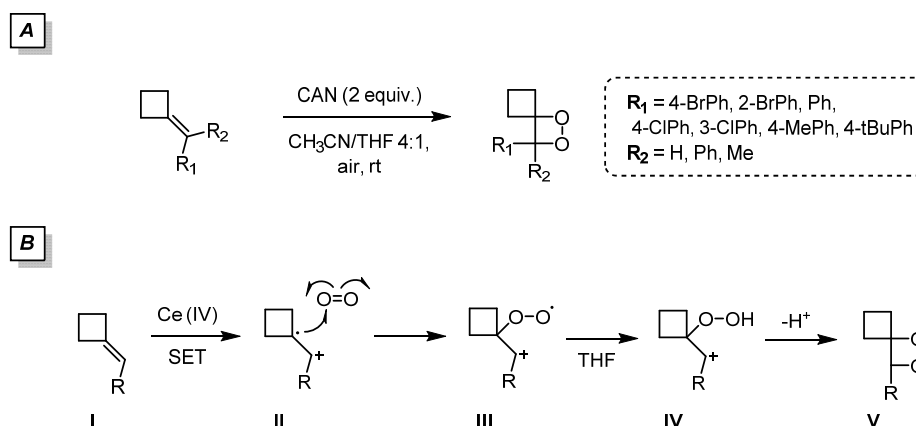
calcium peroxide diperoxohydrate ($\text{CaO}_2 \cdot 2\text{H}_2\text{O}_2$) can be employed.⁷⁹ The reagent is compatible with different solvents and is easily recovered by filtration. Both the reagents have been recently exploited for the synthesis of adamantylidene adamantane-1,2-dioxetane (**1**) from the corresponding olefin **23** (**Scheme 12**).⁷⁹



Scheme 12. Synthesis of adamantylidene adamantane-1,2-dioxetane (**1**) *via* calcium peroxide diperoxohydrate ($\text{CaO}_2 \cdot 2\text{H}_2\text{O}_2$) and molybdate ions ($\text{MoO}_4^{2-}/\text{H}_2\text{O}_2$ system).

A recent work of Yu and colleagues reported the synthesis of stable spirocyclobutyl-1,2-dioxetanes in good yields (50-86%) by cerium (IV) ammonium nitrate (CAN) under air atmosphere and room temperature (**Scheme 13A**).⁹¹ The reaction proved effective on cyclobutenes and on electron rich substrates, exclusively. The plausible mechanism consists of an initial single electron transfer (SET) promoted by CAN to **I** generating a radical cationic specie **II**. The radical intermediate **II** is oxidated by the atmospheric oxygen to form a radical peroxide **III** and hydroperoxide **IV** as the result of a radical H transfer with the solvent (THF). Finally, the peroxide free radical **IV** cyclizes to give the desired spirocyclobutyl-1,2-dioxetane **V** (**Scheme 13B**).

1.5 Decomposition mechanisms of 1,2-dioxetanes

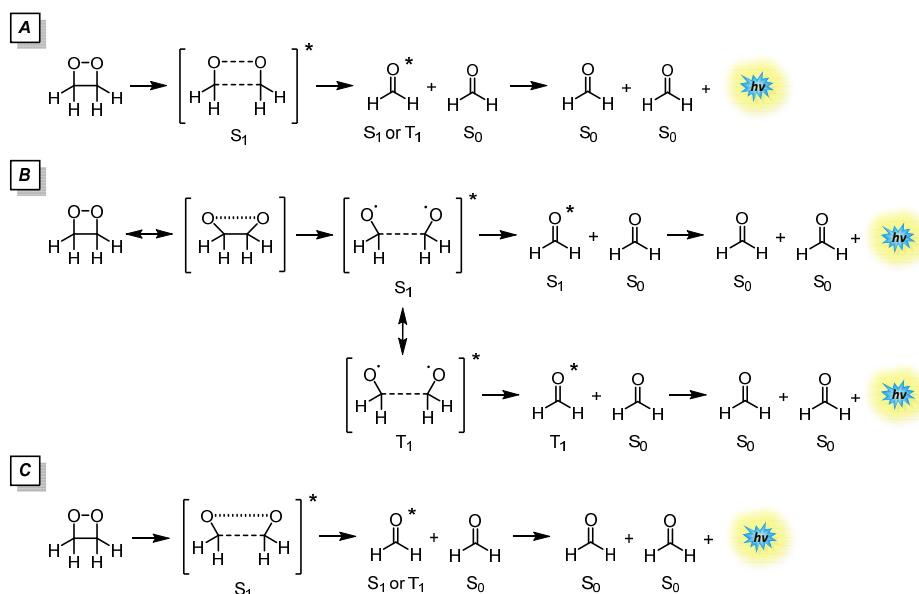


Scheme 13. A) Synthesis of spirocyclobutyl-1,2-dioxetanes through CAN-mediated oxidation. B) Proposed mechanism for the formation of spirocyclobutyl-1,2-dioxetanes involving CAN, air, and CH₃CN/THF mixture as system solvents.

1.5 Decomposition mechanisms of 1,2-dioxetanes

As early discussed, 1,2-dioxetanes tend to undergo a thermal or chemical decomposition generating two carbonyl fragments, one of which is in the excited state (singlet) and is responsible for the generation of light. Several plausible theories have been proposed over the years to explain the mechanisms whereby the endoperoxide group generates an electronically excited fragment, but none of them has provided a comprehensive theory for the chemiexcitation step. The decomposition pathways are strongly influenced by the thermal and chemical stability of 1,2-dioxetane, as well as by the yield of excited state products.

Basically, three different pathways for the decomposition of 1,2-dioxetanes have been proposed: A) synchronous or concerted, B) stepwise or biradical, and C) asynchronous or merged mechanisms (**Scheme 14**).⁹²



Scheme 14. Plausible decomposition pathways of 1,2-dioxetane ring. A) Synchronous or concerted, B) stepwise or biradical, and C) asynchronous or merged mechanisms.

The first mechanism proposed by McCapra and Kearns consisted in a symmetry forbidden pericyclic rearrangement involving the simultaneous homolytic scission of O-O and C-C bonds (**Scheme 14A**).⁹³ Investigating the synchronous theoretical principle, Turro and Devaquet predicted the excited carbonyl fragments populate conveniently the triplet excited states compared to singlet ones by introducing the phenomenon of spin-orbit coupling (SOC) in the ISC.^{41c,94} Based on this theory, the ground state dioxetane surface intersects the various excited states surfaces and that the crossing probabilities, along with the energy levels, determine which path is ultimately taken. In order to occur the transition, a change in electron spin has to happen. This “spin flip” is faster for the transition to the $n-\pi^*$ triplet than to the $\pi-\pi^*$ triplet because the former moves an electron from the O-O bond to an orbital perpendicular to the O-O bond. In this case, the transition is highly favoured compared to the $\pi-\pi^*$ transition (**Figure 10**).

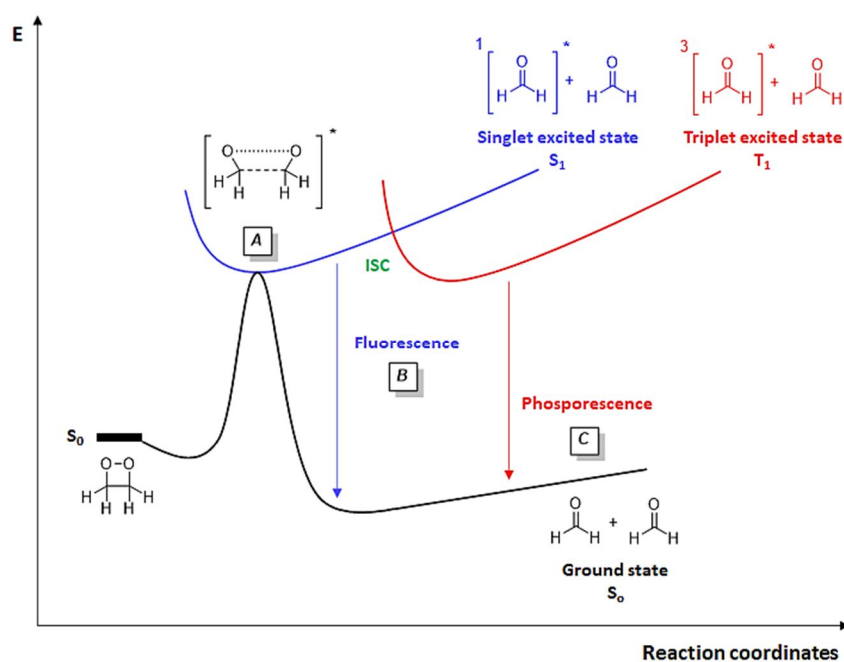


Figure 10. Representation of Turro-Devaquet diagram of the population of the excited states during the 1,2-dioxetane fragmentation.^{24a} A) Dark decomposition (no luminescence) in response to the C-C bond breaking and relaxation to the S_0 . B) C-C bond rupture at the S_1 and de-excitation to the S_0 : fluorescence (*blue*). C) De-excitation across the T_1 following ISC from the S_1 : phosphorescence (*red*).

Subsequently, Richardson and O'Neal suggested a stepwise mechanism with the initial formation of a biradical singlet intermediate after the homolytic cleavage of O-O bond (**Scheme 14B**).⁹⁵ The intermediate may be subjected to different fates: *i*) closure of the four-membered ring to the early 1,2-dioxetane, *ii*) C-C cleavage generating a singlet excited and a ground state carbonyl products, and/or *iii*) relaxation to the close triplet state (biradical triplet intermediate) through the reversible ISC before reaching the ground state (**Scheme 14B**). This theory was further supported by kinetic and *ab initio* calculations.^{46,96} Both mechanisms lead to the formation of two carbonyl fragments where the

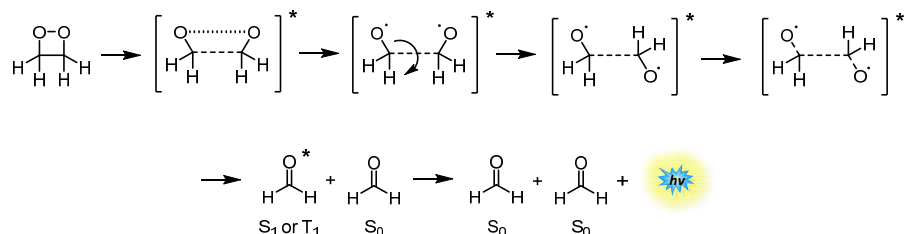
electronically excited one (S_1 or T_1) decays to the ground state and releases energy as photon.

Computational studies have demonstrated that the substitution pattern of 1,2-dioxetanes profoundly affects the decomposition pathway. In particular, aliphatic compounds favour the concerted process,^{97,98} while the presence of aromatic rings or heteroatoms encourages the biradical mechanism.^{96,99}

Currently, the merged (hybrid) mechanism is likely to be the most accepted decomposition pathway (**Scheme 14C**). In this case, the C-C bond stretches along the reaction coordinate supporting a rather concerted, although not simultaneous, cleavage of both C-C and O-O bonds corresponding to a concerted biradical-like mechanism. The mechanism was firstly proposed by Adam and Baader to rationalize both the thermal stability and the singlet/triplet quantum yields of methyl-substituted 1,2-dioxetanes.⁴⁵ The high stability of methyl series was found to depend on the nonbonding repulsive interactions of the methyl groups on C-C and O-O bonds. The concerted almost simultaneous decomposition of methyl-substituted 1,2-dioxetanes without the contribution of radicals provided a high chemiexcitation efficiency, whereas the unsubstituted 1,2-dioxetane preferred a biradical-like decomposition to afford mainly ground state carbonyl products. In summary, the efficient chemiexcitation and the consequent good stability of variably substituted 1,2-dioxetanes could be associated to a concerted mechanism, while 1,2-dioxetanes involved in a biradical-like process are generally characterized by lower excitation efficiency.

More recently, De Vico and co-workers formulated a more comprehensive theory directing their attention on the dissociation rather than the transition state.^{100,101} The turn of events leading to the cleavage of endoperoxide ring could be summarized as a sequence of four steps based on specific geometrical conditions: *i*) stretching of the O-O and C-C bonds, *ii*) torsion of the dihedral angle O-C-C-O, *iii*) asymmetric stretching of both O-C bonds, and *iv*) asymmetric pyramidalization of the C-C atoms affording the final products (**Scheme 15**).

1.5 Decomposition mechanisms of 1,2-dioxetanes



Scheme 15. Representation of the main subsequential steps leading to the opening of the 1,2-dioxetane ring.

De Vico proposed the existence of the “entropic trapping” effect in the decomposition mechanism of 1,2-dioxetanes.¹⁰² Basically, the potential energy surface (PES) for the ground state of the parent dioxetane was calculated and a minimal energy path (MEP), starting from the S_0 transition state along the rotation of the dihedral angle O-C-C-O, was found. The biradical intermediate can explore different torsional configurations generally at equivalent energy in the MEP. However, only specific dihedral angles allow the trajectories to escape from the MEP back to the ground state PES. Consequently, the longer the intermediate remains in the entropic trap, more time it needs to dissociate into the products, thus a longer chemiluminescence event occurs. Furthermore, both the S_1 and T_1 become degenerate when the dioxetane is in the proximity of the transition state (O-O bond cleavage) and they remain so along all the entropic trap region (**Figure 11**). This evidence suggests the positive effect of substituents upon the chemiexcitation efficiency. In particular, enhancing the number of substituents the possible conformations increase, therefore, the time spent in the entropic trap.

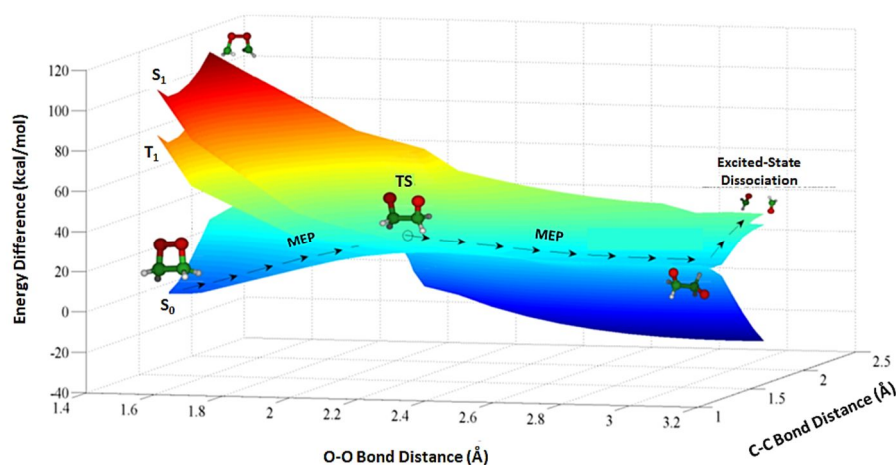


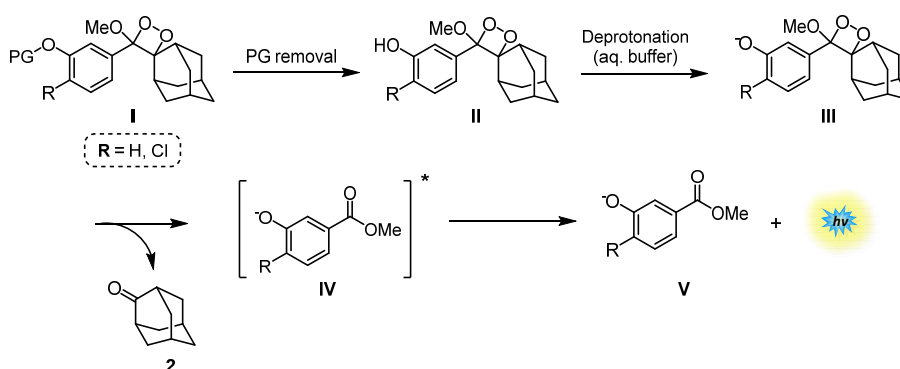
Figure 11. Representation of the entropic trapping effect hypothesized by De Vico and co-workers.^{92,103}

A ground-breaking progress in the decomposition pathway of the 1,2-dioxetanes was the discovery of chemically-triggerable 1,2-dioxetanes by Schaap and Gagnon's groups that synthesized a new class of phenol substituted 1,2-dioxetanes equipped with an enzyme- or analyte-responsive substrate.¹⁰⁴ After the initial chemical removal of the protecting group (PG) and the formation of a phenolate intermediate, a remarkable increase in CL yield and decomposition rate with the predominant formation of S_1 was detected. By carefully selecting the appropriate PG at proper position of the aromatic ring and/or the deprotection reagent, the light emission can be triggered by a specific analyte or enzyme. By then, several triggerable 1,2-dioxetanes have been successfully synthesized.¹⁰⁵

Recently, Shabat and colleagues proposed the synthesis of phenoxy 1,2-dioxetane π -electron systems able to amplify the CL emission through an energy-transfer mechanism occurring at physiological conditions.¹⁰⁶ A considerable light emission efficiency was gained by introducing an EW acrylic substituent at the ortho-position of the phenoxy 1,2-dioxetane (**I**, Scheme 16). After the PG removal (**II**) and the formation of a phenolate as the result of the deprotonation

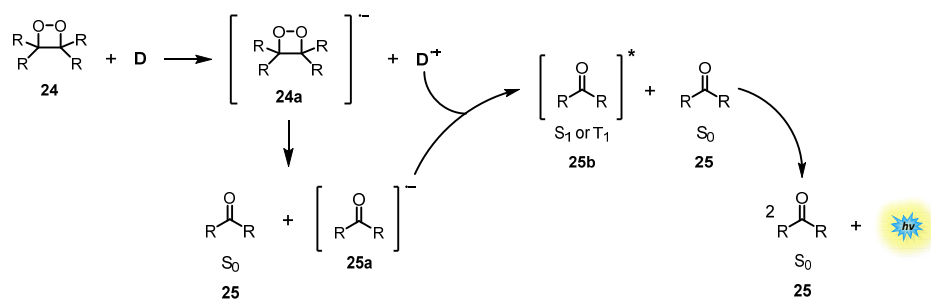
1.5 Decomposition mechanisms of 1,2-dioxetanes

in the aqueous buffer (**III**), the intermediate **III** is excited releasing 2-adamantanone (**2**) and the corresponding phenolate carbonyl fragment (**IV**) which relaxes at its ground state (**V**) producing light (**Scheme 16**). The chemiluminophores showed impressive properties in water environment acting as single-component probes for *in vitro* and *in vivo* detection, as well as for imaging of various analytes and enzymes.



Scheme 16. General structure and activation pathway of Schaap's dioxetanes.

The previously mentioned CIEEL mechanism was gradually imposed as a novel decomposition mechanism to explain the highly efficient chemiluminescence properties of triggered 1,2-dioxetanes.¹⁰⁷ According to the CIEEL mechanism reported in **Scheme 17**, the first step consists in a SET from a donor compound (**D**) to the 1,2-dioxetane **24**, giving the intermediate **24a** which decomposes generating a radical anion **25a**. Then, **25a** reacts with the previously generated radical cation of the donor compound (**D⁺**) within a solvent cage affording the final excited product **25b** which relaxes to the ground state (**25**) emitting light.^{17a}



Scheme 17. CIEEL mechanism for the thermal decomposition of 1,2-dioxetane derivatives.

Aims of the Work

Since the late 1980s, when the TCL phenomenon was firstly suggested as innovative luminescence detection technique in immunoassays, adamantylidene adamantane-1,2-dioxetane (**1**) remained the only stable TCL-based label used in bioanalytical applications until nowadays. Nevertheless, the above-mentioned limitations concerning the poor luminescence intensity and the excessive TCL triggering temperatures, the possibility to generate light in response to the easy thermal degradation of the intrinsically unstable 1,2-dioxetane compounds continue to stimulate interesting research activities in several fields.

To further advance the progress in the development of ultrasensitive TCL probes, this Doctorate work aims to design, prepare, and characterize a set of novel *N*-substituted acridine-containing 1,2-dioxetanes featuring optimal emission triggering temperatures and higher detectability. Accordingly, the study was focussed on the following main aspects:

- Evaluation of the pairing of stability and luminescence efficiency by investigated the effects of EDGs and EWGs at the 2- and 7-positions of acridine moiety;
- Optimization of the key photooxygenation step by using continuous flow technology;
- Computational prediction of the olefins reactivity and 1,2-dioxetanes stability in the crucial [2+2]-cycloaddition reaction;
- Photophysical characterization of final products and evaluation of derivatives in distinct environments (solid state, optical glue and nanocarriers) to provide the proof of concept and potential application in cell-based assays;
- Functionalization of *N*-acridine side chain for the development of new bioconjugated probes based on TCL phenomenon.

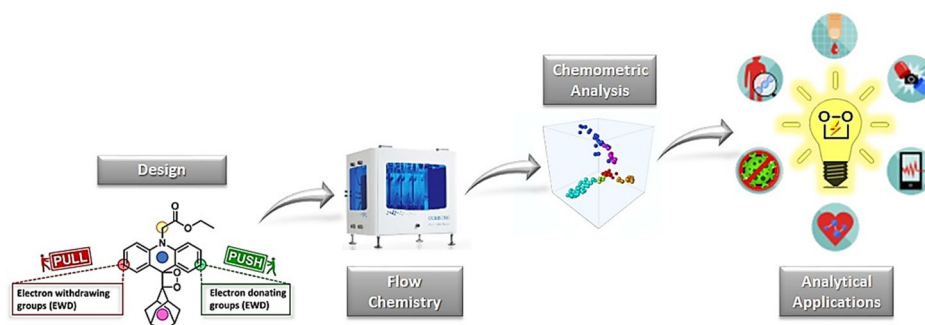


Figure 12. Workflow diagram for the design, synthesis, and characterization of novel *N*-substituted acridine containing 1,2-dioxetanes as ultrasensitive TCL probes for bioanalytical applications.

Chapter 2. Results and Discussion

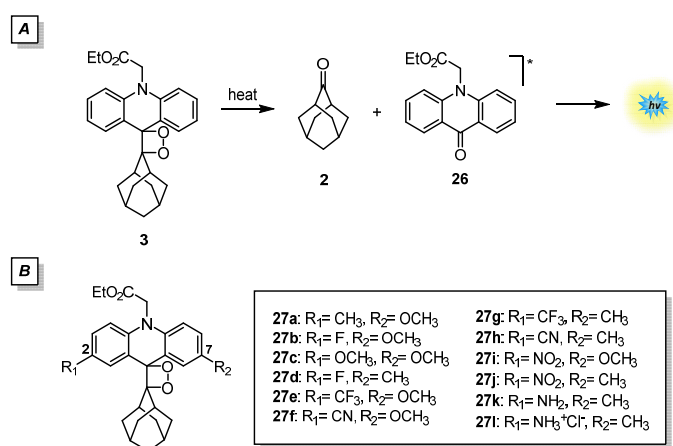
2.1 Design of novel *N*-acridine containing 1,2-dioxetanes

As discussed in the previous Chapter, 1,2-dioxetanes containing an acridine and an adamantyl moieties are considered valuable luminescent probes for bioanalytical applications. The incorporation of 1,2-dioxetane scaffold into the acridine framework was proved as an efficient approach to generate fluorophores endowed of adequate photochemical properties and intense TCL emissions. In particular, compound **3** showed a relatively low trigger temperature (< 100 °C) generating two carbonyl fragments, 2-adamantanone (**2**) and ethyl 9-oxo-10(9*H*)-acridine acetate (**26**), responsible for the light generation (**Scheme 18A**).^{25c,108} The adamantyl moiety sterically protects and stabilizes the 1,2 dioxetane portion from the ring opening, while the acridine scaffold represents the fluorophore unit able to trigger the TCL visible light emission. In addition, the ester group provides a possible binding site for labelling antibodies or other biomolecules such as bt-SA system. Further efforts have been directed towards the development of new bioconjugated probes based on TCL phenomenon (*see* Paragraph 2.5).

Recently, Roda and co-workers exploited the effect of different substituents (-F, -CH₃) on diverse positions of the acridine moiety.^{25a-b} A very interesting point

emerged from these results. The decorations at the acridine fluorophore of **3** can modulate the photophysical properties and the activation parameters for the thermal decomposition of TCL labels. As a general trend, the introduction of EDGs produced higher Φ_F and light emissions, but it was detrimental in terms of thermal stability. On the contrary, EWGs yielded the opposite effects, providing more stable and easier to handle 1,2-dioxetanes with lower Φ_F .^{25a-b} Therefore the approach adopted, i.e., decorating the ring moiety with same electronic nature substituents, was likely to not provide optimal TCL labels featured by high light emission efficiency together with reasonable stability at 25 °C. Moreover, it was previously observed that substituents in C3- and/or C6-positions of the acridine moiety drastically reduce Φ_F compared to the C2- and/or C7-counterparts.^{25a}

To further investigate the effect of substituents at the fluorophore moiety and in the attempt to obtain new TCL probes characterized by a relatively high stability at room temperature and efficient Φ_F for biosensing applications, herein we report the synthesis of a series of novel acridine-containing 1,2-dioxetanes **27** characterized by both EDGs and EWGs at the C2- and C7-positions of the acridine moiety (**Scheme 18B**).



Scheme 18. A) Thermally induced decomposition of acridine-based 1,2-dioxetane **3**.

B) Structures of the novel series of acridine-containing 1,2-dioxetanes (**27a-l**).

2.2 Synthesis

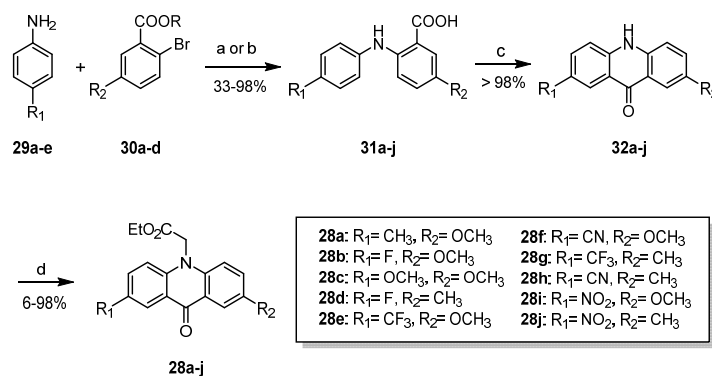
Substituents with different electronical nature (EDGs and EWGs) were sought to be able to balance the electron density inside the molecule and ensure a good compromise between the synthetic feasibility and the chemical instability. For this reason, a series of different substituents was selected, including *a*) EDG by resonance (-OCH₃ and -NH₂), *b*) EDG by hyperconjugation (-CH₃), *c*) EWG by resonance (-CN and -NO₂), *d*) EWG by induction (-CF₃ and -NH₃⁺Cl⁻), and *e*) both EWG by induction and EDG by resonance (-F) (**Scheme 18B**). Previous studies have shown that the effect of the substituents on the photophysical properties and activation parameters of the TCL labels was higher in the 2- and/or 7-positions of the acridine moiety.^{25a-b} Accordingly, C2- and C7-positions were identified as the ideal positions to be explored. Modifications of acridine *N*-side chain have been evaluated by removing or elongating the ester group present in the parent compounds **3**.^{25a} Although the replacement of the ethyl acetate on the nitrogen with alkyl or aryl substituents provided an expected enhancement of Φ_F of the corresponding acridones, a lower thermal stability of the final 1,2-dioxetanes was observed with respect to the reference compound **3**.^{25a} It was found that the ester chain exerts a peculiar stabilizing effect on the 1,2-dioxetane scaffold due to its EW character,^{25c,109} as well as it provides a useful appendage for conjugation with biomolecules. Consequently, the acetate moiety was fixed as the side chain, combining both TCL efficiency and the thermal stability.

2.2 Synthesis

2.2.1 Synthesis and photophysical properties of acridone intermediates

The novel series of acridine-containing 1,2-dioxetanes **27a**, **27d-e**, **27g** characterized by both EDGs and EWGs at the C2- and C7-positions of the acridine moiety were synthesized according to **Scheme 19**. The synthetic route

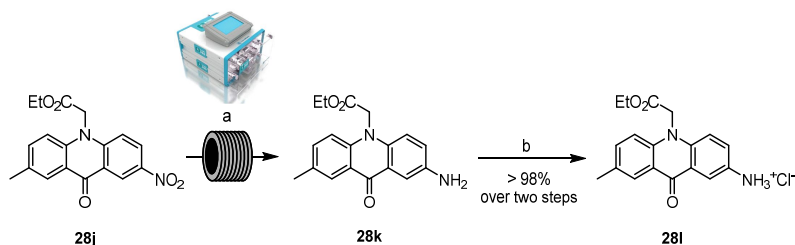
was based on Ullmann or Buchwald-Hartwig couplings, a cyclization step, and an alkylation reaction to afford the corresponding ethyl acridone acetates as key intermediates (**28a-j**).^{25a,110} In particular, Ullmann-type coupling (Cu/K₂CO₃) between substituted anilines **29a-c** and 2-bromo-5-methoxy-benzoic acid **30a** in refluxing DMF gave the corresponding 2-aminoarylbenzoic acids **31a-c**.^{25b,111} Under these conditions, the reaction with methyl 2-bromo-benzoates **30b-d** failed to provide the desired intermediates **31d-j** that were then prepared by Buchwald-Hartwig reaction.¹¹² Accordingly, esters **30b-d** were reacted with Pd₂(dba)₃·CHCl₃, (±)-BINAP and Cs₂CO₃ in toluene at reflux to furnish the resulting adducts that were readily submitted to basic hydrolysis (NaOH, MeOH) providing **31d-j** (Scheme 19).¹¹³ The cyclization step was performed by using the Eaton's reagent in neat conditions at 90 °C affording the desired 2,7-disubstituted 10*H*-acridin-9-ones **32a-j** in nearly quantitative yields (Scheme 19).¹¹⁴ Finally, ethyl 9-oxo-10(9*H*)-acridine acetates **28a-j** were obtained by reaction of **32a-j** with ethyl bromoacetate in the presence of NaH and Bu₄NI in DMF at room temperature (Scheme 19).^{25c}



Scheme 19. Synthesis of ethyl acridone acetates **28a-j**. *Reagents and conditions:* a) Cu, K₂CO₃, DMF, reflux; b) i) Pd₂(dba)₃ CHCl₃, (±)-BINAP, Cs₂CO₃, toluene, 110-130 °C; ii) NaOH, MeOH, r.t.; c) Eaton's reagent, 90 °C; d) NaH, BrCH₂COOEt, Bu₄NI, DMF, 0 °C → r.t..

2.2 Synthesis

To further explore the effect of different substituents, the nitro compound **28j** was reduced into the corresponding amine **28k** (Scheme 20).¹¹⁰ This modification was aimed to confer a polar nature to the molecule by improving the water solubility and to add an additional useful binding site for coupling biomolecules and therefore suitable for bioanalytical applications. The reaction was realized by using a continuous-flow hydrogenation reactor (H-Cube[®], ThalesNano) able to generate high-pressure hydrogen (H₂) from the electrolysis of water.¹¹⁵ The risks associated with the handling of pyrophoric catalysts and the hazardous nature of the gaseous reactant have been completely minimized through *in situ* H₂ generation and the use of sealed catalyst cartridges (CatCarts[®]). Thus, the hydrogenolysis reaction was carried out under continuous flow conditions using palladium on carbon (Pd/C), at 1 bar of pressure, 30 °C and a total flow rate of 1 mL min⁻¹ in MeOH. The product **28k** obtained in quantitative yield was treated with HCl in dioxane to get the corresponding hydrochloride **28l**.

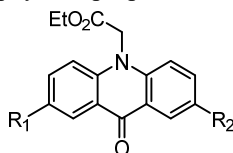


Scheme 20. Synthesis of acridones **28k-l**. *Reagents and conditions:* a) H₂, Pd/C 10%, MeOH, 1 mL min⁻¹, 1 bar, 30 °C, 2 h; b) HCl 4 M in 1,4-dioxane solution, r.t., 6 h, > 98% (over two steps).

We next investigated the photophysical properties of the synthesized ethyl acridone acetates **28a-l** that represent the emitting portion of the 1,2-dioxetane molecules (Table 3). The unsubstituted acridone **26** was employed as reference compound. The experiments were carried out by measuring spectroscopic properties, in terms of maximum absorption, emission wavelengths (λ_{abs} and λ_{em}),

and fluorescence quantum yields (Φ_F). Φ_F was calculated employing the common relative method which relies on the use of well-characterized reference standard with known Φ_F value and optical properties closely matching the unknown sample of interest.¹¹⁶ The absorption and fluorescence emission spectra of **28a-l** were recorded in acetonitrile (CH₃CN) solution and the relative Φ_F values were determined using quinine sulphate as standard ($\Phi_F=0.53$ in H₂SO₄ 0.05 mol L⁻¹), a UV-Vis spectrophotometer (Varian Cary 50) and a spectrofluorometer (Varian Cary Eclipse), respectively.

Table 3. Photophysical properties of acridones **28a-l**.



Compound	R ₁	R ₂	λ_{abs} (nm) ^a	λ_{em} (nm) ^a	Φ_F ^{a,b}
26	H	H	390	403	0.11
28a	CH ₃	OCH ₃	414	441	0.55
28b	F	OCH ₃	417	451	0.67
28c	OCH ₃	OCH ₃	424	457	0.56
28d	F	CH ₃	406	429	0.59
28e	CF ₃	OCH ₃	407	451	0.59
28f	CN	OCH ₃	410	450	0.50
28g	CF ₃	CH ₃	394	413	0.23
28h	CN	CH ₃	385	411	0.21
28i	NO ₂	OCH ₃	364	^c n.e.	^d n.d.
28j	NO ₂	CH ₃	358	543	0.02
28k	NH ₂	CH ₃	430	514	0.14
28l	NH ₃ ⁺ Cl ⁻	CH ₃	401	423	0.18

^a Determined in CH₃CN solution. ^b Determined using quinine sulfate as standard ($\Phi_F=0.53$ in H₂SO₄ 0.05 mol L⁻¹). ^c n.e.= No emission. ^d n.d.= Not determined.

The effect of the nature of the substituents at C2- and C7-positions of the acridones on the electronic structure of the chromophores has been carefully evaluated. Based on the various substituents employed (*see* Paragraph 2.1), the acridone molecules reported in **Table 3** can be classified into *push-pull* acridones (**28b**, **28d-e**, **28f-i**, **28j** and **28l**) when they are constituted by an EWG and an EDG, and *not push-pull* acridones (**28a**, **28c** and **28k**) when they possess two EDGs.

Compounds **28a**, **28c** and **28k** showed a remarkable bathochromic shift of maximum absorbance wavelengths (λ_{abs}) with respect to reference compound **26**, as previously observed. In addition, the acridone **28b**, characterized by the presence of a strong EDG (-OCH₃) and a fluorine substituent due to its electronic double nature as stated above, showed a comparable shift. In general, other *push-pull* acridones (**28d-g**, **28l**) showed a common very slight red shift (from 4 to 20 nm) compared to unsubstituted acridone **26**. Conversely, the compounds **28h-j** characterized by the presence of resonance EWGs (-NO₂ or -CN) showed a hypsochromic shift (from 5 to 32 nm). These results are confirmed by previous findings showing a bathochromic shift of λ_{abs} upon introduction of EDGs on the acridone molecule. It is thus confirmed that the electron density enrichment generates a red shift of the absorbance spectrum.^{25b}

Concerning the effects of the substituents on the maximum fluorescent emission wavelength (λ_{em}), except for the derivative **28i**, all the other compounds showed a red shift compared to the unsubstituted acridone **26**, suggesting an effect of perturbation of the excited state symmetry that reduces the distance between HOMO and LUMO orbitals. It can be additionally noted that compound **28j**, although displaying a very low Φ_{F} value, provided the highest bathochromic shift of fluorescence emission, leading to a large Stokes shift. This can be ascribed to the presence of the nitro substituent and to the conditions employed for photophysical properties measurement. Indeed, it is known that fluorophores containing nitro groups display a strong emission solvatochromism because of

the remarkable change of the dipole moment between ground and excited states. Since the fluorescence emission spectra were recorded in CH₃CN, the solvent polarity enhanced the ability of -NO₂ to stabilize the charge transfer state, thus producing the λ_{em} red shift.¹¹⁷

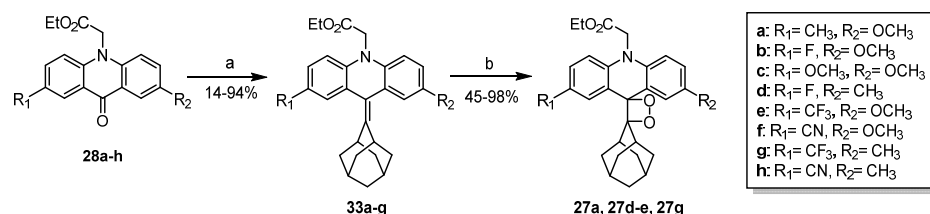
A significant improvement of the Φ_F values can be observed into compounds **28a** and **28c** bearing only EDGs, compared to the unsubstituted derivative **26**, as expected, while only a slight improvement was observed for compound **28k**. The *push-pull* systems displayed an increase of Φ_F ($0.21 \leq \Phi_F \leq 0.67$), as opposed to nitro derivatives (**28i** and **28j**) and to a lesser extent for **28l** that show weak fluorescent emission intensities, in agreement with previously reported results.^{118,119} It can be observed that Φ_F values are strongly influenced by the electron density enrichment of the aromatic system determined by the decoration of diversified substituents on the acridone ring. This effect is particularly evident valuating compounds **28e** and **28f** (*push-pull* acridones in which the EDG acts by resonance) which have higher Φ_F values with respect to compounds **28g** and **28h** (*push-pull* acridones in which the EDG acts by induction). As concerns *push-pull* compounds **28i** and **28j**, the well-known quenching effect of the -NO₂ substituent is confirmed by our findings. Generally, it is indeed known that the Φ_F of a fluorophore containing nitro groups is extremely low because of the decrease in the radiative rate and the increase in the internal conversion rate of the excited state fluorophore.¹¹⁷

2.2.2 Synthesis of acridine containing 1,2-dioxetanes

We next proceeded with the synthesis of 1,2-dioxetanes **27** from the corresponding acridones **28** (**Scheme 21**), selected on the basis of synthetic feasibility and Φ_F values. Thus, the McMurry-type olefination was realized on promising acridones **28a-h** under standard conditions by adding 2-adamantanone

2.2 Synthesis

(**2**) to a suspension of Zn powder and TiCl₄ (1 M in CH₂Cl₂) in anhydrous THF (**Scheme 21, step a**).^{25a} As previously reported, the different substitution pattern at the C2- and C7-positions of the acridine moiety influenced the reaction outcome as a consequence of both electronic and steric effects. However, McMurry reaction did not occur with **28h** and failed to give the corresponding olefin **33h**. Olefins **33a-g** thus formed were submitted to the photooxidation reaction (**Scheme 21, step b**), the limiting step of the whole synthetic strategies.



Scheme 21. Synthesis of acridine-containing 1,2-dioxetanes (**27**) by McMurry (*step a*) and photooxygenation (*step b*) reactions. *Reagents and conditions:* a) **2**, TiCl₄ (1 M in CH₂Cl₂), Zn, anhydrous THF, reflux; b) MB, -20 °C, CH₂Cl₂, lamp, O₂ (1 atm, balloon).

The photooxygenation of the tetrasubstituted double bond certainly represent the critical step of the synthetic pathway. It consists of a [2+2]-cycloaddition reaction where ¹O₂ originated from a sensitizer upon light irradiation is added to an olefin system. The reaction is particularly sensitive to the π-electron density of the double bond, thus electron rich olefins readily react to these conditions.^{51,54j,120} Consequently, the reactivity of the olefin in the photooxygenation process strongly depends on substitution pattern of the acridine ring.

The [2+2]-cycloaddition of ¹O₂ to an alkene was preferred over the classical Kopecky method as direct and convenient synthetic route to obtain 1,2-dioxetanes. In fact, the synthetic approach is characterized by a high atom

economy, good yields, and the employ of green reagents, including catalytic amount of photosensitizer and light source.

Initially, the photooxygenation step was realized by using a home-made batch photo apparatus composed of a double jacketed-bottom flask filled with O₂, a cryostat to refrigerate the reactor flowing coolants (e.g., glycol), and a 500 W halogen lamp equipped with an UV 460 nm cut-off filter (**Figure 13A**).^{25a} The reaction was further performed by using a 1000 W red light-emitting diode (LED) instead of the halogen lamp as earlier described,¹¹⁰ significantly increasing the reaction yield from 30 to 94% (**Figure 13B**). Moreover, the LED technology ensures several benefits including: *i*) restricted spectrum of colours, *ii*) low heat generation limiting thermal decomposition and side-products formation, *iii*) high energy saving and longer lifetime of the light source (**Figure 13C**).¹²¹ The LED wavelength was fixed at 700 nm to favour the only excitation of the MB used as photosensitizer, according to the reagent maximum absorption. Thus, compounds **33a-g** were dissolved in CH₂Cl₂ in presence of MB and irradiated at -20 °C under O₂ atmosphere.

2.2 Synthesis

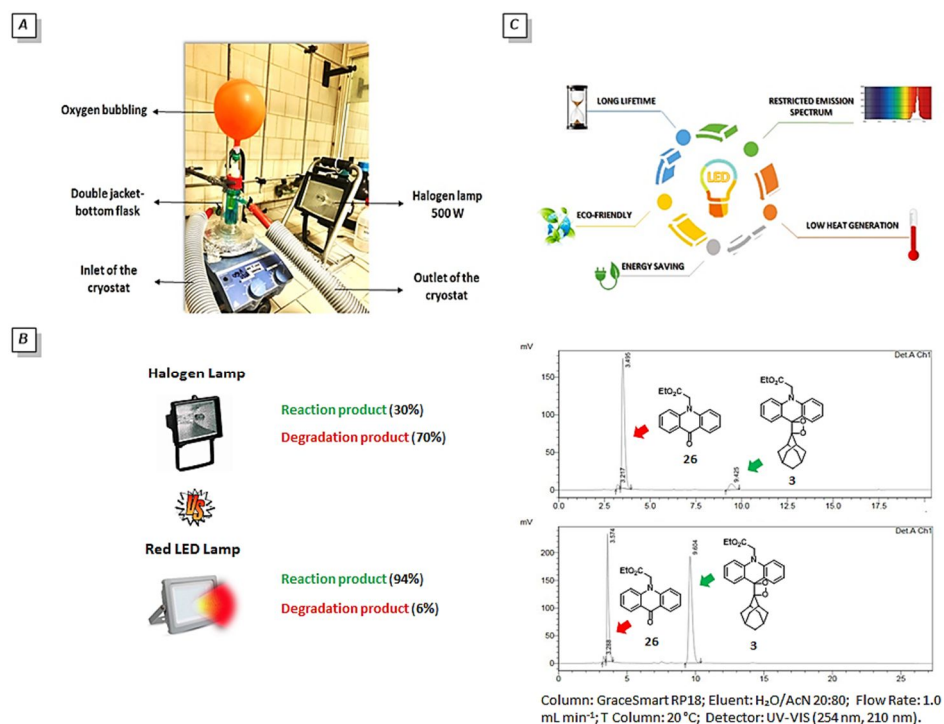
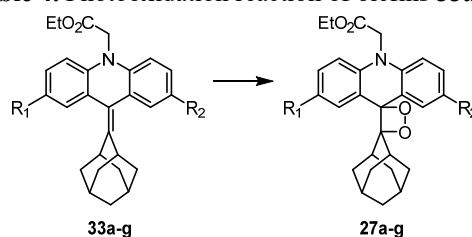


Figure 13. A) Batch photo apparatus for the [2+2]-cycloaddition reaction. B) HPLC analysis of photooxygenation reaction by comparing halogen lamp vs red LED for the synthesis of unsubstituted 1,2-dioxetane **3**. C) Advantages of LED technology.

The success of the reaction basically depends on the kinetic operating conditions.¹²² In particular, low temperatures (below 0 °C) avoid the decomposition of 1,2-dioxetane scaffold into the ketone intermediates and, at the same time, drastically increase the lifetime of the ¹O₂. As expected, the rate of formation of 1,2-dioxetane derivatives was strongly dependent on the substitution pattern that modulates the π -electron density on the double bond.^{25a,54j,118,119} The position and the electronic/steric properties of the substituents on the acridine ring can determine not only the success or the failure of the ¹O₂ addition to the tetrasubstituted double bond of **33a-g**, but also the stability of the corresponding 1,2-dioxetanes. As a result, compounds **27d** and **27g** were obtained in high yield

(79% and 93%, respectively) as for the unsubstituted parent compound **3** (Table 4). Conversely, with all the alkenes possessing the methoxy group on the aromatic rings (**33a-c** and **33f**), we were unable to collect the desired products, with the exception of the derivative **33e** that provided the corresponding 1,2-dioxetane in moderate yield (45%) (Table 4).¹¹⁰

Table 4. Photooxidation reaction of olefins **33a-g**.^a



Compound	R ₁	R ₂	Yield (%) ^b
3	H	H	94
27a	CH ₃	OCH ₃	complex crude
27b	F	OCH ₃	complex crude
27c	OCH ₃	OCH ₃	complex crude
27d	F	CH ₃	79
27e	CF ₃	OCH ₃	45
27f	CN	OCH ₃	complex crude
27g	CF ₃	CH ₃	93

^a Reagents and conditions: MB, -20 °C, CH₂Cl₂, lamp, O₂ (1 atm, balloon). ^b Determined by ¹H-NMR analysis.

It is worth noting that in most cases, products were formed but readily decomposed in the reaction mixtures or during the purification because of their instability. These findings seem to suggest that the strong ED ability of the methoxy group greatly destabilizes the acridine-based 1,2-dioxetane derivatives.

2.2 Synthesis

Only when the effect is mitigated by an inductive EWG (-CF₃) the desired product becomes isolable.

2.2.3 Chemometric analyses and computational prediction of the photooxygenation step reactivity

The reactivity of acridine-derived alkenes (**33**) in the formal [2+2]-cycloaddition of ¹O₂ affording the corresponding 1,2-dioxetanes (**27**) was investigated based on the different substitution pattern using a straightforward chemometric approach.¹¹⁰ The study was conducted in collaboration with Prof. Marco Lombardo and Dr. Arianna Quintavalla from the University of Bologna. Principal component analysis (PCA) was used to derive a predicting model able to discriminate the most important structural and electronic molecular descriptors of alkenes **33**, crucial in determining the photooxygenation reactivity. Moreover, supervised linear discriminant analysis (LDA) was applied to predict the reactivity of new alkenes. It was demonstrated that the reactivity of alkenes **33** in the photooxygenation reaction was mainly due to steric effects, caused by the presence of substituents in the proximity of the double bond, and only marginally to electronic factors. Therefore, a series of DFT calculations on the new alkenes **33a-g** was carried out according to the same level of theory used in the previously reported PCA model to rationalize the reactivity results here reported,^{25a} as well as to better understand the effects of the electronic density on the double bond from the substitution pattern on the acridine ring.

Analogues of alkenes **33a-g**, namely **34a-g**, with a methyl ester group on the *N*-side chain, and the corresponding unsubstituted olefin **34**, were considered in order to simplify the prediction model. This allowed to considerably reduce the number of potential conformers, since the electronic distribution and the structural parameters of the aromatic rings are not affected by the nature of ester

moiety to a significant extent. Therefore, **34a-g** were first screened by molecular mechanics (MM force field) and the conformers obtained in an 8 kcal·mol⁻¹ window were further optimized by using Density-Functional Theory (DFT) at the B3LYP/6-31G(d) level of theory. The most stable conformers were finally determined by Boltzmann analysis, using the Gibbs free energies obtained after vibrational frequency calculations.¹¹⁰ The 14 structural and electronic parameters used in building the previous PCA and LDA models for acridine-like alkenes were recovered from these optimized structures and used to estimate the probability that the new set of alkenes **34a-g** belongs to the class of reactive (mean of canonical variables= 6.48) or unreactive (mean of canonical variables= -11.8) starting materials (**Table 5**).¹¹⁰ The LDA model predicted all alkenes **34a-g** to be potentially reactive in the photooxygenation reaction, with raw canonical scores very close to the mean of the reactive class (**Table 5**). This is supported by the fact that all alkenes **34a-g** were partially or totally consumed during the photooxygenation reaction. However, some final 1,2-dioxetanes were not stable enough and decomposed during the reaction course or the isolation stage.

Table 5. LDA raw canonical scores for alkenes **34a-g**.

Compound	R₁	R₂	LDA score^a
34a	CH ₃	OCH ₃	5.66
34b	F	OCH ₃	7.31
34c	OCH ₃	OCH ₃	7.11
34d	F	CH ₃	7.81
34e	CF ₃	OCH ₃	8.34
34f	CN	OCH ₃	8.64
34g	CF ₃	CH ₃	6.43

^a Mean for reactive class= 6.48; mean for unreactive class= -11.8.

DFT calculations demonstrated that 1,2-dioxetanes deriving from alkenes possessing only EDGs on the aromatic rings (**27a** and **27c**) were extremely unstable, suggesting that the stability strongly depends on the electron density and that it can be eventually modulated by inserting both an EDG and an EWG on the aromatic framework (*push-pull* effect). To confirm this hypothesis, atomic charges for the analogues 1,2-dioxetanes **3** and **27a-g** with a methyl ester on the side chain, namely **35** and **35a-g**, were calculated using Multiwfn software with different partition schemes.¹²³ In particular, we noticed that the negative charge of C9 atom of the double bond increases with raising of electron density on the aromatic framework. The results obtained using PEOE (partial equalization of orbital electronegativity)¹²⁴ and Hirshfeld partition schemes are displayed in **Figure 14**.¹²⁵

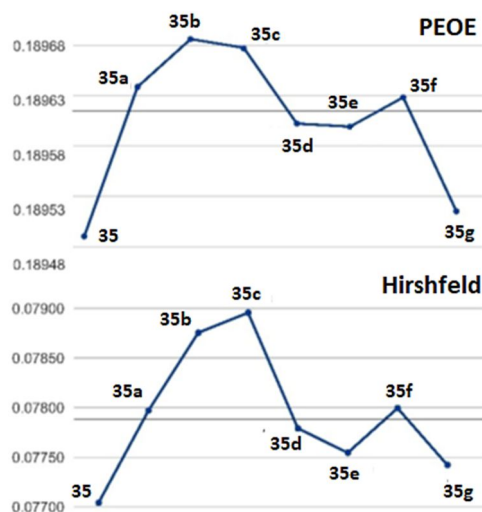


Figure 14. Calculated PEOE and Hirshfeld charges on atom C9 for 1,2-dioxetanes **35** and **35a-g**.

DFT calculations demonstrated that the most stable dioxetanes in the series (**3** and **27g**) are related to analogues characterized by an electron deficiency on C9

atom (**35** and **35g**), while the most unstable products are the ones corresponding to the analogues with the largest charge values (**35a-c** and **35f**), with **35d** and **35e** giving intermediate results (**Figure 15A**). The effect of the different substituents on the electron density distribution can be visually appreciated also by inspecting the corresponding ESPs (Electrostatic Potential mapped on the total electron density iso-surfaces), reported in **Figure 15B**, for the two relatively stable new dioxetanes analogues (**35d** and **35g**) and for the unstable one (**35c**). These findings suggest that the strong mesomeric electron donating effect of the two methoxy groups greatly destabilizes the corresponding acridine-based 1,2-dioxetane enhancing the negative charge density on the aromatic rings (**35c**, **Figure 15B**). On the other hand, the presence of both a weak EDG (-CH₃) for hyperconjugation and an EWG (-F or -CF₃) *via* inductive effect in the molecule (**35d** and **35g**, **Figure 15B**) reduces the electron density from the aromatic rings by conferring more stability at the final 1,2-dioxetanes towards thermic degradation.¹¹⁰

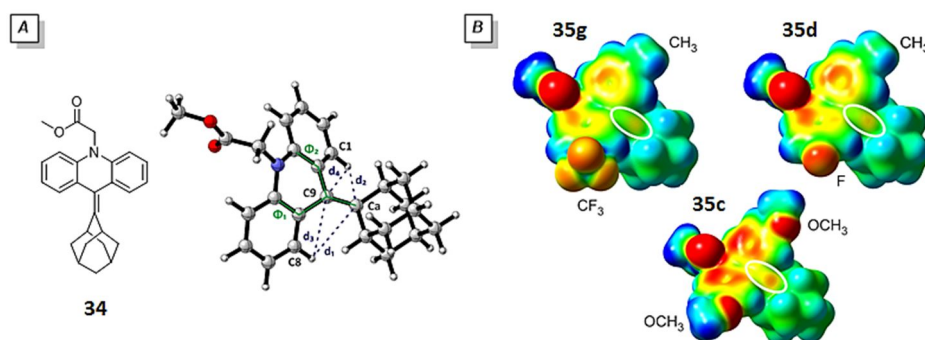


Figure 15. A) DFT-optimized structure of unsubstituted olefin **34** and structural molecular descriptors employed in the PCA and LDA analyses. B) Calculated ESP surfaces for dioxetanes **35c-d** and **35g**. Negative charges are colored in red, while positive charges in blue. The white oval identifies the position of the double bond.

Finally, it should be mentioned that the accepted mechanism for the degradation of 1,2-dioxetanes involves the formation of oxygen biradicals and can be theoretically studied accurately only using complete active space SCF methods (CASSCF). Theoretical analyses of 1,2-dioxetanes decomposition have been reported so far only for very simple molecules,^{102,103,126} and they would be extremely computationally demanding on more complex substrates, such as **3** or **27**.

2.3 Optimization of photooxygenation step by continuous flow technology

The last decades have witnessed a renewed interest and subsequent growing development of photochemical reactions in both academia and industry.¹²⁷

The use of photons as “clean and traceless reagents” to generate high molecular complexity, such as natural products and useful building blocks, is driven by the desire to realize more sustainable approaches for target molecules synthesis. This purpose has been partially reached thanks to the increasing availability of reliable light sources, i.e., LEDs, as well as to the introduction of “enabling technologies”, such as the continuous flow chemistry, to overcome limitations of conventional batch photosynthesis.¹²⁸ A variety of photochemical transformations ranging from cycloaddition to functionalization reactions, including halogenations,¹²⁹ trifluoromethylations,¹³⁰ C-H activations,¹³¹ and in particular oxygenations,^{127c,132} has been successfully developed under continuous flow fashion.

Box 2. Basic concepts of continuous flow photochemistry technology

Batch reactions performed in traditional round-bottom flasks are replaced with broader surface-to-volume ratio flow-type tubing within which reactions take place. Specific pumps are embedded into the flow set-up to convey feed solutions of starting materials and reactants into transmittable reactor devices. A typical flow photo apparatus generally consists of pumping and reaction modules (photoreactor and light source), but additional components can be easily assembled on demand to create several combinations and customizable set-ups (Figure 16).¹³³

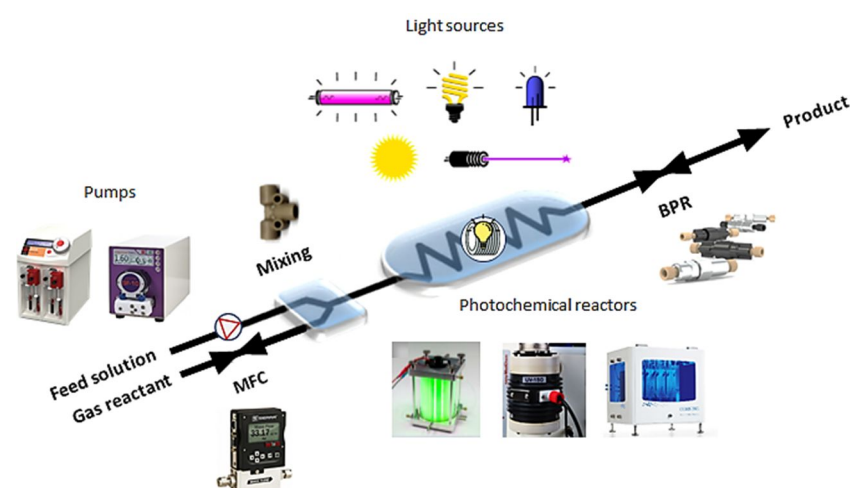


Figure 16. Illustration of a general photochemical flow set-up involving gas as reactant.

Although commercial dedicated continuous flow platforms with integrated or interchangeable lamps are commercially available,^{134,135} “home-made” flow photoreactors and attached components may be designed by using 3D-printers providing a flexible, versatile, economic, and smart alternative to researchers.^{128d,136} The flow system is fed with the solution of reagents and starting materials through different pumps (HPLC, syringe, peristaltic and rotary pumps) or eventually pre-loaded in sample loops generating a continuous flow streaming headed for the reactor. A range of fitting parts such as Swagelok, nuts and ferrules are essential accessories for assembling and connecting the different bespoke flow set-ups.¹³⁷ The tubing materials including glass, silicon, and polymers shall be properly chosen according to the working conditions, chemical compatibility, and operational needs. Generally, photoreactors are realized with light transparent materials able to hold the light without any scattering phenomena. The light source represents one of the most important components in photochemical reactions.¹³⁸ The selection of the appropriate light source depends mainly on the overlap between the emission spectrum and the absorption characteristics of the photoactive reactants or catalysts. Other fundamental criteria to be considered include costs, energy efficiency, lifetime and dimension. Traditional light sources such as halogen, pressurized mercury vapor lamps, and fluorescent light bulbs are gradually replaced by more efficient LEDs exploiting extensive advantages in microfluidic applications.¹³⁹ Advanced LED technology is characterized by a narrow pseudo-monochromatic light emission minimizing the energy dissipation and the heat generation. Furthermore, the small size and the affordable price make them particularly suitable for the integration with flow reactor modules. A multitude of LEDs in the visible light spectrum are commercially available providing access to a wide range of wavelengths and intensities.

Continuous flow chemistry represents a powerful technology to assist the development process from early drug discovery to manufacturing.¹⁴⁰ Commercial flow apparatus are engineered to ensure a precise control over the experimental reaction parameters (concentration, temperature, pressure, and reaction time) with an appreciable positive impact on higher product quality, more reliable methods and a smaller footprint in scaling-up operations.¹⁴¹ Substrates and reagents are efficiently mixed to ensure fast and homogeneous heat/mass transfers (especially in gas-liquid reactions) thus resulting in an increased reaction rate and productivity. Moreover, pressurization regimes allow to operate at superheated conditions amplifying the reactivity window. Hazardous and gaseous reactants can be used by dosing their streams in each unit of the flow synthesizers.¹⁴² Remarkably, flow systems can be integrated with downstream units enabling the in-line work-up, purification, and analysis of the products. The addition of several devices in parallel reduces the risks of manual chemical manipulation and/or isolation stage of dangerous intermediates which are rapidly quenched or consumed immediately during telescoped or multistep synthesis in fully automated and/or self-optimizing processes.

In the case of photochemical reactions, the miniaturized components and the narrow channels of flow reactors ensure a homogenous irradiation and an intense light penetration. Consequently, photoreactions can be significantly accelerated (from days/hours to minutes/seconds) while requiring less amount of the photosensitizer.^{128e} The accurate control over the irradiation time minimizes the formation of thermal side-products increasing the product quality and yield.¹⁴³ Finally, the optimal mass transfer, the high reactive surface and the homogenous and fast thermal exchange can result in a greater reaction reproducibility and scalability.

The optimization of the key [2+2]-cycloaddition step towards the target 1,2-dioxetane **3** was performed in collaboration with the research group of Prof. Jean-Christophe Monbaliu (CiTOS, Belgium, Liege) where I spent my period abroad.

The miniaturized devices and the compact flow reactor elements employed in this Project can indeed improve the light-matter interaction phenomena ensuring an excellent mass/heat transfer and preventing the thermal decomposition of the final product. In fact, the reactor size is very important to explain the mixing phenomena in continuous flow photochemistry according to the Bouguer-Lambert-Beer law. The following equation correlates the light absorption (A) with the compound molar extinction coefficient (ϵ), the relative concentration (c), and the path length of light propagation (l):

$$A = \epsilon cl$$

Small radius reactors ensure a short length scale and an optimal energy distribution with a dramatic increase of the reaction rate, lower catalyst loading, and less by-products formation.^{128d} In addition, continuous flow reactors grant straightforward scalability and the possibility to safely use potentially explosive gaseous reactants, such as high energetic and short-lived oxygen species. The aforementioned challenges and the total lack of previous flow synthetic approaches reported in literature make the synthesis of 1,2-dioxetanes an appealing reaction to be translated under continuous flow conditions.

To this aim, a home-made coil flow reactor connected to LED technology was designed and realized. Firstly, the reaction system was investigated carrying out various sets of experiments to determine the preliminary flow operating conditions. The photooxygenation step was subsequently optimized by using an advanced LED-driven flow reactor module (Corning® Advanced-Flow™ Lab Photo Reactor, Corning Proprietary)¹⁴⁴ achieving a preliminary experimental protocol for the synthesis of 1,2-dioxetanes.

Compound **36** was selected as the model olefin (**Figure 17**). Reactions were performed at low concentration (0.025 M) in order to obtain selectivity and avoid the undesirable excitation of the starting material that could act as a reaction

2.3 Optimization of photooxygenation step by continuous flow technology

quenching molecule. Moreover, the selection of a proper solvent was crucial to guarantee a certain solubility of reaction components, reactive oxygen species lifetime, and process scaling-up.¹⁴⁵ In particular, the solvent shall allow the complete dissolution of all the chemicals and products to prevent the reactor clogging and an undesired light scattering. Notably, chlorinated and, in particular, deuterated solvents afford a longer $^1\text{O}_2$ lifetime than the polar protic ones. Furthermore, the common organic dyes used as sensitizers are highly soluble in halogenated solvents. For these reasons, dichloromethane (CH_2Cl_2) was selected as the reaction solvent, and it was preferred to deuterated chloroform (CDCl_3) because of its acidity which would encourage a faster degradation of the final product (**3**) into the corresponding ketones (**2** and **26**).

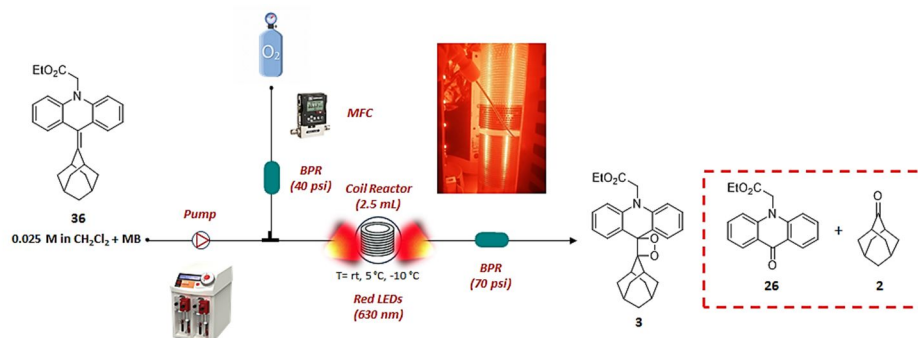


Figure 17. General flow set-up for the synthesis of parent 1,2-dioxetane TCL probe **3**.

The feed solution of olefin **36** (0.025 M) and a variable amount of MB were dissolved in CH_2Cl_2 and were conveyed to a Syrris pump equipped with Asia red syringes at different flow rates (**Figure 17**). The solution was mixed *via* a T-shape mixer with a stream of O_2 controlled by a Bronkhorst® F210CTM mass flow controller (MFC) and pumped into a reactor coil ($V=2.5$ mL) irradiated with 630 nm LEDs at different temperatures. Back pressure regulators (BPRs) were inserted at the outlets of MFC (40 psi) and reactor (70 psi), respectively (**Figure**

17). Then, the crude was filtered through a small pad of silica gel (5 mm layer) or charcoal, alternatively, by using CH_2Cl_2 as eluent and the solution was evaporated at 25 °C under vacuum. Using this flow set-up a number of experiments were carried out as reported in **Table 6**.

Table 6. Preliminary screening of flow reaction conditions for the synthesis of TCL dioxetane probe (**3**).

Entry	MB (mol %)	Solvent flow rate (mL min ⁻¹)	O ₂ flow rate (mL min ⁻¹)	T (° C)	Conversion (%) ^a	Yield (%) ^a	Products from degradation (%) ^a
1*	6	-	-	-5	100	34	66
2	6	0.2	2	25	100	44	56
3	6	0.2	2	-5	100	66	34
4	6	1.25	12.5	-5	100	94	6
5	1	1.25	12.5	25	82	68	14
6	1	1.25	12.5	-5	94	91	3
7	6	1.25	12.5	-10	78	75	3

All reactions were performed on 20 mg scale. *Entry 1**: Batch conditions after 1 h.

^aDetermined by ¹H-NMR of the crude reaction mixtures.

Entry 1 was carried out under batch conditions showing variable and poorly reproducible results in terms of yield and reaction rate using the photo apparatus described in detail in Paragraph 2.2.2 (**Figure 18**).

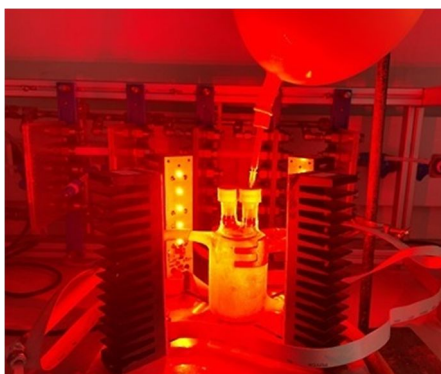


Figure 18. Photooxygenation reaction of olefin **36** under batch conditions. *Reagents and conditions:* MB, -5 °C, CH₂Cl₂, 630 nm LEDs, O₂ (1 atm, balloon), 1 h.

As expected, both temperature and reaction time strongly influenced the formation of decomposition products (**2** and **26**). In particular, reactions carried out at -5 °C gave a lower decomposition rate in comparison to 25 °C (*entry 2 vs 3, Table 6*). Moreover, longer residence times was found to promote the thermal decomposition of final product (*entry 3 vs 4, Table 6*). However, lower temperatures (i.e., -10 °C) afforded low conversion yields (*entry 7, Table 6*). A poor conversion was also observed with a reduction of the amount of photosensitizer (*entry 5 and 6, Table 6*). The best results were obtained at -5 °C using 6% mol of photosensitizer to achieve a complete consumption of the starting material in only 50 seconds, excellent yield (94%) with traces of the degradation product (6%), and a productivity of 1.4 g h⁻¹ (*entry 4, Table 6*).

The conversion and product yield, as well as the formation of degradation products, were determined by ¹H-NMR analysis of crude reaction mixtures (**Figure 19**). NMR spectra revealed substantial differences in the chemical shifts of indicative signals due to the anisotropic shielding effect of protons in α -positions of adamantane fragment. In particular, the broad singlet (brs, 2H) of 1,2-dioxetane **3** is upfield shifted at 2.28 ppm in comparison to the corresponding olefin **36** (3.44 ppm) and 2-adamantanone **2** (2.55 ppm) (**Figure 19**).

Alternatively, aromatic region can be useful to compare different compound signals related to acridine ring protons.

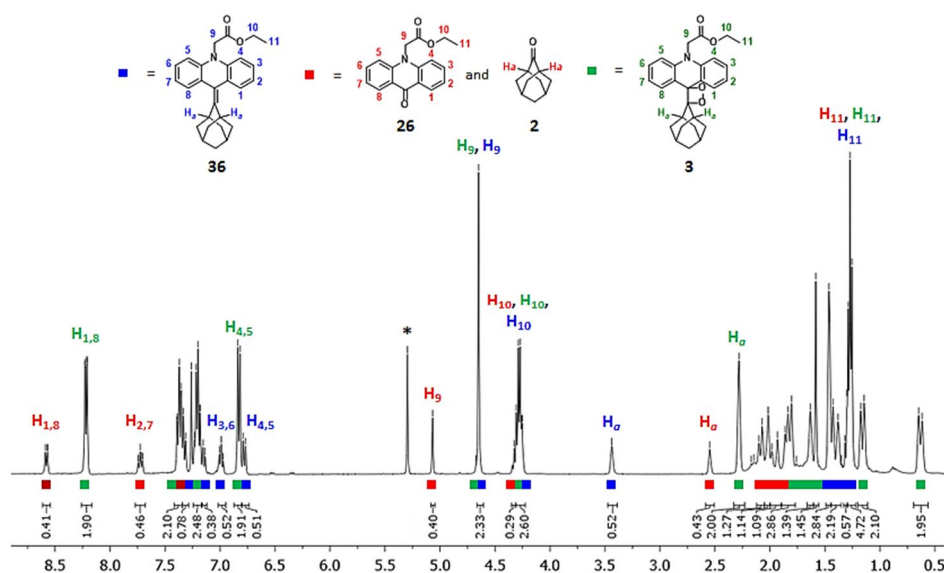


Figure 19. Assignment of NMR signals corresponding to unreacted SM (36) (blue), thermal degradation by-products (2 and 26) (red), and 1,2-dioxetane (3) (green) in a complex crude (entry 5, Table 6). * CH₂Cl₂ (reaction solvent).

The concept of reaction time in a flow process is expressed by the residence time, i.e., the time reagents spend in the reactor zone, and it is calculated from the volume (V) of the reactor and the total flow rate:

$$\text{Residence time} = \frac{V \text{ (mL)}}{\text{flow rate (mL min}^{-1}\text{)}}$$

The residence time of gas-liquid flow reactions is deeply affected by both the solvent flow rate and the O₂ stream used. The most common segmented flow consists of an alternation of liquid “slug” and gas bubbles.¹⁴⁶ The succession of gas-liquid segments ensures an improvement of mixing and interfacial mass

2.3 Optimization of photooxygenation step by continuous flow technology

transfer phenomena with higher safety compared to gaseous batch photoreactions. Tailored flow patterns are generated through a MFC meter which adjusts variable doses of gas into the liquid stream. The size and the frequency of these slugs can be modulated by varying the flow rate of the liquid and/or the gas stream in order to expose a larger surface area to the gas at any time.^{147,148} The O₂ flow rate has been initially set to ensure slugs flow with small and comparable size segments between O₂ and solvent (**Figure 20**).

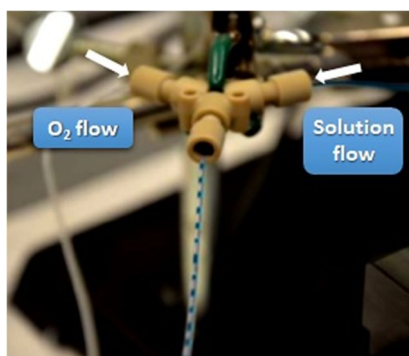


Figure 20. Taylor flow in gas-liquid reaction under continuous flow conditions. Solution segments containing SM (**36**) and MB dissolved in CH₂Cl₂ (*blue*) and O₂ segments (*transparent*).

Accordingly, employing the equation reported below, the moles of O₂ used in the photooxygenation reaction using 12.5 mL min⁻¹ as flow rate of O₂ at 25 °C were calculated.¹⁴⁹

$$n_{O_2} = \frac{P_N(\text{atm}) V_N(\text{L})}{R(\text{L}\cdot\text{atm}\cdot\text{mol}^{-1}\cdot\text{K}^{-1}) T_N(\text{K})} = \frac{1 \cdot 0.0125}{0.082 \cdot 273.15} = 0.56 \text{ mmol}$$

Consequently, the O₂ used in the first screening reactions conditions was approximatively 7:1 mol ratio in comparison with **36** (0.56/0.0786 mmol). The excess of O₂ was next decreased (1:1, O₂:SM mol ratio, *entry 5-7, Table 7*) in order to develop a greener and cheaper flow process.

The photooxygenation reaction was further optimized using Corning® Advanced-Flow™ Lab Photo Reactor (Corning Proprietary) equipped with a lab scale mesofluidic reaction glass module (V= 2.6 mL) and irradiated by internal red LEDs (Figure 21) (see Paragraph 3.1 for the detailed instrumental description).

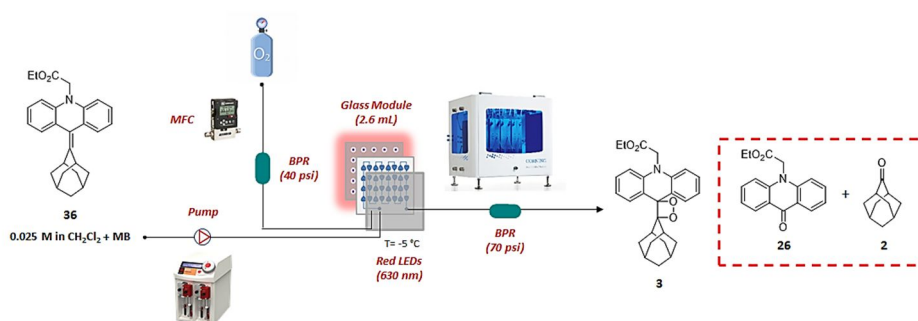


Figure 21. Corning reactor flow set-up for the photooxygenation step of **3**.

Table 7. Optimized flow reaction conditions for the synthesis of TCL model probe (**3**).

Entry	MB (mol %)	Solvent flow rate (mL min ⁻¹)	O ₂ flow rate (mL min ⁻¹)	O ₂ :SM mol ratio ^a	Lamp intensity (%)	Conv. (%) ^b	Yield (%) ^b	Products from degradation (%) ^b
1*	6	1.25	12.5	11:1	-	100	94	6
2	6	1.25	12.5	11:1	100	100	80	20
3	6	1.25	12.5	11:1	50	100	88	12
4	6	1.25	12.5	11:1	10	100	93	7
5	6	1.25	1.25	1:1	10	100	92	8
6	3	1.25	1.25	1:1	10	100	97	3
7	3	1.25	1.25	1:1	10	65	60	5

All reactions were performed on 20 mg scale except for *Entry 7* (64 mg scale, 0.1 M). *Entry 1**. The reaction was carried out using the home-made photo apparatus (Table 6).

^a Determined according to the equation $nO_2 = Pn \cdot \text{flow rate MFC} / R \cdot T_n$.¹⁴⁹

^b Determined by ¹H-NMR analysis of the crude reaction mixtures.

2.4 Characterization

An excess formation of degradation products (**2** and **26**) was obtained repeating the reaction under the same reaction conditions but using the Corning reactor rather than the home-made photo apparatus (*entry 1 vs 2*, **Table 7**). The decomposition has been supposed to be due to the different lamp intensity applied. Consequently, the intensity of the lamp was gradually decreased to guarantee a complete conversion (*entry 3 and 4*, **Table 7**). The photoreaction was further optimized by reducing both the O₂ flow rate (*entry 5*) and the amount of photosensitizer (*entry 6*) (**Table 7**). The reaction was then repeated according to the best conditions using a 0.1 M solution of the starting material (*entry 7*, conv. 65%, **Table 7**). In this case, the conversion was not complete implying that the reaction probably required longer reaction time. *Entry 6* showed the best flow reaction conditions with excellent yield (97%) and good productivity (600 mg h⁻¹) in short reaction time (2 minutes) (**Table 7**). The promising results obtained in terms of yields, reaction rate, and especially reproducibility, prompt us to extend the use of this technology for the synthesis of the other functionalized 1,2-dioxetanes, in particular of the unstable derivatives.

2.4 Characterization

2.4.1 TCL measurements of the final products

The activation parameters according to the Arrhenius equation of the final products **27a**, **27d-e**, and **27g** were initially determined in the solid dioxetane samples after solvent evaporation (**Table 8**).¹¹⁰ The analytical measurements and the photophysical characterizations were conducted with the support of Prof. Massimo Guardigli and Dr. Donato Calabria from the University of Bologna. CH₃CN was selected as solvent of choice since it guaranteed a good solubility of the test samples, with a few exceptions in which the addition of some drops of

DMSO was required (*see* Paragraph 2.5.1). Moreover, CH₃CN has an adequate boiling point (82 °C) which is compatible with the operating temperature range employed in the TCL measurements on solid state.

The TCL apparatus was composed of a dark box equipped with a thermally cooled charge-coupled device (CCD) back side illuminated camera light as detector and a mini heater to trigger the TCL emission at different temperatures controlled by a potentiostat (**Figure 22**). The heating plate was connected to a temperature controller able to reach the required temperature with an exact heating rate (150° min⁻¹). This aspect is not trivial since the decomposition temperature of the TCL compounds is a critical chemical-physical parameter that plays an important role in the kinetics. The detector was combined with a computer showing live the TCL emission. Digital images were analyzed employing ImageJ software and the intensity of the TCL signal was measured in the area corresponding to the test spot.²⁶

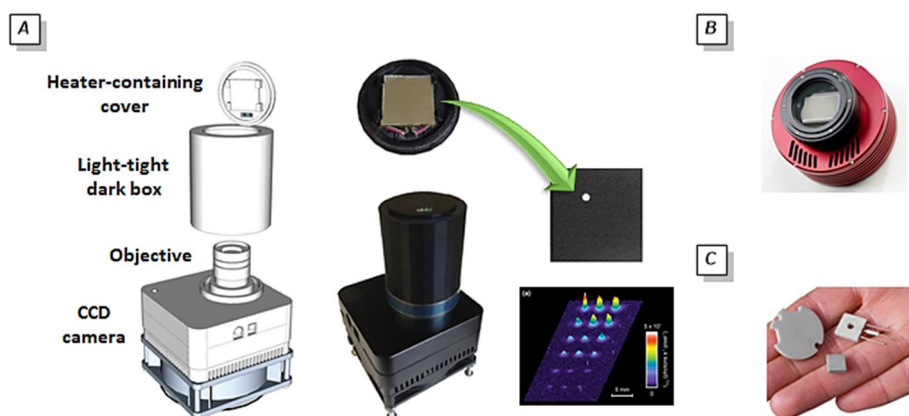


Figure 22. A) Analytical apparatus for TCL imaging. B) Detector: CCD camera back side illuminated thermally cooled portable device (double Peltier). C) Mini heater: thermocouple “K type” Watlow series Ultramic fabricated in aluminum nitride (AlN) (dimensions: 25 × 25 × 2.5 mm, working temperature: up to 400 °C).

2.4 Characterization

The decay kinetics of the light emitted by TCL molecules upon heating was studied in a range of temperatures between 100-140 °C by depositing a drop (5-10 μL) of 1,2-dioxetane solution in CH_3CN (corresponding to 5×10^{-9} mol). Upon the complete solvent evaporation, the light signal kinetics was measured after heating at the predetermined temperature. Consecutive acquisitions were performed on the same sample using the same exposure time until the signal completely disappeared to reconstruct the decay kinetics of the TCL signal. The TCL kinetic parameters ($\ln A$ and E_a) of the new set of 1,2-dioxetanes (**27a**, **27d-e**, and **27g**) along with the $t_{1/2}$ values calculated for the solid compounds at 25 °C were compared with not-decorated 1,2-dioxetane **3** values (**Table 8**). Finally, the limits of detection (LOD) were calculated at 100 °C measuring the area under the curve (AUC) up to 400 sec where all the kinetic curves of investigated 1,2-dioxetanes reached a plateau (**Table 8**).

Table 8. Activation parameters for the thermal decomposition of 1,2-dioxetanes **3**, **27a**, **27d-e** and **27g**.

Cmpd	R ₁	R ₂	$\ln A^a$	E_a^b (kcal mol ⁻¹)	$t_{1/2}^c$ (months)	LOD ^d (mol spot ⁻¹)
3	H	H	37 ± 1	32 ± 1	7	$(3.5 \pm 0.5) \times 10^{-13}$
27a	CH ₃	OCH ₃	24 ± 1	23.2 ± 0.7	1	$(1.6 \pm 0.1) \times 10^{-14}$
27d	F	CH ₃	18 ± 4	17 ± 2	0.01	$(4.5 \pm 0.1) \times 10^{-11}$
27e	CF ₃	OCH ₃	33 ± 4	29 ± 3	2	$(3.5 \pm 0.2) \times 10^{-14}$
27g	CF ₃	CH ₃	46 ± 8	43 ± 7	> 100 (years)	$(2.7 \pm 0.2) \times 10^{-13}$

All the measurements were determined according to the Arrhenius equation (see Paragraph 3.3 for details). ^a Pre-exponential factor. The logarithmic form is expressed in s⁻¹. ^b Activation energy. ^c Calculated for the solid compound at 25 °C. ^d Limit of detection (calculated as mean + 3 SD of three independent measurements).

A typical kinetics of the light signal at different temperatures ranging from 100 to 140 °C for compound **27e** is reported in **Figure 23A**. Lower temperatures were not reported, as very low TCL signals were obtained. The signal profile varies

with temperature, although the AUC of the signal vs time is quite constant and related to the concentration of the TCL compound. The calibration curve carried out at a trigger temperature of 100 °C is reported in **Figure 23B**, where the signal is well correlated to the probe concentration in a range of linearity from 3.5×10^{-14} to 6.0×10^{-13} with a LOD of 3.5×10^{-14} moles analyzed. The normalized TCL decay (**Figure 23C**) and the TCL Arrhenius plot (**Figure 23D**) allowed to calculate the kinetic parameters previously reported.

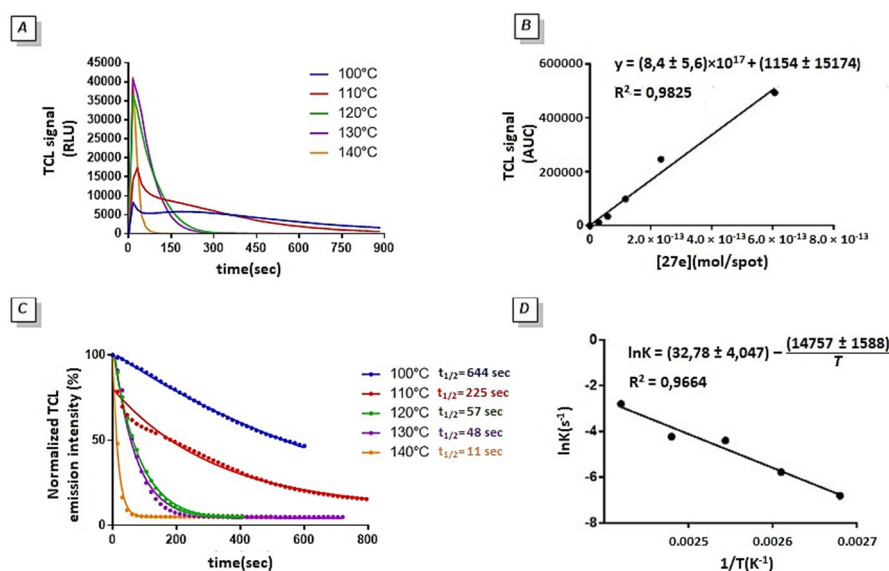


Figure 23. A) TCL kinetic profiles of **27e** at different temperatures (range 100-140 °C). B) Calibration curve of TCL probe constructed plotting the AUC of TCL kinetic profiles recorded at 100 °C for increasing concentration of **27e** (range 3.5×10^{-14} - 6×10^{-13} mol spot⁻¹). C) TCL decay profiles and half lifetimes ($t_{1/2}$) of **27e** at different temperatures. Each curve is normalized to its maximum value. D) Arrhenius plot of **27e**.

As previously observed,^{25a-b} the variations of the activation energy (E_a) in the presence of different substituents are paralleled by an analogous modification in the pre-exponential factor ($\ln A$). This can be explained considering that $\ln A$

represents the frequency of collisions between the reactant molecules used in this case to describe a unimolecular reaction. As the TCL reaction was triggered upon the complete evaporation of the solvent, the molecules packing in the dried solid state might have an influence on the TCL emission Arrhenius parameters. The packing density, the orientation of the molecules and their steric hindrance aggregated in the solid state are strongly influenced by the electronic structure and by the weak electron interactions, such as π - π , between different substituents of the aromatic moieties.^{150,151} Consequently, an amount of heat supplied to trigger the TCL reaction is partly necessary to destabilize these characteristic interactions of the solid state favouring the molecules thermal decomposition.¹⁵² These considerations must be taken into account to explain and to understand the trends observed for the values of $\ln A$ in the 1,2-dioxetane probes investigated (**27a**, **27d-e** and **27g**).

The acridine moiety substituents pattern influences both the 1,2-dioxetane Arrhenius parameters and the acridone Φ_F . Compound **27a** does not correspond to the stringent definition of a *push-pull* system containing two EDGs, one by resonance and one by induction. As expected, this compound exhibited a remarkable increase in the Φ_F , but with kinetic parameters leading to lower stability. In fact, a trigger temperature close to 100 °C is related to poor handling and less stable TCL probes at room temperature, not suitable for analytical purposes. This finding accords with the results achieved in the previous work showing the same behaviour in the presence of EDGs.^{25b} As concerns compounds **27d-e** and **27g**, which display a *push-pull* substituents pattern, the mesomeric or inductive nature of EDG and EWG provided TCL compounds with different photophysical properties. In particular, compound **27d**, in which the methyl group exerts the action of EDG by inductive effect and the fluorine atom owing a double nature, and compound **27e**, possessing an inductive-based EWG ($-\text{CF}_3$) and a resonance-based EDG ($-\text{OCH}_3$), provided a similar behaviour, decreasing the Arrhenius parameters with respect to unsubstituted compound **3**. As

previously reported, EDG by mesomeric effect, such as $-\text{OCH}_3$, promote O-O bond cleavage by resonance interaction through the π -electrons of the aromatic moiety in 1,2-dioxetanes.¹⁵³ In addition, such substitution pattern significantly improved the Φ_F of the corresponding acridones **28** compared to **26**. On the contrary, compound **27g**, containing an EDG and an EWG both by induction, displays a different and very intriguing behaviour reversing the trend observed up to now. Indeed, along with a relative increase of the acridone Φ_F with respect to the unsubstituted compound **26** (0.23 and 0.11, respectively), a surprisingly high stability at room temperature (> 100 years) has been recorded. In particular, the comparison of compounds **27e** and **27g** shows a dramatic difference obtained by simply substituting a resonance-based perturbation with an inductive effect. Observing the results, it can be evidenced that, even when a *push-pull* approach is adopted, the mesomeric electronic enrichment of the acridine moiety generally causes a reduction of the E_a of the TCL reaction. Conversely, a fully inductive *push-pull* substitution pattern appears to provide positive features to the TCL molecules, greatly increasing the stability at room temperature without reducing the efficiency of the TCL emission and LODs.

Approximate values for the TCL efficiency (Φ_{TCL}) of synthesized *push-pull* compounds (**27d-e** and **27g**) were estimated by comparing the signal output obtained with Φ_{CL} values reported in the literature for the luminol- H_2O_2 reaction catalyzed by horseradish peroxidase (HRP) (*see* Paragraph 3.3 for protocol and data).¹⁵⁴ Thus, all the tested compounds displayed significantly higher efficiency with respect to that reported for adamantylidene adamantane-1,2-dioxetane (**1**).^{19b} In addition, compound **27g** provided the highest efficiency, although lower than that measured for luminol, thus confirming its positive features. These results clearly suggested that *push-pull* 1,2-dioxetane systems offer an optimal solution to improve the TCL emission properties, providing better stability at room temperature with respect to the not-decorated compound **3** and still higher TCL emission efficiency. In particular, the new dioxetane **27g** proves to be the most

2.4 Characterization

promising TCL candidate of the series representing the right compromise between relatively intense TCL signal and remarkable higher stability at 25 °C.

The effect of different substituents on TCL efficiency was further investigated by comparing the photophysical behaviour of the unsubstituted compound **3** and the *push-pull* 1,2-dioxetane **27g** in distinct environments (solid state, optical glue and nanocarriers). The surrounding environment had a considerable impact on the mechanism and TCL performance. TCL experiments were carried out in collaboration with the research group of Prof. Luca Prodi from the University of Bologna, by using the TCL apparatus previously described (**Figure 22**). In addition, the TCL decays were detected either using a CCD camera (**Figure 24A**) and an electron multiplying charge coupled device (EMCCD) (**Figure 24B**), alternatively, to compare the TCL signals, in particular the effect of the noise on the tail of the TCL emission profile and the consequent kinetic and thermodynamic parameters. Detectors were connected to a computer showing the real-time TCL emissions. Moreover, the superior performance of EMCCD allowed to detect and quantify single photon events through a unique electron multiplying structure into the chip offering a high resolution for low signals.¹⁵⁵

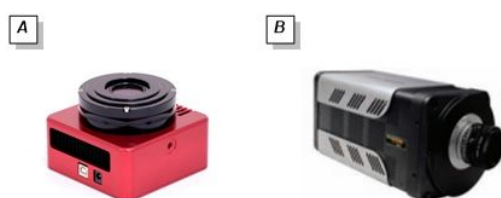


Figure 24. A) CCD camera. Optical parameters: diaphragm aperture at the maximum value; exposure time 20 s at 80 °C and 10 s at 90-120 °C; delay: 0 s. B) EMCCD camera. Optical parameters: diaphragm aperture at the maximum value; exposure time: 1 s; gain: 4000; accumulation: 2.

Firstly, solutions of two dioxetanes **3** and **27g** (0.5 mM in 0.5 μ L of CH₃CN) were spread on a square glass slide (BELLCO 9 \times 9 mm cover slip) and dried for

spontaneous solvent evaporation. The TCL emissions were measured at 80 °C using different concentrations through multilayer samples depositions (repeated drop solution-dry steps) to ensure a homogeneous distribution of the molecules in a small portion of the same plate. As previously mentioned, the random deposition of compounds **3** and **27g** on glass slide, as the result of aggregates formation in the same spot, generated various TCL decay trends according to different TCL mechanisms (**Figure 25**).¹⁵²

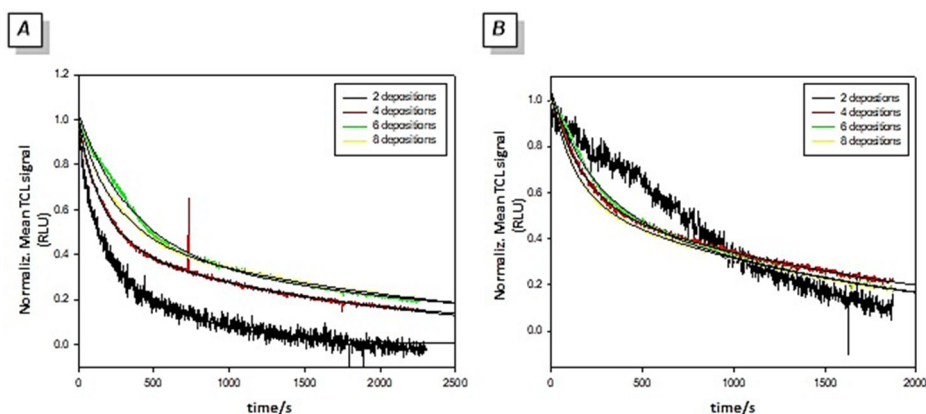


Figure 25. Normalized TCL emission decays at 80°C of **3** (A) and **27g** (B) via EMCCD detection in solid state. Black coded lines represent the fitting of the decay curves with a multiexponential equation. Each curve is normalized to its maximum value.

The non-homogenous deposition of the samples highly made difficult the extrapolation of the results. Therefore, it was not possible to determine accurate evaluations for 1,2-dioxetanes **3** and **27g** in terms of TCL intensity, since it strongly depended on the deposition manner of the two compounds on the glass slide. In particular, double or even triple exponentials were required to obtain the right fitting of the curves suggesting that the decay profiles did not respect a classical first order kinetic in solid state but rather they were a sum of first order kinetics, thus a lifetimes distribution.

2.4 Characterization

Based on these considerations, a different approach involving the dispersion of compound **3** and **27g** into an optical glue was applied to overcome the poor reproducibility issues caused by the formation of aggregates observed in solid state and responsible to different kinetics. Solutions (12.5 mM, 20 μ L) of two samples **3** and **27g** in CH₃CN dispersed in a liquid photopolymer (Norland Optical Adhesive 61, NOA 61) were exposed under UV irradiation for 10 minutes to trigger the polymerization (**Figure 26**).

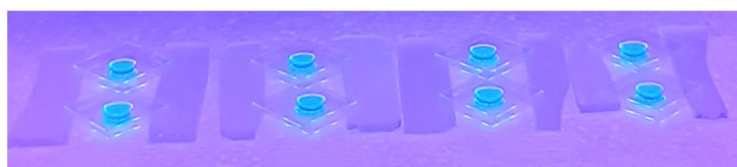


Figure 26. Samples **3** and **27g** dispersed in optical glue NOA 61 under UV light.

After that, the samples were placed on the heating plate in the dark box and heated at a set of temperatures ranging from 80 to 120 °C, while acquiring the signals with both detectors in duplicate (**Table 9**).

Table 9. Emission lifetimes for compound **3** and **27g** with a CCD and an EMCCD detectors in optical glue at different temperatures.

	$t_{1/2}$ (s) ^a 3		$t_{1/2}$ (s) ^a 27g	
	CCD	EMCCD	CCD	EMCC
80 °C	2000	1796	1137	1479
90 °C	1026	1063	1729	801
100 °C	616	760	615	541
110 °C	376	429	327	349
120 °C	189	220	202	195

All the measurements were determined by fitting the decay profile of the TCL emission with a first order equation in duplicate. ^a Calculated in optical glue at different temperatures (80-120 °C).

The normalized TCL decay and the TCL Arrhenius plot allowed to calculate the kinetic parameters. More in detail, for each temperature, the kinetic constants (k) of the TCL process were calculated by fitting the decay profile of the TCL emission with the first order decay equation and then the E_a and the $\ln A$ of the TCL process were determined by using the logarithmic form of the Arrhenius equation:

$$\ln K = \ln A - \frac{E_a}{RT}$$

The activation parameters of 1,2-dioxetane **3** and **27g** were extrapolated and reported in **Table 10**.

Table 10. Activation parameters of compound **3** and **27g** using CCD and EMCCD cameras in optical glue.

	3		27g	
	CCD	EMCCD	CCD	EMCC
$\ln A^a$	21.88 ± 4.87	19.61 ± 10.20	28.23 ± 10.22	39.34 ± 10.08
E_a^b (kcal mol⁻¹)	16.73 ± 3.67	13.88 ± 0.68	14.81 ± 7.49	22.12 ± 8.00

All the measurements were determined according to the Arrhenius equation in duplicate. ^a Pre-exponential factor. The logarithmic form is expressed in s⁻¹. ^b Activation energy (calculated as mean SD of two independent measurements using both detectors).

The statistically significant differences observed by recording the activation parameters using different cameras, especially for **27g** compound, can be explained by considering the substantial changes on the TCL curve profile in response to the high noise over long times, although the problem can be considerably reduced with appropriate fittings. By comparing the TCL emission profiles of dioxetane **3** and **27g** it emerged that the *push-pull* compound intensifies the TCL emission in terms of a higher mean TCL signal, as shown in

Figure 27, and increases the detectability, respectively. This finding could be probably related to an increased efficiency of the excited state formation.

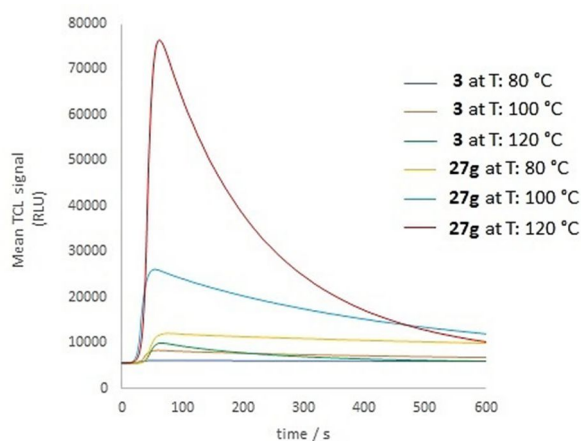


Figure 27. Comparison of TCL signals between **3** and **27g** at different temperatures in optical glue performed with the EMCCD for a single experiment.

The TCL emission profiles of 1,2-dioxetanes **3** and **27g** showed a first order kinetic trend in optical glues using both detectors. No substantial differences emerged by comparing 1,2-dioxetanes of interest (**3** and **27g**) dispersed in optical glue in terms of TCL emission duration and activation parameters. In particular, the presence of substituents in C2- and C7-positions indeed seems to not alter the thermodynamic and kinetic parameters, but rather it has a tangible effect on the TCL intensity according to the enhanced efficiency of excited state formation. Consequently, the thermal stability of the 1,2-dioxetane is basically independent from the *push-pull* substitution.

TCL experiments performed in optical glue with both CCD and EMCCD cameras have been taken as references to determine the TCL efficiencies (Φ_{TCL}), since they provided the most reproducible results. The efficiency of the TCL process is related to the probability of populating the excited state (singlet) through the cleavage of the dioxetane unit, and the consequent emission in a

radiative way, thus delivering photons. The $B^*\tau$ value as the product of B value of the fitting equation and the half lifetime of the TCL decay at different temperatures was considered to better exploit the relationship between TCL efficiency and temperature. Consequently, the $B^*\tau$ values for the 1,2-dioxetanes **3** and **27g** have been obtained from the exponential decays of the TCL emission, then normalized and plotted as a function of the temperature (**Figure 28**).

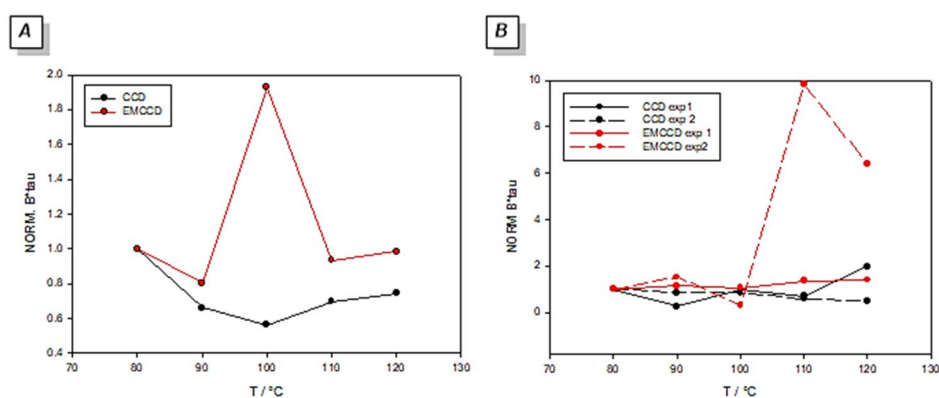


Figure 28. TCL efficiency trends of 1,2-dioxetanes **3** (A) and **27g** (B) in optical glue by using CCD and EMCCD detectors.

The $B^*\tau$ for the CCD experiment of **3** was almost constant with temperature, while the corresponding EMCCD experiment provided a different anomalous trend (**Figure 28A**). Moreover, three of the reported experiments for **27g** showed a constant behaviour of $B^*\tau$ as a function of temperature except for the EMCCD exp. 2 (**Figure 28B**), displaying an increase as the temperature raises. However, a precise and accurate trend for the TCL efficiency parameter is difficult to define, since the systematic slight differences in sample preparation and the temperature gradient variation. In addition, these controversial and unexpected behaviours may depend on the several variables that occur in each TCL experiments. Nevertheless, from this promising results it can be noticed that a significant difference in terms of $B^*\tau$ on the temperature variation between the

unsubstituted 1,2-dioxetanes **3** and the *push-pull* system **27g** was not revealed. As a future perspective, a refinement of instrumental heating device and an evaluation of temperature gradient inside the samples shall be implemented to give us precious information about a better evaluation of the TCL efficiency for the next experiments.

Finally, we have investigated the behaviour of the 1,2-dioxetanes **3** and **27g** incorporated into Pluronic silica nanoparticles (PluS NPs). Silica NPs offer opportunities in several fields, including imaging, drug delivery, sensing and catalysis.¹⁵⁶ Different strategies can be adopted to synthesize the desired size and shape NPs. In this project, two structural elements widely reported in literature, tetraethyl-orthosilicate (TEOS) and the co-polymer Pluronic F127, were selected to build the core-shell nanoparticles.¹⁵⁷ The latter is constituted by a central hydrophobic polypropylene oxide (PPO) block and two ending hydrophilic polyethylene glycol (PEG) chains. A precise amount of the selected 1,2-dioxetanes **3** and **27g** (0.1, 0.2 and 0.3% of dye moles) was dissolved in DMF and NaCl were added to a mixture of Pluronic F127 polymer in AcOH, used both as solvent and as acid catalyzer, to allow the micelle formation. The addition of TEOS provided the condensation following by the hydrolysis of ethoxy group in the acidic environment. Finally, trimethylsilyl chloride (TMSCl) was used as “capping agent” ensuring the core growth interruption and preventing the nanoparticles aggregation. The final structure featured hence an inner sphere in which a portion of the hydrophobic PPO chain was entrapped within a silica matrix and an entirely polymeric outer shell. This last part was divided in a first narrow hydrophobic sector near the solid nucleus and a second one that presented the hydrophilic chain of PEG ending with a -OH group available for further functionalization (**Figure 29**).¹⁵⁸



Figure 29. Structure of a core-shell silica nanoparticle (*left*) and structure of Pluronic F127 (*right*).

The photophysical and morphological characterization of Plus NPs were performed (*see* Paragraph 3.3 for details). In particular, absorption and emission spectra, luminescence lifetimes of three suspensions of **3** and **27g**-dopes Plus NPs differing on the initial doping level (0.1, 0.2 and 0.3% moles of dyes *vs* moles of TEOS) were detected. The photophysical properties of **3** and **27g**-doped Plus NPs (0.3% for **3**-doped Plus NPs and 0.2% for **27g**-doped Plus NPs) were compared with those of the corresponding free 1,2-dioxetanes **3** and **27g** in H₂O solution at 25 °C (**Table 11**).

Table 11. Comparison of absorption and fluorescence data between **3**-doped Plus NPs_0.3% and **27g**-doped Plus NPs_0.2% and free **3** and **27g** in H₂O at r.t..

	λ_{abs}^a (nm)	λ_{em}^a (nm)	Φ_F^b	τ^c (ns)	χ^2^d
3-doped Plus NPs_0.3%	386	420	0.96	12.8	1.146
3	402	421	0.93	13.0	1.071
27g-doped Plus NPs_0.2%	397	428	0.17	12.89	1.119
27g	410	429	0.30	15.33	1.034

^a Determined in H₂O solution. ^b Determined using quinine sulfate as standard ($\Phi_F = 0.53$ in H₂SO₄ 0.05 mol L⁻¹). ^c Fluorescence lifetime decay. ^d Coefficient of determination (chi-squared).

2.4 Characterization

The NPs suspensions displayed a slight blue shift in absorption with respect to the free 1,2-dioxetane **3** and **27g** in H₂O solution. The two systems exhibited similar Φ_F , significantly higher in H₂O (0.93 for **3** and 0.30 for **27g**, **Table 11**) than in CH₃CN (0.11 and 0.23, respectively). The molar extinction coefficient (ϵ) of 1,2-dioxetanes **3** and **27g** in H₂O was determined to establish the final doping level of the NPs suspension of interest, according to the equation reported below:

$$EE \% = \frac{\text{mol diox. inside}}{\text{initial mol of TEOS}} \times 100$$

In particular, ϵ were calculated at $\lambda_{\text{abs}} = 402$ nm and 410 nm (**3** and **27g**, **Table 11**) corresponding to 6000 M⁻¹ cm⁻¹ and 2100 M⁻¹ cm⁻¹, respectively. Consequently, the entrapment efficiency of the 0.3% suspension for **3** and 0.2% suspension for **27g**, was 0.002% and 0.005%, respectively. However, low doping levels complicated a sensible estimation of the average number of molecules for NPs at this preliminary stage. The photophysical results above mentioned for the synthesized PluS NPs suspensions suggested that 1,2-dioxetane derivatives **3** and **27g** can be encapsulated with a relatively low efficiency. Yet, despite this low encapsulation efficiency, the NPs environment provides the possibility of investigating the TCL mechanism in a confined space, different from those previously studied.¹⁵⁹ For this reason, preliminary TCL experiments involving 1,2-dioxetane-doped NPs suspensions **3** and **27g** were performed. The doped NPs suspensions (5 μ L, 10 μ M, expressed as TCL compound concentration) were spread on a glass slide and then put in a vacuum dryer to remove water. The rest of experiment was carried out according to the general TCL procedure previously described. The unsubstituted 1,2-dioxetane **3**-doped PluS NPs showed a clear but weak signal (**Figure 30A**). The TCL emission profile displayed a peak which deviated from the background of just 200 absolute units and that rapidly disappeared with first order decay kinetics. However, any TCL emission was detected by performing the same experiment at the same concentration with the

free TCL label **3** in CH₃CN. Controversy, the restricted and protected environment offered by NPs favoured the thermolysis and then the emission.

27g-doped Plus NPs provided a higher emission signal than its parent compound **3** according to results carrying out in optical glue, deviating from the background of 1000 absolute units, in terms of mean TCL signal (**Figure 30B**). However, as well as **3**-doped NPs, even with a *push-pull* system, the TCL signal decreased with first-order decay kinetics. Despite not having sufficient data to fully support this evidence, the environment seems to assist in the high efficiency of the excited state in addition to the *push-pull* effect. The light signals provided by the two suspensions are reported in **Figure 30**.

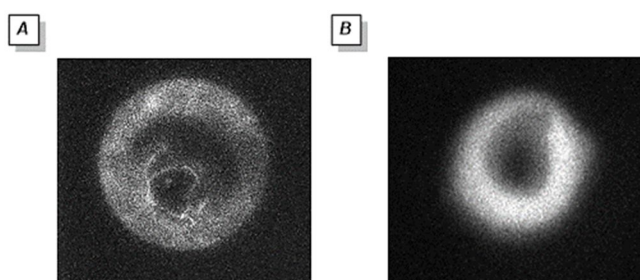


Figure 30. TCL images: maximum TCL emission of **3**-PluS NPs (A) and **27g**-PluS NPs (B) heated at 140°C using EMCCD camera as detector. Optical parameters: diaphragm aperture at the maximum value; exposure time 1 s; accumulation 2; gain 4000.

In summary, we have demonstrated that the investigated compounds (**3** and **27g**) can be easily trapped into the silica matrix remaining still active and efficient for TCL applications. In addition, the lifetimes of TCL compounds should be calculated at different temperatures (4 °C, -20 °C, and -80 °C) to establish an estimate of the potential TCL efficiencies in the different environments evaluated and to develop specific diagnostic tests for various storage conditions.

2.4 Characterization

2.4.2 TCL imaging of the unsubstituted probe model: proof of concept

As a preliminary proof of concept, the representative dioxetane parent compound (**3**) was diluted in saline solution and then incubated at 25 °C for 30 minutes with aneuploid immortal keratinocyte cell line from adult human skin (HaCaT, 1×10^6 cells).¹¹⁰ Cells were then washed in saline solution and deposited on a cellulose disc. The TCL signal was measured by heating the disc using the above-described imaging apparatus. An equal volume of supernatant from the last washing step was deposited on a paper disk and subjected to the same measurement, as the blank. A rather intense light signal can be observed from the cells pellet, while very low signal (almost the thermal noise of the instrument) was observed for the supernatant (**Figure 31A-B**). It was thus confirmed that the relatively high lipophilicity (O/W Log P= 2.5) of this molecule facilitates the entry into the cell membrane allowing to image the cells as evaluated in the microscope imaging of the cells plated on glass. The light signal was acquired with a very sensitive B/W cooled CCD camera and transformed in pseudo color scale (**Figure, 31C-D**).

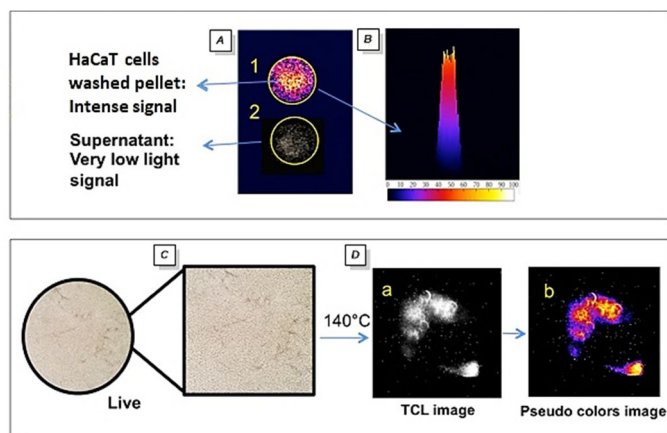


Figure 31. A) TCL pseudo color image of HaCaT cells pellet deposited on a cellulose disc (1 cm diameter) after washing with saline solution and heated at 140 °C in comparison with (1) and the blank (2) of the same volume of the supernatant. B) Surface 3D plot of TCL image acquired from the HaCaT cells pellet. C-D) Microscope image using ultrasensitive B/W CCD camera: TCL imaging of HaCaT cells plated on cover glass (cells frozen at -20 °C with EtOH/CH₃CN, 1/1, v/v). C) Cells live image. D) TCL intracellular microscope (a) and pseudo colors image (b).

These preliminary data encourage the use of such TCL probes coupled with biomolecules for the development of reagentless ultrasensitive biosensors, a bioanalytical method competing with conventional biochemiluminescence probes, which are still sensitive but requiring the addition of the substrate to trigger the CL process.

2.5 Development of new bioconjugated probes based on TCL phenomenon

The recent COVID-19 pandemic has highlighted the relevance of novel ultrasensitive biosensors in compact formats able to provide real-time information at relatively low cost and POC application.¹⁶⁰ The rapid detection of

specific target molecules in complex samples can find application in many areas, including clinical diagnostic, drug discovery, environmental monitoring, and food safety assessment.^{1a} Although bioanalytical applications of TCL probes are limited because of chemical instability and low water solubility, 1,2-dioxetane analogues have been recently repropose as ultrasensitive probes in immuno- and gene assays.^{25a-b,31} Some efforts have been directed towards the development of new bioconjugated probes based on the TCL phenomenon in order to realize robust, universal, and easy-to-handle TCL-based immunoassays. For this reason, synthetic functionalization on the ester appendage were designed to provide novel sites for labelling antibodies or other biomolecules such as bt-SA system.

Three different strategies, including directly conjugated (**Figure 32A**), biotinylated (**Figure 32B**), and sulfonated probes (**Figure 32C**), were investigated to create new TCL molecular labels through the direct derivatization of the structural core of the parent 1,2-dioxetane **3** with bioactive portions.

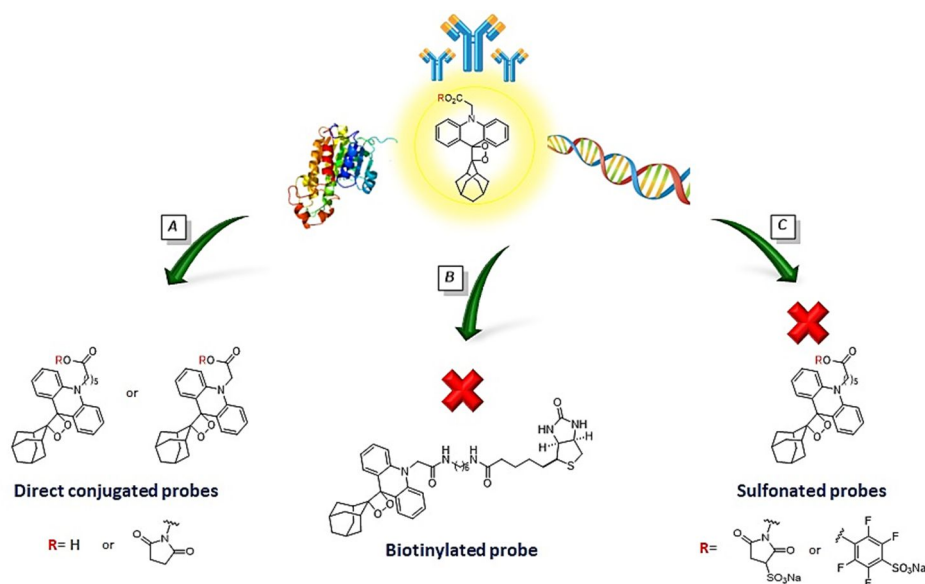


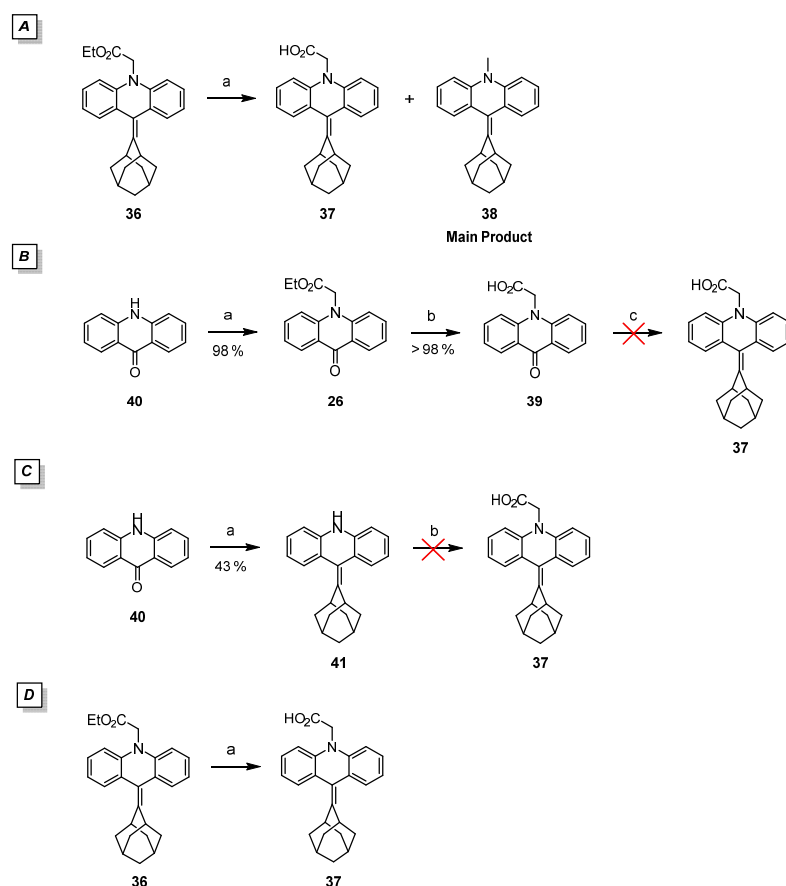
Figure 32. Strategies adopted for the synthesis of bioconjugated TCL probes. A) Direct conjugation, B) biotinylation, and C) synthesis of sulfonated probes.

2.5.1 Directly conjugated probes

Among the functional groups available in proteins and other biomolecules of interest, primary amines (-NH₂) are certainly the most employed groups for bioconjugation purposes.^{161,162} Primary amines are characterized by a positive charge at physiologic pH and a strong nucleophilicity, encouraging the conjugation with reactive groups.¹⁶³ Generally, amine-reactive chemical groups, including free carboxylic acids and *N*-hydroxysuccinimide (NHS) esters, are incorporated in probes to bind primary amines in target biological materials for protein crosslinking and labelling.^{164,165} For these reasons, the ester moiety of 1,2-dioxetane **3** was functionalized to react with amine groups.

Firstly, different approaches were applied to synthesize the acid intermediate **37**. During the classical alkaline hydrolysis procedure (LiOH in refluxing EtOH) of **36**, a partial decarboxylation of the side chain was observed affording the by-product **38** (**Scheme 22, path a**). The second strategy consisted of the McMurry reaction of intermediate **39** obtained by way of the alkaline hydrolysis in quantitative yield of alkylated acridone **26** (**Scheme 22, path b**).^{25a-c,166} McMurry reaction was also carried out starting from the commercial acridone **40** with the subsequential alkylation of **41** using chloroacetic acid (**Scheme 22, path c**).^{25a-c} However, the last procedures failed to afford the desired product. Finally, the acid intermediate **37** was synthesized according to a patent protocol (aqueous solution of NaOH 15%, w/w, EtOH at reflux for 10 minutes) (**Scheme 22, path d**).¹⁶⁷

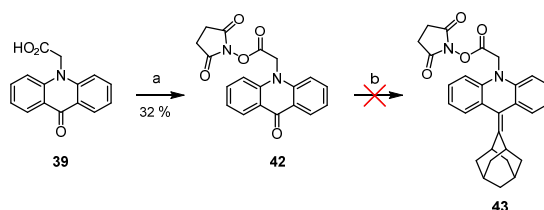
2.5 Development of new bioconjugated probes based on TCL phenomenon



Scheme 22. Synthesis of acid intermediate **37**. *Reagents and conditions: Path a.* a) LiOH, EtOH, reflux, 7 h. *Path b.* a) NaH, BrCH₂COOEt, Bu₄NI, DMF, 0 °C → r.t., 24 h, 98%; b) NaOH, EtOH, reflux, 7 h, 98%; c) **2**, TiCl₄ (1 M in CH₂Cl₂), Zn, anhydrous THF, reflux, 48 h. *Path c.* a) **2**, TiCl₄ (1 M in CH₂Cl₂), Zn, anhydrous THF, reflux, 24 h, 43%; b) NaH, ClCH₂COOH, Bu₄NI, DMF, 0 °C → r.t., 48 h. *Path d.* a) NaOH, EtOH, reflux, 10 min.

To avoid the isolation of unstable intermediate **37**, a direct acylation of acid intermediate **39** was carried out. **39** was reacted with *N*-hydroxysuccinimide (NHC), *N,N'*-dicyclohexylcarbodiimide (DCC) in anhydrous THF at 25 °C for 48 hours affording the product **42** in low yield (32%, **Scheme 23**).^{168,169} However,

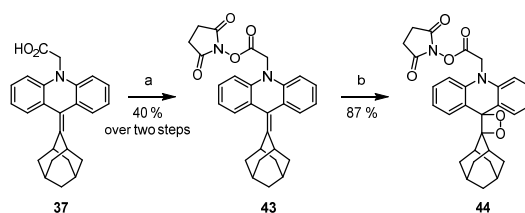
the subsequent reductive coupling did not occur probably because of the complexation of titanium species at the several carbonyl functionalities of the molecule (**Scheme 23**).



Scheme 23. First attempt for the synthesis of NHS ester olefin **43**. *Reagents and conditions:* a) NHS, DCC, anhydrous THF, r.t., 48 h, 32%; b) **2**, TiCl₄ (1 M in CH₂Cl₂), Zn, anhydrous THF, reflux, 48 h.

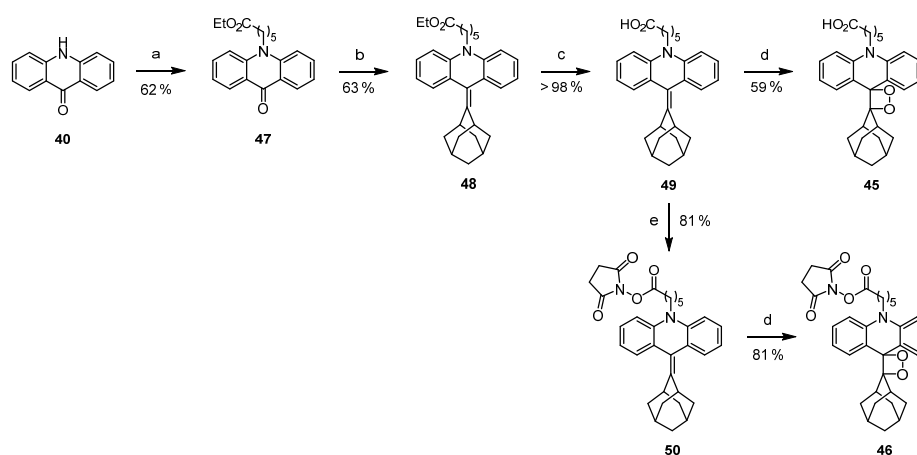
The experimental evidence supports that terminal carboxylic acids or steric hindered amide on the side chain compete with acridone ketone as the result of the formation of coordination complexes, decreasing the reactivity in McMurry reaction at the target carbonyl group. Consequently, the crude acid intermediate **37** was used in the synthesis of corresponding NHS ester probe **44** (**Scheme 24**), while the synthesis of the short chain 1,2-dioxetane derivatives was abandoned.

NHS esters are reactive groups formed by carbodiimide-activation of carboxylate molecules. Succinimidyl esters show high chemical stability forming stable amide bonds with aliphatic amines in physiologic to slightly alkaline conditions (pH from 7.2 to 9).¹⁶³ **37** was functionalized in acylation reaction by using NHC, 1-hydroxybenzotriazole (HOBt) hydrate, *N*-methyl morpholine and 2-(1*H*-benzotriazole-1-yl)-1,1,3,3-tetramethylaminium tetrafluoroborate (TBTU) in anhydrous DMF at 25 °C affording the desired intermediate **43** in moderate yield (40% over two steps, **Scheme 24**). The thus formed intermediate **43** was submitted to the photooxygenation reaction affording the short chain NHS ester probe **44** in high yield (87%, **Scheme 24**).¹⁷⁰



Scheme 24. Synthesis of the short chain NHS ester probe **44**. *Reagents and conditions:* a) NHS, *N*-Me morpholine, HOBT hydrate, TBTU, anhydrous DMF, r.t., 16 h, 40% (over two steps); b) MB, -20 °C, CH₂Cl₂, lamp, O₂ (1 atm, balloon), 16 h, 87%.

The elongation of the *N*-side chain by using the commercially available ethyl 6-bromohexanoate was also evaluated to avoid the formation of the by-product **38**. Moreover, the dependence among the side chain length and the corresponding 1,2-dioxetane stability, as well as the TCL properties, was intensively investigated by inserting a six-carbon atoms arm on the ester acetate. Consequently, the longer chain acid **45** and the corresponding NHS ester **46** 1,2-dioxetanes were synthesized according to the standard procedures.¹⁷¹ In particular, commercial acridone **40** was alkylated by using ethyl 6-bromohexanoate to provide the resulting adduct **47** that it was submitted to McMurry olefination for 48 hours (**48**) and subsequential basic hydrolysis providing the acid alkene derivative (**49**, **Scheme 25**). **49** was used in acylation reaction with NHC and the resultant intermediate **50** was submitted to [2+2]-cycloaddition step affording the final long chain succinimidyl 1,2-dioxetane product **46** in good yield (81%, **Scheme 25**). The long chain acid olefin **49** was also directly submitted to the photooxygenation step obtaining the final long chain acid 1,2-dioxetane **45** with moderate yield (59%, **Scheme 25**).¹⁷⁰



Scheme 25. Synthesis of final products **45** (long chain acid 1,2-dioxetane) and **46** (long chain NHS ester 1,2-dioxetane). *Reagents and conditions:* a) NaH, Br(CH₂)₅COOEt, Bu₄Ni, DMF, 0 °C → r.t., 16 h, 63%; b) **2**, TiCl₄ (1 M in CH₂Cl₂), Zn, anhydrous THF, reflux, 63%; c) LiOH, EtOH, reflux, 16 h, > 98%. d) MB, -20 °C, CH₂Cl₂, lamp, O₂ (1 atm, balloon), 16 h (**45**: 59% and **46**: 81%). e) NHS, *N*-Me morpholine, HOBT hydrate, TBTU, anhydrous DMF, r.t., 16 h, 81%.

The new directly bioconjugated 1,2-dioxetanes (**45** and **46**) were evaluated in terms of TCL efficiency and LODs, while the results for the 1,2-dioxetane **44** are presently ongoing. Both **45** and **46** were investigated at 100 °C and the activation parameters were extrapolated according to the Arrhenius equation. The long chain acid 1,2-dioxetane **45** had a weak signal and a low intensity emission, while the corresponding succinimide derivative **46** showed a stable signal, affording comparable kinetic profile and thermodynamic parameters in tune with the series of new 1,2-dioxetanes synthesized (**27a**, **27d-e**, **27g**) and their parent compound **3** ($E_a = (28 \pm 6) \text{ kcal mol}^{-1}$; $\text{LOD} = (5,7 \pm 0,5) \times 10^{-11} \text{ mol spot}^{-1}$). The problems related to the poor solubility of the new probes in CH₃CN used as the solvent system in TCL assays can be associated with the increase in lipophilicity as a consequence of the *N*-side chain elongation. The introduction of more polar sulfonated esters on the terminal acid chains was further adopted (*see* Paragraph

2.5.3).¹⁶³ So far, the long chain succinimidyl 1,2-dioxetane **46** represents a valid candidate to proceed with the bioconjugation as the stability of endoperoxide unit seems not particularly affected by the side chain length.

2.5.2 Biotinylated probe

The second bioconjugation stage consisted of the direct functionalization of TCL substrate with biotin (bt) to exploit the biotin-streptavidin (bt-SA) interaction in enzyme recognition. The molecular probe characterized by three different portions, i.e., TCL scaffold, biomarker unit, and connecting spacer (Figure 33).

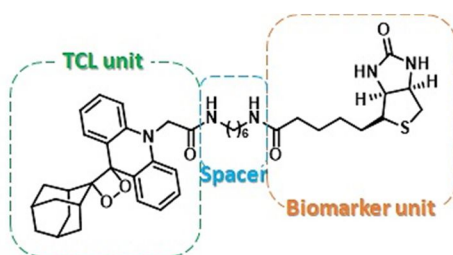
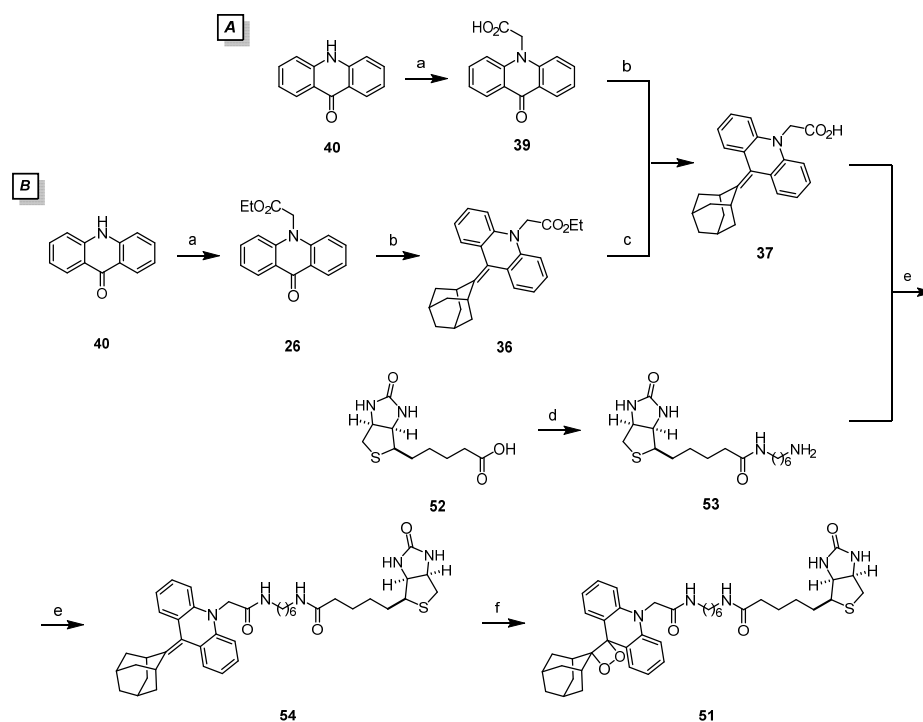


Figure 33. Molecular structure of biotin TCL probe **51**.

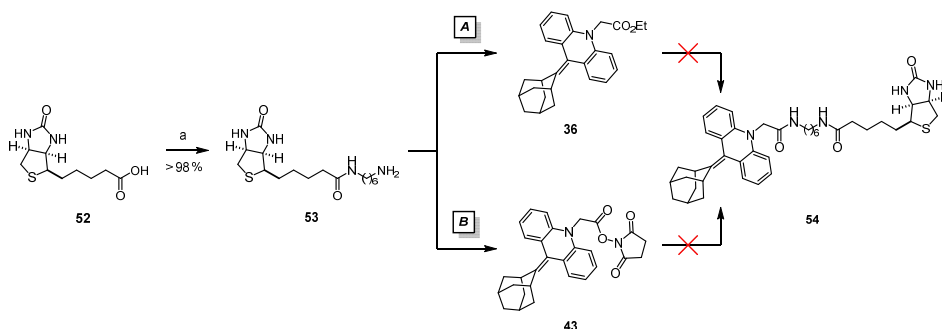
Bt-SA complex is widely described on literature to establish the strongest enzyme-substrate non-covalent interactions, with a dissociation constant (K_d) in the femtomolar range.^{172,173} Furthermore, this interaction is resistant to harsh experimental conditions including variations in pH values and high temperatures. Thus, the streptavidinated enzymes commercially available and low-cost biotinylation reagents, make the bt-SA technology particularly suitable for the development of universal reagents for immunoassays development. Finally, the spacer unit, a six-carbon atoms space unit was selected to preserve the bt-SA interaction.¹⁷⁴

Firstly, a convergent strategy was attempted to generate synthons to be combined at the later stage achieving the target molecule **51** (Scheme 26).¹⁷⁵ The synthesis started from the respective acid derivative **37** following a direct alkylation of acridone **40** (Scheme 26, path a) or through hydrolysis of McMurry adduct **36** (Scheme 26, path b), alternatively. Two sequential coupling reactions between a) D-bt (**52**) and 1,6-hexanediamine, and b) the terminal amine intermediate **53** with acid McMurry adduct **37** led to the formation of the biotinylated olefin **54** followed by the final photooxygenation step to obtain the biotinylated TCL probe **51** (Scheme 26).



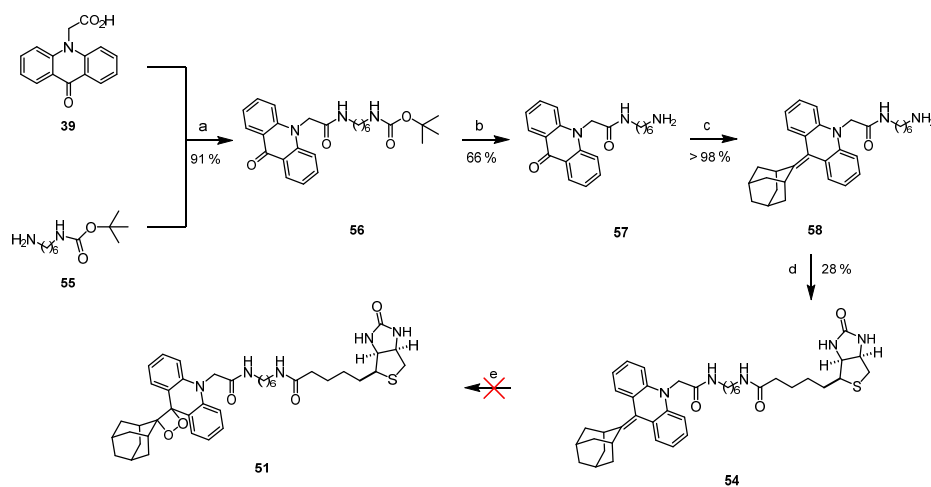
Scheme 26. Convergent synthetic strategy for obtaining the biotinylated TCL probe (**51**).
Reagents and conditions: a) NaH, dry DMF, ClCH₂COOH (*path a*) or BrCH₂COOEt (*path b*), Bu₄NI, DMF, 0 °C → r.t.; b) **2**, TiCl₄ (1 M in CH₂Cl₂), Zn, anhydrous THF, reflux; c) NaOH, EtOH, reflux; d) 1,6-hexanediamine, DSC, Et₃N, anhydrous DMF, r.t.; e) EDC, CHCl₃, 0 °C → r.t.; f) MB, -20 °C, CH₂Cl₂, lamp, O₂ (1 atm, balloon).

By adopting this strategy, a series of difficulties was encountered related to the instability of the key intermediate **37**. Thus, alternative routes have been pursued by reacting **52** with 1,6-hexanediamine to afford the corresponding conjugate **53** in quantitative yield (**Scheme 27**).¹⁷⁶ Next, the conjugated bt-hexanediamine **53** was submitted to a direct coupling with the corresponding ester McMurry derivative (**36**) using zinc triflate at reflux in anhydrous DMF for 48 hours (**Scheme 27, path a**). Alternatively, the key intermediate succinimide olefin (**43**) was reacted under basic conditions in anhydrous DMF at 100 °C overnight (**Scheme 27, path b**).¹⁷⁷



Scheme 27. Alternative strategies for the synthesis of biotinylated olefin **54**. *Reagents and conditions:* a) 1,6-hexanediamine, DSC, Et₃N, anhydrous DMF, r.t., 24 h, > 98%; *path a:* Zn triflate, anhydrous DMF, reflux, 48 h; *path b:* Et₃N, DMAP, anhydrous DMF, 100 °C, 24 h.

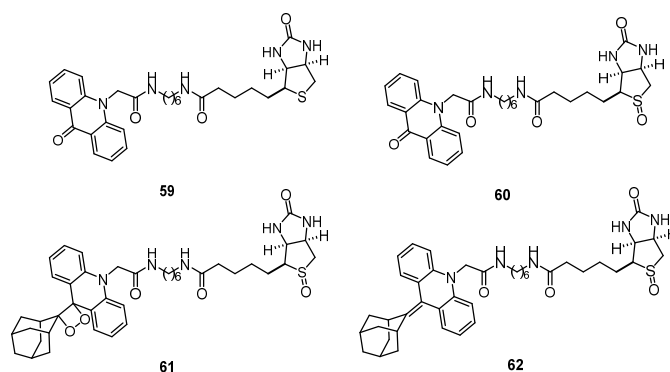
Unfortunately, both procedures failed to provide the desired product (**54**), prompting us to explore an alternative synthetic pathway (**Scheme 28**). Thus, the coupling between **39** and *N*-mono Boc 1,6-hexanediamine **55** obtained by using di-*tert*-butyl dicarbonate (Boc₂O)¹⁷⁸ in CHCl₃ starting from 1,6-hexanediamine at 25 °C gave the intermediate **56**.¹⁷⁹



Scheme 28. Second synthetic strategy for obtaining the biotinylated TCL probe **51**. *Reagents and conditions:* a) COMU, DIPEA, anhydrous DMF, 0 °C → r.t., overnight, 91%; b) TFA, CH₂Cl₂, 0 °C → r.t., 3 h, 66%; c) **2**, TiCl₄, Zn, anhydrous THF, reflux, 45 min, > 98%; d) **52**, COMU, DIPEA, anhydrous DMF, 0 °C → r.t., 3 h, 28%; e) MB, -20 °C, CH₂Cl₂, lamp, O₂ (1 atm, balloon).

The adduct **56** was deprotected in acid conditions for trifluoroacetic acid (TFA) at 25 °C in quantitative yield (**57**). Then, McMurry reaction was carried out obtaining **58** and the subsequent coupling reaction with **52** led to the desired biotinylated olefin intermediate **54** in low yield (28%, **Scheme 28**).¹⁷⁹ However, solubility issues were encountered in the synthesis of the new intermediates, especially during the photooxygenation step. A slow conversion of the olefin **54** was observed by NMR analysis of crude after 5 hours of irradiation. This result strongly depended on the low solubility of precursor **54** in the reaction solvent (CH₂Cl₂), consequently few drops of MeOH were added to provide a complete solubilization of the starting material. Unfortunately, a mixture of sulfone and sulfoxide derivatives was obtained after 10 hours of irradiation, (**59-62**, **Scheme 29**) probably caused by the increase of solubility after MeOH addition.

2.5 Development of new bioconjugated probes based on TCL phenomenon



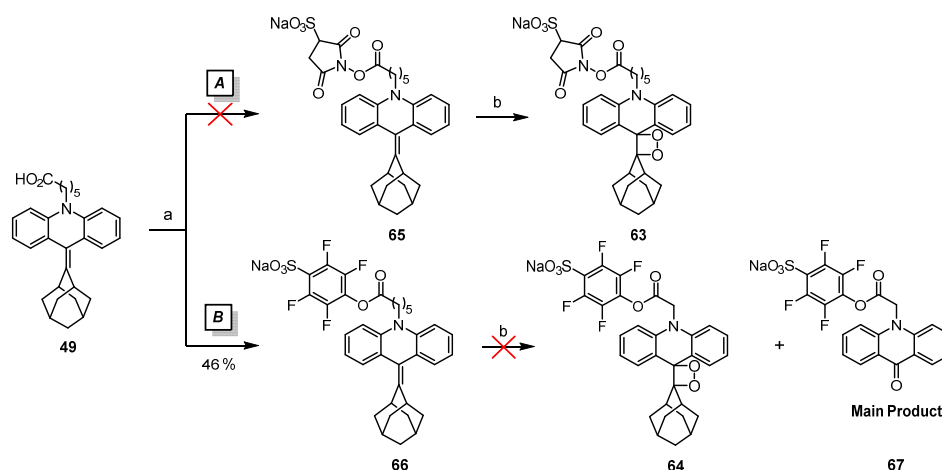
Scheme 29. Molecular structures of by-products (**59-62**) obtained under photooxygenation conditions from biotinylated olefin **54**.

2.5.3 Sulfonated probes

The water solubility frequently represents a difficult obstacle to overcome for labelling molecules attachment. The high hydrophobicity and the poor solubility of NHS esters in aqueous media make them often incompatible with specific bioanalytical applications. In appropriated quantities, the addition of organic co-solvents such as DMF or DMSO is required to improve solubility of the reactive esters, while an excess could compromise the stability of biopolymer.¹⁶⁴

To solve solubility issues, more polar sulfo *N*-hydroxysuccinimidyl (sulfo-NHS) and 4-sulfotetra fluorophenyl (STP) esters have been designed to realize bioconjugation reaction in aqueous buffers.^{180,181} The classical coupling procedure using a third generation coupling agent (1-cyano-2-ethoxy-2-oxoethylideneaminoxy)dimethylamino-morpholino-carbenium hexafluorophosphate (COMU) and DIPEA in anhydrous DMF at 25 °C was applied to obtain the long chain sulfo-NHS and STP 1,2-dioxetanes (**63** and **64**, **Scheme 30**).¹⁷⁹ Extraction from the reaction crude of the sulfo-NHS olefin **65** was particularly tedious because of its high affinity with water limiting the

purification of **65** (Scheme 30, path a). Conversely, the isolation of STP olefin **66** resulted easier, even though the complete degradation of STP 1,2-dioxetane **64** was observed in the following photooxygenation step (Scheme 30, path b).



Scheme 30. Synthesis of sulfonated probes **63** and **64**. *Reagents and conditions:* a) Sulfo-NHS or STP, COMU, DIPEA, anhydrous DMF, 0 °C → r.t., o.n. (**66**: 46%). b) MB, -20 °C, CH_2Cl_2 , lamp, O_2 (1 atm, balloon).

The preliminary results about the functionalization of side chain appendage to afford TCL probes useful in bioconjugation assays provided promising results. However, the encountered solubility issues as well as the synthetic infeasibility of some intermediates and final products certainly require further studies and deepening.

Concluding Remarks and Future Perspectives

Among the well-established luminescence techniques, TCL represents a promising and innovative approach for realizing bioanalytical assays. Despite its potential, only recently this technique has been broadly explored with the development of novel 1,2-dioxatane derivatives, in particular *N*-substituted acridine-containing compounds, as ultrasensitive TCL labels.

In this Thesis work, the acridine ring has been decorated at the C2- and C7-positions with both EWGs and EDGs to fine-tune the photophysical and TCL properties of the target 1,2-dioxetane compound **3**. We proved both experimentally and with the support of computational analysis, that the efficiency of the photooxidation reaction, resulting into the TCL compounds properties, is markedly influenced by the different substitution pattern of the acridine moiety. Synthetic limitations due to the poor scalability and reproducibility of the key photooxidation step were solved with the recourse of enabling chemical technologies making the preparation of the 1,2-dioxetane unit more accessible. In particular, the critical [2+2]-photocycloaddition was performed under continuous flow conditions furnishing a simple method to prepare efficiently variably functionalized 1,2-dioxetanes. Among the synthesized derivatives, dioxetane **27g**, containing an EDG and an EWG both by induction, was identified

as the best compound combining an intense TCL signal with a remarkable higher stability at room temperature. The effect of substitutions on mechanism and TCL performance was investigated by comparing the photophysical behaviour of the unsubstituted compound **3** with the *push-pull* 1,2-dioxetane **27g** in different environments (solid state, optical glue and Plus NPs). Moreover, experiments carried out on HaCaT cell lines demonstrated that compound **3** can be detected in real biological samples as cell-based assays. Next, the functionalization of *N*-acridine side chain was attempted to provide the site for coupling with proteins such as streptavidin, biotin or protein A, and facilitate their binding to antibody or DNA probes. Preliminary studies on the insertion of TCL probes into functionalized nanoparticles gave promising results in view of an improved stability in solution and enhancing the number of tracers *per* molecule, i.e., a high signal/mass for ultrasensitive detection. Further screening of specific materials, such as glass and plastics, will be evaluated to avoid the rapid decomposition of TCL probes and find the optimal working conditions (temperature, pH, ionic strength, and protein content) to make this approach universal to trace any biospecific reaction from immune- to gene-assays.

Chapter 3. Experimental Section

3.1 Synthesis

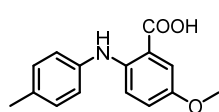
General methods

Unless otherwise noted, chemicals were obtained from commercial suppliers and used without further purification. NMR spectra were recorded on a Bruker AC 400 MHz spectrometer in the indicated solvent. Chemical shifts are reported in parts per million (ppm) and are relative to CDCl₃ (7.26 ppm and 77.0 ppm), CD₃OD (3.31 ppm and 49.0 ppm) DMSO-d₆ (2.50 ppm and 39.52 ppm) or acetone-d₆ (2.05 ppm and 29.84 ppm). The abbreviations used are as follows: s, singlet; brs, broad singlet; d, doublet; dd, double doublet; dt, double triplet; t, triplet; q, quartet; m, multiplet; brm, broad multiplet. Hydrogenation reaction was performed on a H-Cube system (ThalesNano). Flash column chromatography was performed using Biotage Isolera One. Thin-layer chromatography was performed using glass plates coated with silica gel 60 F-254. Spots were visualized by UV detector (λ : 254 nm).

General procedure for Ullmann coupling reaction (31a-c).^{25b,111}

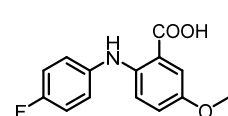
A suspension of *p*-substituted aniline (**29a-c**, 1 equiv.), 2-bromo 5-methoxy benzoic acid (**30a**, 0.72 equiv.), anhydrous K₂CO₃ (1 equiv.), and copper (0.14 equiv.) in anhydrous DMF was heated under reflux and nitrogen atmosphere, until the complete disappearance of the starting material monitored by TLC. Then, the mixture was cooled to r.t., quenched with H₂O and extracted with CH₂Cl₂. The water phase was acidified with HCl 3 N up to pH= 3 and extracted with CH₂Cl₂. The combined organic phases were washed with water, brine and dried over anhydrous Na₂SO₄. The crudes were concentrated under reduced pressure to dryness to give the desired products **31a-c** that were submitted for the next step without further purifications.

Ethyl 2-(9-((5*r*,7*r*)-adamantan-2-ylidene)acridin-10(9*H*)-yl)acetate (31a)



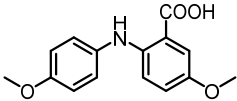
150 mg (0.58 mmol). Yield: 63%. Yellow solid. ¹H-NMR (CDCl₃, 400 MHz): δ 2.36 (s, 3H), 3.81 (s, 3H), 7.03 (m, 1H), 7.14 (m, 5H), 7.54 (m, 1H). ¹³C-NMR (CDCl₃, 100.6 MHz): δ 20.3, 55.2, 109.9, 113.3, 115.6, 122.0, 123.7, 129.4, 132.6, 137.8, 143.4, 150.2, 173.1.

2-((4-fluorophenyl)amino)-5-methoxybenzoic acid (31b)



1.53 g (5.86 mmol). Yield: 65%. Green solid. ¹H-NMR (DMSO-d₆, 400 MHz): δ 3.72 (s, 3H), 7.05-7.22 (m, 6H), 7.38 (m, 1H), 9.10 (bs, 1H). ¹³C-NMR (DMSO-d₆, 100.6 MHz): δ 55.6, 114.4, 115.0, 116.5, 116.7, 116.9, 122.4, 122.8, 122.9, 138.6, 141.8, 151.5, 157.1, 159.5 170.0. ¹⁹F-NMR (DMSO-d₆, 376 MHz): -121.41.

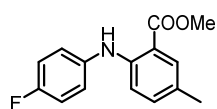
5-methoxy-2-((4-methoxyphenyl)amino)benzoic acid methyl (31c)


 1.24 g (4.54 mmol). Yield: 56%. Yellow solid. ¹H-NMR (CDCl₃, 400 MHz): δ 3.80 (s, 3H), 3.90 (s, 3H), 6.87-6.93 (m, 2H), 6.95-7.02 (m, 2H), 7.12-7.18 (m, 2H), 7.48-7.51 (m, 1H). ¹³C-NMR (CDCl₃, 100.6 MHz): δ 55.6, 55.9, 109.9, 114.0, 114.8, 115.8, 124.6, 125.6, 134.0, 145.3, 150.6, 156.6, 173.5.

General procedure for Buchwald-Hartwig cross-coupling reaction and hydrolysis (31d-j).^{112,113}

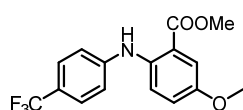
A suspension of tris(dibenzylideneacetone)dipalladium (0)-chloroform adduct (0.036 equiv.) and (±)-BINAP (0.07 equiv.) in anhydrous toluene was stirred under nitrogen atmosphere at r.t. for 30 minutes. To the deep red solution, 2-bromo 5-substituted methoxy benzoate (**30b-d**, 1 equiv.), *p*-substituted aniline (**29a-e**, 0.86 equiv.), and Cs₂CO₃ (1 equiv.) were added, and the mixture was stirred at 110-130 °C until the complete disappearance of the starting material monitored by TLC. The mixture was cooled to r.t., diluted with H₂O and extracted with CH₂Cl₂. The combined organic phases were washed with H₂O, brine, dried over anhydrous Na₂SO₄ and evaporated under reduced pressure co-distilling with acetone. To a solution of the corresponding ester coupling derivative (1 equiv.) in MeOH an aqueous solution of NaOH 5% (v/v) was added and the reaction mixture was stirred at r.t. until the complete disappearance of starting material. The mixture was concentrated under reduced pressure, diluted with HCl 3 N up to pH= 3 and extracted with CH₂Cl₂. The combined organic phases were washed with H₂O, brine, dried over anhydrous Na₂SO₄ and evaporated under vacuum. The crudes were purified by automated flash chromatography to give the desired adducts **31d-j**.

Methyl 2-((4-fluorophenyl)amino)-5-methylbenzoate (31d)



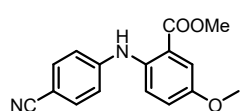
187 mg (0.72 mmol). Yield: 33%. Colorless oil. $^1\text{H-NMR}$ (CDCl_3 , 400 MHz): δ 2.26 (s, 3H), 3.90 (s, 3H), 6.99-7.06 (m, 2H), 7.11-7.15 (m, 1H), 7.15-7.20 (m, 2H), 7.77 (s, 1H), 9.25 (bs, 1H). $^{13}\text{C-NMR}$ (CDCl_3 , 100.6 MHz): δ 19.7, 51.4, 110.9, 113.2, 115.3, 115.5, 123.9, 124.0, 125.6, 130.7, 134.6, 136.5, 145.6, 159.7, 168.3. $^{19}\text{F-NMR}$ (CDCl_3 , 376 MHz): -119.84.

Methyl 5-methoxy-2-((4-(trifluoromethyl)phenyl)amino)benzoate (31e)



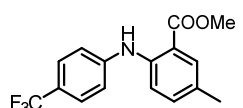
1.33 g (4.0887 mmol). Yield: > 98%. Yellow oil. $^1\text{H-NMR}$ (CDCl_3 , 400 MHz): δ 3.80 (s, 3H), δ 3.90 (s, 3H), 7.03 (dd, 1H, $J_1 = 2.70$, $J_2 = 9.00$), 7.18 (m, 2H), 7.37 (m, 1H), 7.49 (m, 3H). $^{13}\text{C-NMR}$ (CDCl_3 , 100.6 MHz): δ 13.5, 20.4, 51.4, 55.0, 59.7, 113.8, 114.7, 117.4, 117.6, 121.2, 125.9, 126.0, 138.7, 144.8, 151.9, 167.6. $^{19}\text{F-NMR}$ (CDCl_3 , 376 MHz): -62.12.

Methyl 2-((4-cyanophenyl)amino)-5-methoxybenzoate (31f)



510 mg (1.81 mmol). Yield: 44%. Yellow solid. $^1\text{H-NMR}$ (CDCl_3 , 400 MHz): δ 3.80 (s, 3H), δ 3.89 (s, 3H), 7.04 (dd, 1H, $J_1 = 3.07$, $J_2 = 9.05$ Hz), 7.11 (m, 2H), 7.37 (m, 1H), 7.47 (m, 3H). $^{13}\text{C-NMR}$ (CDCl_3 , 100.6 MHz): δ 51.6, 55.41, 102.1, 114.1, 116.0, 116.5, 118.6, 119.1, 120.8, 133.0, 137.1, 146.0, 152.7, 167.4.

Methyl 5-methyl-2-((4-(trifluoromethyl)phenyl)amino)benzoate (31g)

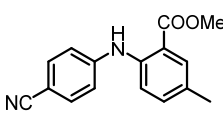


1.2 g (3.88 mmol). Yield: 60%. Colorless oil. $^1\text{H-NMR}$ (CDCl_3 , 400 MHz): δ 2.30 (s, 3H), 3.90 (s, 3H), 7.18-7.25 (m, 2H), 7.30-7.40 (m, 1H), 7.49-7.59 (m, 2H), 7.81 (m, 1H), 9.48 (s, 1H). $^{13}\text{C-NMR}$ (CDCl_3 , 100.6 MHz): δ 14.3, 20.5, 52.0, 60.5, 114.0,

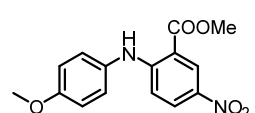
3.1 Synthesis

115.8, 119.0, 126.6, 128.5, 131.7, 135.1, 143.4, 145.0, 168.8. ^{19}F -NMR (CDCl_3 , 376 MHz): -62.15.

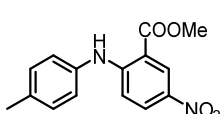
Methyl 2-((4-cyanophenyl)amino)-5-methylbenzoate (31h)

 705 mg (2.65 mmol). Yield: 41%. Yellow solid. ^1H -NMR (CDCl_3 , 400 MHz): δ 2.30 (s, 3H), 3.88 (s, 3H), 7.13-7.22 (m, 2H), 7.32-7.38 (m, 1H), 7.39-7.46 (m, 1H), 7.49-7.56 (m, 2H), 7.81 (s, 1H), 9.53 (s, 1H). ^{13}C -NMR (CDCl_3 , 100.6 MHz): δ 19.9, 51.5, 102.7, 114.4, 116.1, 117.4, 119.0, 124.7, 127.8, 128.3, 129.1, 129.9, 131.2, 133.0, 134.3, 141.3, 142.7, 167.9, 177.4.

Methyl 2-((4-methoxyphenyl)amino)-5-nitrobenzoate (31i)

 167 mg (0.55 mmol). Yield: 48%. Yellow solid. ^1H -NMR (CDCl_3 , 400 MHz): δ 3.86 (s, 3H), 3.97 (s, 3H), 6.85-6.92 (m, 1H), 6.94-7.02 (m, 2H), 7.15-7.23 (m, 2H), 7.81 (s, 1H), 8.90-8.93 (m, 1H), 9.53 (s, 1H), 10.01 (brs, 1H). ^{13}C -NMR (CDCl_3 , 100.6 MHz): δ 52.5, 55.7, 109.5, 113.0, 115.2, 127.1, 129.2, 129.5, 130.9, 137.0, 154.1, 158.3, 168.0.

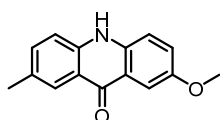
Methyl 5-nitro-2-(p-tolylamino)benzoate (31j)

 602 mg (2.10 mmol). Yield: 55%. Yellow solid. ^1H -NMR (CDCl_3 , 400 MHz): δ 2.39 (s, 3H), 4.00 (s, 3H), 7.00 (d, 1H, 9.45), 7.14 (d, 2H, $J = 7.93$), 7.24 (d, 2H, 8.17), 8.08 (dd, 1H, $J_1 = 2.12$, $J_2 = 9.35$), 8.90 (d, 1H, 2.28), 10.09 (brs, 1H). ^{13}C -NMR (CDCl_3 , 100.6 MHz): δ 21.2, 52.5, 109.8, 113.1, 124.9, 129.2, 129.4, 130.5, 135.6, 136.4, 137.1, 153.4, 167.9.

General procedure by Eaton's acid-mediated cyclization step (31a-j).¹¹⁴

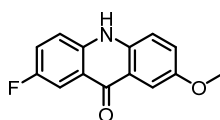
In a flask containing the corresponding acid coupling derivative (**31a-j**, 1 equiv.), Eaton's reagent (10 wt % P₂O₅ solution in methanesulfonic acid) was added, and the reaction mixture was then stirred at 90 °C for ca. 3 hours. After cooling to r.t., the mixture was diluted with H₂O and EtOAc. The crude was treated with NaHCO_{3(ss)} up to pH= 7 and extracted with EtOAc. The combined organic phases were washed with H₂O, brine, dried over anhydrous Na₂SO₄ and concentrated under vacuum. The crudes were used for the next step without further purifications.

2-methoxy-7-methylacridin-9(10H)-one (32a)

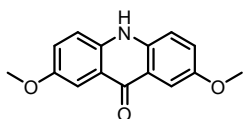


1.6 g (6.69 mmol). Yield: > 98%. Yellow solid. ¹H-NMR (DMSO-d₆, 400 MHz): δ 2.40 (s, 3H), 3.84 (s, 3H), 7.36 (dd, 1H, J₁ = 2.79, J₂ = 9.03), 7.14 (m, 1H), 7.50 (m, 2H), 7.59 (m, 1H), 8.01 (m, 1H), 11.68 (brs, 1H). ¹³C-NMR (DMSO-d₆, 100.6 MHz): δ 21.0, 55.7, 105.1, 117.7, 119.6, 119.9, 121.2, 124.6, 125.3, 130.0, 130.2, 135.0, 136.1, 139.0, 154.2, 176.3.

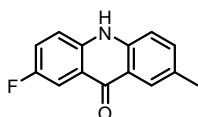
2-fluoro-7-methoxyacridin-9(10H)-one (32b)



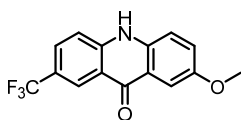
1.6 g (6.58 mmol). Yield: > 98%. Yellow solid. ¹H-NMR (DMSO-d₆, 400 MHz): δ 3.85 (s, 3H), 7.40 (m, 1H), 7.53-7.66 (m, 4H), 7.85 (m, 1H), 12.07 (bs, 1H). ¹³C-NMR (DMSO-d₆, 100.6 MHz): δ 55.9, 105.0, 109.8, 110.0, 119.9, 120.6, 122.5, 122.8, 125.2, 136.3, 137.8, 154.7, 156.1, 158.4 176.0. ¹⁹F-NMR (DMSO-d₆, 376 MHz): -121.59.

2,7-dimethoxyacridin-9(10H)-one (32c)

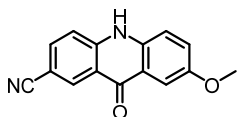
93 mg (0.36 mmol). Yield: > 98%. Yellow solid. ¹H-NMR (DMSO-d₆, 400 MHz): δ 3.83 (s, 6H), 7.33-7.40 (dd, 2H, J₁ = 3.00, J₂ = 9.03), 7.50-7.57 (d, 2H, J = 9.00), 7.57-7.62 (d, 2H, J = 3.00), 11.83 (brs, 1H). ¹³C-NMR (DMSO-d₆, 100.6 MHz): δ 55.4, 104.5, 119.4, 120.1, 124.3, 135.5, 153.9, 175.4.

2-fluoro-7-methylacridin-9(10H)-one (32d)

230 mg (1.01 mmol). Yield: > 98%. Pale yellow solid. ¹H-NMR (DMSO-d₆, 400 MHz): δ 2.40 (s, 3H), 7.42-7.48 (m, 1H), 7.54-7.66 (m, 4H), 7.80-7.88 (dd, 2H, J₁ = 2.62, J₂ = 9.30), 7.99 (m, 1H), 11.79 (brs, 1H). ¹³C-NMR (DMSO-d₆, 100.6 MHz): δ 21.0, 109.9, 110.2, 117.8, 119.9, 120.3, 120.4, 121.2, 122.5, 122.7, 125.3, 130.8, 135.6, 138.0, 139.3, 156.0, 158.3, 176.3. ¹⁹F-NMR (DMSO-d₆, 376 MHz): -121.62.

2-methoxy-7-(trifluoromethyl)acridin-9(10H)-one (32e)

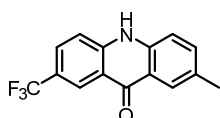
630 mg (2.15 mmol). Yield: > 98%. Yellow solid. ¹H-NMR (CD₃OD, 400 MHz): δ 3.94 (s, 3H), 7.46 (dd, 1H, J₁ = 2.69, J₂ = 9.02), 7.55 (m, 1H), 7.67 (m, 1H), 7.77 (m, 1H), 7.91 (m, 1H), 8.65 (m, 1H). ¹³C-NMR (CD₃OD, 100.6 MHz): δ 56.1, 108.6, 117.3, 119.7, 120.1, 120.5, 122.3, 123.0, 124.1, 125.7, 133.4, 137.8, 147.7, 154.6, 176.5. ¹⁹F-NMR (CD₃OD, 376 MHz): -63.77.

7-methoxy-9-oxo-9,10-dihydroacridine-2-carbonitrile (32f)

1.00 g (4.00 mmol). Yield: > 98%. Yellow solid. ¹H-NMR (DMSO-d₆, 400 MHz): δ 3.84 (s, 3H), 7.43-7.50 (m, 1H), 7.54-7.62 (m, 3H), 7.94-7.99 (m, 1H), 8.54 (m,

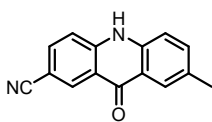
1H), 12.24 (brs, 1H). ¹³C-NMR (DMSO-d₆, 100.6 MHz): δ 55.3, 102.3, 104.9, 118.7, 118.9, 119.5, 121.5, 124.8, 132.0, 134.1, 135.2, 142.2, 154.7, 175.0.

2-methyl-7-(trifluoromethyl)acridin-9(10H)-one (32g)



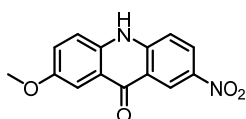
300 mg (1.08 mmol). Yield: > 98%. Yellow solid. ¹H-NMR (DMSO-d₆, 400 MHz): δ 2.41 (s, 3H), 7.50-7.75 (m, 2H), 7.77-7.90 (m, 1H), 7.90-8.12 (m, 2H), 8.45 (m, 1H), 12.87 (s, 1H). ¹³C-NMR (DMSO-d₆, 100.6 MHz): δ 21.1, 118.4, 119.5, 119.7, 121.2, 124.2, 125.5, 129.3, 131.8, 139.6, 143.4, 176.7. ¹⁹F-NMR (DMSO-d₆, 376 MHz): -60.57.

7-methyl-9-oxo-9,10-dihydroacridine-2-carbonitrile (32h)

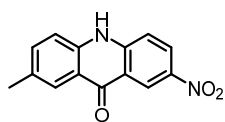


100 mg (0.43 mmol). Yield: > 98%. Orange solid. ¹H-NMR (DMSO-d₆, 400 MHz): δ 2.40 (s, 3H), 7.11-7.59 (m, 3H), 7.99-8.35 (m, 2H), 8.70-8.93 (m, 1H), 12.87 (brs, 1H). ¹³C-NMR (DMSO-d₆, 100.6 MHz): δ 20.6, 117.2, 117.5, 119.4, 120.7, 125.2, 126.3, 126.5, 130.9, 132.1, 135.2, 138.9, 142.4, 167.4, 176.7.

2-methoxy-7-nitroacridin-9(10H)-one (32i)



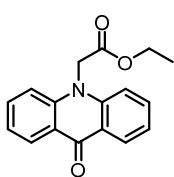
110 mg (0.41 mmol). Yield: > 98%. Yellow solid. ¹H-NMR (CDCl₃, 400 MHz): δ 4.07 (s, 3H), 7.45-7.51 (m, 1H), 7.59 (dd, 1H, J₁ = 1.60, J₂ = 8.97), 8.07-8.16 (m, 1H), 8.23-8.31 (m, 1H), 8.43 (dd, 1H, J₁ = 1.60, J₂ = 9.20), 9.30-9.35 (m, 1H). ¹³C-NMR (CDCl₃, 100.6 MHz): δ 56.1, 99.9, 122.2, 122.3, 123.0, 126.2, 128.4, 131.9, 132.0, 145.8, 147.8, 148.3, 159.3, 171.9.

2-methyl-7-nitroacridin-9(10H)-one (32j)

400 mg (1.57 mmol). Yield: > 98%. Yellow solid. ¹H-NMR (CDCl₃, 400 MHz): δ 2.66 (s, 3H), 7.73-7.81 (m, 1H), 8.11-8.24 (m, 2H), 8.26-8.35 (m, 1H), 8.42-8.51 (m, 1H), 9.31-9.38 (m, 1H). ¹³C-NMR (CDCl₃, 100.6 MHz): δ 22.4, 122.7, 122.8, 123.1, 123.3, 129.5, 131.6, 134.1, 136.2, 139.2, 142.8, 143.0, 152.4, 175.1.

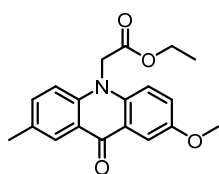
General procedure for the alkylation step (26 and 28a-j).^{25c}

To a suspension of the corresponding cyclization derivative (**32a-j** and **40**, 1 equiv.) in anhydrous DMF, NaH (60% dispersion in mineral oil, 1.2 equiv.) was added dropwise, and the mixture was stirred for 30 minutes at r.t.. After cooling to 0°C, ethyl 2-bromoacetate (1.5 equiv.), and tetrabutylammonium iodide (0.01 equiv.) were added and the solution was stirred for further 24 hours at r.t. The mixture was diluted with H₂O and extracted with EtOAc. The combined organic phases were washed with H₂O, brine and dried over anhydrous Na₂SO₄. The crudes were evaporated under vacuum and purified by flash chromatography to give the desired compounds (**26**, **28a-j**).

Ethyl 2-(9-oxoacridin-10(9H)-yl)acetate (26)

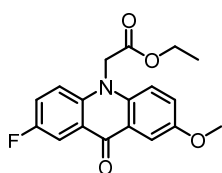
2.81 g (9.99 mmol). Yield: 98%. Pale yellow solid. ¹H-NMR (CDCl₃, 400 MHz): δ 1.29 (t, 3H, J = 7.1 Hz), 4.30 (q, 2H, J = 7.12 Hz), 5.04 (s, 2H), 7.31-7.27 (m, 4H), 7.71-7.66 (m, 2H), 8.54-8.52 (m, 2H). ¹³C-NMR (CDCl₃, 100.6 MHz): δ 14.3, 48.5, 62.3, 114.3, 121.9, 122.6, 128.0, 134.2, 142.3, 168.4, 178.2.

Ethyl 2-(2-methoxy-7-methyl-9-oxoacridin-10(9H)-yl)acetate (28a)



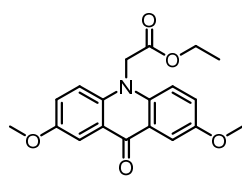
47 mg (0.14 mmol). Yield: 81%. Yellow solid. $^1\text{H-NMR}$ (CDCl_3 , 400 MHz): δ 1.27 (t, 3H, $J = 7.02$ Hz), 2.44 (s, 3H), 3.92 (s, 3H), 4.27 (q, 2H, $J = 6.97$), 5.01 (s, 2H), 7.18 (m, 1H), 7.18 (m, 1H), 7.23 (m, 1H), 7.30 (dd, 1H, $J_1 = 2.64$, $J_2 = 6.52$), 7.48 (m, 1H), 7.92 (m, 1H), 8.31 (m, 1H). $^{13}\text{C-NMR}$ (CDCl_3 , 100.6 MHz): δ 14.3, 20.7, 48.5, 55.9, 62.2, 107.0, 114.1, 116.0, 121.7, 123.1, 124.5, 127.2, 131.2, 135.3, 137.0, 140.0, 154.6, 168.5, 177.6.

Ethyl 2-(2-fluoro-7-methoxy-9-oxoacridin-10(9H)-yl)acetate (28b)

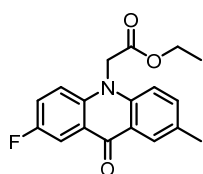


31 mg (0.09 mmol). Yield: 42%. Yellow solid. $^1\text{H-NMR}$ (CDCl_3 , 400 MHz): δ 1.29 (t, 3H, $J = 6.51$ Hz), 3.92 (s, 3H), 4.29 (q, 2H, $J = 6.74$), 5.03 (s, 2H), 7.22-7.44 (m, 4H), 7.86 (m, 1H), 8.15 (m, 1H). $^{13}\text{C-NMR}$ (CDCl_3 , 100.6 MHz): δ 14.3, 48.9, 55.9, 62.4, 106.8, 112.1, 112.3, 116.1, 116.36, 116.43, 122.2, 122.4, 122.6, 122.7, 122.8, 125.0, 137.0, 138.5, 154.9, 156.6, 159.0, 168.3, 176.9. $^{19}\text{F-NMR}$ (CDCl_3 , 376 MHz): -121.41.

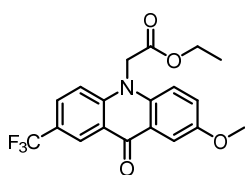
Ethyl 2-(2,7-dimethoxy-9-oxoacridin-10(9H)-yl)acetate (28c)



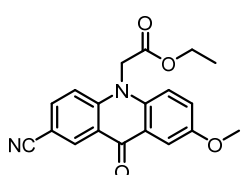
504 mg (1.48 mmol). Yield: 72%. Yellow solid. $^1\text{H-NMR}$ (CDCl_3 , 400 MHz): δ 1.26 (t, 3H, $J = 6.69$ Hz), 3.93 (s, 6H), 4.27 (q, 2H, $J = 6.88$), 5.03 (s, 2H), 7.22-7.29 (m, 2H), 7.30-7.38 (m, 2H), 7.89-8.00 (m, 2H). $^{13}\text{C-NMR}$ (CDCl_3 , 100.6 MHz): δ 14.2, 48.6, 55.9, 62.2, 106.8, 115.9, 122.5, 124.5, 136.7, 154.6, 168.4, 177.1.

Ethyl 2-(2-fluoro-7-methyl-9-oxoacridin-10(9H)-yl)acetate (28d)

35 mg (0.11 mmol). Yield: 40%. Pale yellow solid. $^1\text{H-NMR}$ (CDCl_3 , 400 MHz): δ 1.29 (t, 3H, $J = 7.09$ Hz), 2.45 (s, 3H), 4.29 (q, 2H, $J = 7.02$), 5.03 (s, 2H), 7.15-7.23 (m, 1H), 7.25-7.30 (m, 1H), 7.37-7.45 (m, 1H), 7.49-7.55 (m, 1H), 8.12-8.19 (m, 1H), 8.54 (s, 1H). $^{13}\text{C-NMR}$ (CDCl_3 , 100.6 MHz): δ 14.1, 20.5, 48.6, 61.4, 62.2, 112.2, 112.4, 114.1, 115.7, 116.1, 116.2, 121.6, 122.0, 122.2, 125.8, 127.1, 131.7, 134.3, 135.7, 138.6, 140.2, 156.4, 158.9, 168.1, 177.3. $^{19}\text{F-NMR}$ (CDCl_3 , 376 MHz): -121.37.

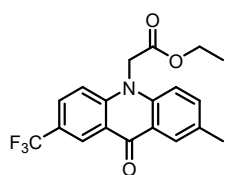
Ethyl 2-(2-methoxy-9-oxo-7-(trifluoromethyl)acridin-10(9H)-yl)acetate (28e)

20 mg (0.05 mmol). Yield: 77%. Yellow solid. $^1\text{H-NMR}$ (CDCl_3 , 400 MHz): δ 1.30 (t, 3H, $J = 7.12$ Hz), 3.94 (s, 3H), 4.33 (q, 2H, $J = 7.10$), 5.07 (s, 2H), 7.30 (m, 1H), 7.37 (m, 2H), 7.86 (dd, 1H, $J_1 = 2.00$, $J_2 = 9.04$), 7.92 (m, 1H), 8.83 (m, 1H). $^{13}\text{C-NMR}$ (CDCl_3 , 100.6 MHz): δ 13.5, 48.0, 55.3, 61.8, 106.5, 114.3, 115.6, 116.5, 117.6, 124.4, 125.4, 129.2, 149.0, 154.2, 167.2, 176.3. $^{19}\text{F-NMR}$ (CDCl_3 , 400 MHz): -62.22.

Ethyl 2-(2-cyano-7-methoxy-9-oxoacridin-10(9H)-yl)acetate (28f)

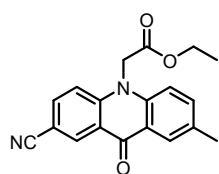
74 mg (0.22 mmol). Yield: 30%. Yellow solid. $^1\text{H-NMR}$ (CDCl_3 , 400 MHz): δ 1.32 (t, 3H, $J = 7.12$ Hz), 3.96 (s, 3H), 4.33 (q, 2H, $J = 7.11$), 5.08 (s, 2H), 7.30-7.35 (m, 1H), 7.37-7.41 (m, 2H), 7.85-7.90 (m, 1H), 7.92-7.95 (m, 1H), 8.89 (s, 1H). $^{13}\text{C-NMR}$ (CDCl_3 , 100.6 MHz): δ 14.1, 48.6, 55.9, 62.6, 105.0, 107.4, 115.4, 116.4, 117.6, 122.3, 124.4, 125.3, 133.7, 135.4, 137.8, 144.2, 156.1, 168.8, 176.3.

Ethyl 2-(2-methyl-9-oxo-7-(trifluoromethyl)acridin-10(9H)-yl)acetate (28g)



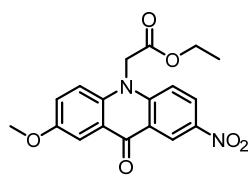
110 mg (0.30 mmol). Yield: 28%. White-pale yellow solid. $^1\text{H-NMR}$ (CDCl_3 , 400 MHz): δ 1.29 (t, 3H, $J = 7.12$ Hz), 2.41 (s, 3H), 4.29 (q, 2H, $J = 7.07$), 5.03 (s, 2H), 7.10-7.22 (m, 1H), 7.22-7.39 (m, 1H), 7.42-7.55 (m, 1H), 7.70-7.87 (m, 1H), 8.21 (s, 1H), 8.72 (s, 1H). $^{13}\text{C-NMR}$ (CDCl_3 , 100.6 MHz): δ 14.2, 20.6, 48.5, 62.5, 114.6, 115.1, 121.7, 122.6, 125.9, 127.3, 129.9, 132.6, 136.0, 140.2, 143.8, 163.9, 177.4. $^{19}\text{F-NMR}$ (CDCl_3 , 376 MHz): -62.25.

Ethyl 2-(2-cyano-7-methyl-9-oxoacridin-10(9H)-yl)acetate (28h)

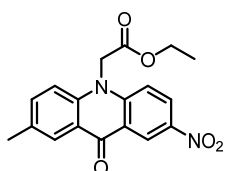


30 mg (0.09 mmol). Yield: 22%. Yellow solid. $^1\text{H-NMR}$ (DMSO-d_6 , 400 MHz): δ 1.23 (t, 3H, $J = 7.12$ Hz), 3.45 (s, 3H), 4.21 (q, 2H, $J = 7.11$), 5.46 (s, 2H), 7.40 (m, 1H), 7.52-7.80 (m, 2H), 8.10-8.33 (m, 2H), 8.89 (s, 1H). $^{13}\text{C-NMR}$ (CDCl_3 , 100.6 MHz): δ 14.7, 21.2, 48.9, 62.2, 101.6, 116.1, 118.9, 119.3, 122.6, 123.2, 128.1, 129.3, 130.5, 133.5, 133.7, 137.3, 145.0, 168.9, 176.3

Ethyl 2-(2-methoxy-7-nitro-9-oxoacridin-10(9H)-yl)acetate (28i)



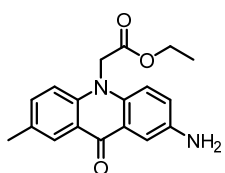
4 mg (0.01 mmol). Yield: 6%. Yellow solid. $^1\text{H-NMR}$ (CDCl_3 , 400 MHz): δ 1.33 (t, 3H, $J = 7.11$ Hz), 3.97 (s, 3H), 4.34 (q, 2H, $J = 7.14$), 5.12 (s, 2H), 7.28-7.35 (m, 2H), 7.37-7.41 (m, 2H), 7.87-7.93 (m, 1H), 8.48-8.52 (m, 1H). $^{13}\text{C-NMR}$ (CDCl_3 , 100.6 MHz): δ 14.3, 48.9, 56.0, 62.7, 114.8, 115.5, 121.7, 122.7, 124.8, 127.7, 128.0, 133.7, 136.5, 140.1, 141.7, 145.5, 167.5, 177.1.

Ethyl 2-(2-methyl-7-nitro-9-oxoacridin-10(9H)-yl)acetate (28j)

4 mg (0.01 mmol). Yield: 6%. Yellow solid. $^1\text{H-NMR}$ (CDCl_3 , 400 MHz): δ 1.28 (t, 3H, $J = 7.11$ Hz), 2.45 (s, 3H), 4.29 (q, 2H, $J = 7.10$), 5.09 (s, 2H), 7.23-7.28 (m, 1H), 7.33-7.40 (d, 1H, $J = 9.43$), 7.53-7.60 (m, 1H), 8.23-8.8.28 (m, 1H), 8.37-8.45 (dd, 1H, $J_1 = 2.63$, $J_2 = 9.36$), 9.28-9.32 (d, 1H, $J = 2.67$). $^{13}\text{C-NMR}$ (CDCl_3 , 100.6 MHz): δ 14.3, 20.7, 48.9, 62.7, 114.8, 115.5, 121.7, 122.7, 124.8, 127.7, 128.0, 133.7, 136.5, 140.1, 141.7, 145.5, 167.5, 177.1.

General procedure for reduction of nitro group under continuous flow conditions and hydrochloride salt formation (28k-l).¹¹⁰

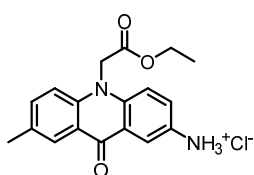
A solution of starting material (**28j**, 1 equiv.) dissolved in MeOH was hydrogenated under continuous flow apparatus H-Cube (ThalesNano)¹¹⁵ using a Pd/C cartridge (10% loading, 30×4 mm, ThalesNano) at 1 bar of pressure, 30 °C and a total flow rate of 1 mL min^{-1} for 2 hours. The crude was evaporated under vacuum obtained the desired product without any further purification. The resultant product **28k** was dissolved in HCl 4 M in 1,4-dioxane solution (1 mL, 0.03 M) and the solution was stirred at r.t. for 6 hours. The solid precipitate formed was filtered and triturated with Et_2O to give **28l** hydrochloride in quantitative yield.

Ethyl 2-(2-amino-7-methyl-9-oxoacridin-10(9H)-yl)acetate (28k)

10 mg (0.03 mmol). Yield: > 98%. Oil. $^1\text{H-NMR}$ (CDCl_3 , 400 MHz): δ 1.28 (t, 3H, $J = 7.14$ Hz), 2.46 (s, 3H), 4.28 (q, 2H, $J = 7.10$), 5.02 (s, 2H), 7.09-7.16 (dd, 1H, $J_1 = 2.58$, $J_2 = 8.94$), 7.16-7.19 (d, 1H, $J = 4.15$), 7.19-7.22 (d, 1H, $J = 3.94$), 7.43-7.53 (dd, 1H, $J_1 = 1.73$, $J_2 = 8.68$), 7.78-7.83 (d, 1H, $J = 2.56$), 8.31-8.35 (m, 1H). $^{13}\text{C-NMR}$ (CDCl_3 , 100.6 MHz): δ 13.6, 18.0, 47.7, 61.4, 110.1,

113.3, 114.7, 121.0, 121.8, 122.8, 126.6, 130.2, 134.6, 135.1, 139.4, 140.5, 168.0, 177.1.

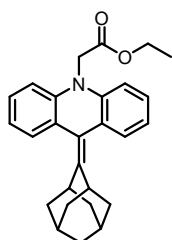
Ethyl 2-(2-amino-7-methyl-9-oxoacridin-10(9H)-yl)acetate hydrochloride (28I)



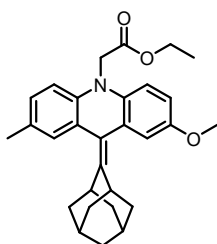
10 mg (0.03 mmol). Yield: > 98%. Brown solid. ¹H-NMR (CD₃OD, 400 MHz): δ 1.31 (t, 3H, J = 7.04 Hz), 2.50 (s, 3H), 4.28 (q, 2H, J = 7.02), 5.40 (s, 2H), 7.53-7.60 (m, 1H), 7.66-7.72 (m, 1H), 7.72-7.78 (m, 2H), 8.24-8.32 (m, 2H). ¹³C-NMR (CD₃OD, 100.6 MHz): δ 13.0, 19.2, 49.5, 61.8, 110.1, 115.1, 117.3, 122.6, 122.8, 126.3, 127.2, 130.2, 133.5, 135.6, 141.0, 142.1, 168.8, 177.3.

General procedure for the McMurry reaction (33a-g and 36).^{25a}

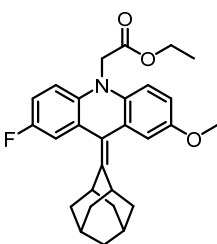
Under a nitrogen atmosphere, zinc powder (13.5 equiv.) was added portionwise to a solution of TiCl₄ (1 M in CH₂Cl₂, 6.1 equiv.) dissolved in anhydrous THF and the suspension was stirred for 10 minutes under reflux. A solution of ketones **26** and **28a-g** (1 equiv.) and **2** (1 equiv.) in anhydrous THF was added dropwise over a period of 30 minutes. The reaction mixture was heated at reflux until the complete disappearance of starting materials monitored by TLC. Then, it was cooled to r.t., quenched with H₂O, treated with HCl 3 N, and extracted with EtOAc. The combined organic layers were washed with H₂O, brine and dried over anhydrous Na₂SO₄. The crudes were evaporated under vacuum and purified by automated flash chromatography to yield the desired adducts (**33a-g**, **36**).

Ethyl 2-((5*r*,7*r*)-adamantan-2-ylidene)acridin-10(9*H*)-yl)acetate (36)

742 mg (1.67 mmol). Yield: 94%. White solid. ¹H-NMR (CDCl₃, 400 MHz): δ 1.28 (t, 3H, J = 7.1 Hz), 1.48-2.28 (m, 12H), 3.44 (s, 2H), 4.27 (q, 2H, J = 7.1 Hz), 4.65 (s, 2H), 6.76-6.79 (m, 2H), 6.97-7.01 (m, 2H), 7.14-7.18 (m, 2H), 7.21-7.23 (m, 2H). ¹³C-NMR (CDCl₃, 100.6 MHz): δ 14.3, 32.3, 37.2, 48.8, 61.5, 112.4, 120.0, 120.6, 126.2, 126.3, 127.6, 143.2, 144.8, 170.0.

Ethyl 2-((*E*)-9-((5*R*,7*R*)-adamantan-2-ylidene)-2-methoxy-7-methylacridin-10(9*H*)-yl)acetate (33a)

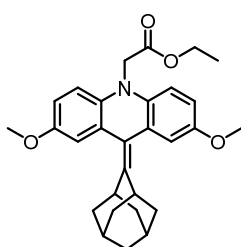
14 mg (0.03 mmol). Yield: 20%. Pale yellow solid. ¹H-NMR (CDCl₃, 400 MHz): δ 1.26 (t, 3H, J = 7.06 Hz), 1.48-2.22 (m, 12H), 2.30 (s, 3H), 3.44 (s, 1H), 3.49 (s, 1H), 3.78 (s, 3H), 4.26 (q, 2H, J = 7.08 Hz), 4.59 (s, 2H), 6.61-6.69 (m, 2H), 6.70-6.75 (m, 1H), 6.77-6.83 (m, 1H), 6.91-6.98 (m, 1H), 7.01 (s, 1H). ¹³C-NMR (CDCl₃, 100.6 MHz): δ 14.4, 20.9, 32.3, 32.5, 37.3, 39.4, 48.9, 55.8, 61.3, 111.4, 112.0, 112.7, 113.5, 120.3, 125.7, 126.9, 127.4, 128.0, 129.4, 137.8, 141.4, 144.7, 153.9, 170.2.

Ethyl 2-((*Z*)-9-((5*S*,7*S*)-adamantan-2-ylidene)-2-fluoro-7-methoxyacridin-10(9*H*)-yl)acetate (33b)

90 mg (0.20 mmol). Yield: 22%. Pale yellow solid. ¹H-NMR (acetone-*d*₆, 400 MHz): δ 1.26 (t, 3H, J = 7.08 Hz), 1.48-2.30 (m, 12H), 3.44 (s, 1H), 3.51 (s, 1H), 3.75 (s, 3H), 4.22 (q, 2H, J = 7.11 Hz), 4.71 (s, 2H), 6.76-6.96 (m, 6H). ¹³C-NMR (acetone-*d*₆, 100.6 MHz): δ 13.6, 32.2, 32.4, 36.5, 39.4, 48.2, 54.8, 60.3, 111.7, 112.3, 112.5, 112.9, 113.2, 113.5, 113.6,

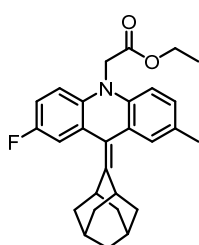
113.7, 119.9, 126.0, 126.5 (x2), 137.4, 140.3, 145.2, 154.1, 156.0, 158.4, 169.1.
¹⁹F-NMR (acetone-d₆, 376 MHz): -121.60.

Ethyl 2-(9-((5*r*,7*r*)-adamantan-2-ylidene)-2,7-dimethoxyacridin-10(9*H*)-yl)acetate (33c)



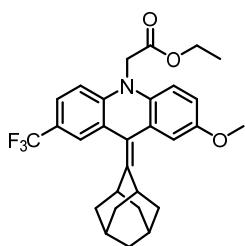
37 mg (0.08 mmol). Yield: 32%. White/pale yellow solid.
¹H-NMR (CDCl₃, 400 MHz): δ 1.27 (t, 3H, J = 7.12 Hz), 1.50-2.30 (m, 12H), 3.49 (s, 2H), 3.77 (s, 6H), 4.26 (q, 2H, J = 7.12 Hz), 4.57 (s, 2H), 6.63-6.70 (m, 2H), 6.70-6.73 (d, 1 H, J = 2.77), 6.73-6.75 (d, 1 H, J = 2.80), 6.77-6.85 (d, 1 H, J = 2.54). ¹³C-NMR (CDCl₃, 100.6 MHz): δ. 14.3, 25.8, 26.1, 32.5 (x2), 37.1, 37.2, 49.0, 55.8, 61.3, 111.5, 112.7, 113.5, 120.3, 127.0, 138.0, 145.3, 153.8, 170.2.

Ethyl 2-((Z)-9-((5*S*,7*S*)-adamantan-2-ylidene)-2-fluoro-7-methylacridin-10(9*H*)-yl)acetate (33d)



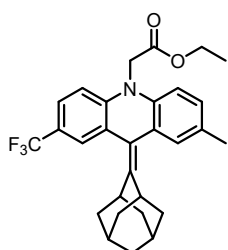
187 mg (0.43 mmol). Yield: 40%. Yellow oil. ¹H-NMR (CDCl₃, 400 MHz): δ 1.28 (t, 3H, J = 7.02 Hz), 1.48-2.24 (m, 12H), 2.32 (s, 3H), 3.43 (s, 2H), 4.27 (q, 2H, J = 7.05 Hz), 4.59 (s, 2H), 6.63-6.71 (m, 2H), 6.81-6.88 (m, 1H), 6.89-6.94 (m, 1H), 6.95-6.98 (m, 1H), 7.01 (s, 1H). ¹³C-NMR (CDCl₃, 100.6 MHz): δ 14.3, 20.9, 32.3, 37.1, 61.5, 112.2, 112.4, 112.6, 112.8, 112.9, 113.8, 114.1, 119.6, 125.5, 127.1, 127.60, 127.64, 128.0, 129.9, 139.9, 141.1, 145.6, 156.5, 158.8, 169.9. ¹⁹F-NMR (CDCl₃, 376 MHz): -125.30.

Ethyl 2-((E)-9-((5R,7R)-adamantan-2-ylidene)-2-methoxy-7-(trifluoromethyl)acridin-10(9H)-yl)acetate (33e)



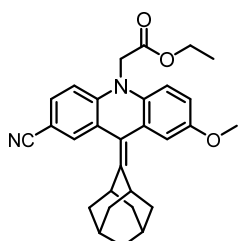
410 mg (0.82 mmol). Yield: 50%. Pale yellow solid. $^1\text{H-NMR}$ (CDCl_3 , 400 MHz): δ 1.30 (t, 3H, $J = 7.12$ Hz), 1.48-2.30 (m, 12H), 3.30 (s, 1H), 3.50 (s, 1H), 3.79 (s, 3H), 4.29 (q, 2H, $J = 7.12$ Hz), 4.63 (s, 2H), 6.69-6.83 (m, 4H), 7.40 (s, 2H). $^{13}\text{C-NMR}$ (CDCl_3 , 100.6 MHz): δ 13.6, 31.7, 31.8, 36.3, 48.2, 55.1, 61.0, 111.0, 111.3, 112.6, 112.7, 118.3, 121.3, 121.6, 122.71 (x2), 123.9 (x2), 124.7, 126.4, 127.6, 128.4, 136.0, 145.4, 146.1, 153.9, 168.8. $^{19}\text{F-NMR}$ (CDCl_3 , 376 MHz): -61.75.

Ethyl 2-((Z)-9-((5S,7S)-adamantan-2-ylidene)-2-methyl-7-(trifluoromethyl)acridin-10(9H)-yl)acetate (33f)



20 mg (0.04 mmol). Yield: 36%. White solid. $^1\text{H-NMR}$ (CDCl_3 , 400 MHz): δ 1.28 (t, 3H, $J = 7.11$ Hz), 1.48-2.25 (m, 12H), 2.32 (s, 3H), 3.29 (s, 1H), 3.44 (s, 1H), 4.27 (q, 2H, $J = 7.22$ Hz), 4.64 (s, 2H), 6.63-6.72 (m, 1H), 6.76-6.82 (m, 1H), 6.94-7.01 (m, 1H), 7.01-7.04 (m, 1H), 7.36-7.43 (m, 2H). $^{13}\text{C-NMR}$ (CDCl_3 , 100.6 MHz): δ 14.3, 20.9, 27.0, 32.3, 37.1, 48.8, 61.6, 112.1, 112.5, 127.2, 128.0, 137.1, 142.5, 148.3, 168.9. $^{19}\text{F-NMR}$ (CDCl_3 , 376 MHz): -61.81.

Ethyl 2-((E)-9-((5R,7R)-adamantan-2-ylidene)-2-cyano-7-methoxyacridin-10(9H)-yl)acetate (33g)

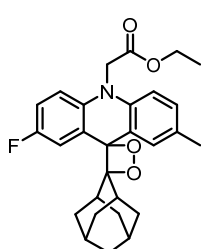


6 mg (0.01 mmol). Yield: 14%. Pale yellow solid. ¹H-NMR (CDCl₃, 400 MHz): δ 1.29 (t, 3H, J = 7.04 Hz), 1.46-2.28 (m, 12H), 3.26 (s, 1H), 3.47 (s, 1H), 3.79 (s, 3H), 4.28 (q, 2H, J = 7.06 Hz), 4.62 (s, 2H), 6.68-6.82 (m, 4H), 7.41 (m, 2H).

Synthesis of 1,2-dioxetanes via photooxygenation reaction under batch conditions (27a, 27d-e, 27g).¹¹⁰

Alkene (**33a**, **33d-e**, **33g**, 16 equiv.) and MB (1 equiv.) were dissolved in CH₂Cl₂ (2 mL/20 mg of SM) inside a home-made photochemical reactor. The solution was cooled at -20 °C, subjected to an oxygen atmosphere (1 atm, balloon) and irradiated by a 1000 W red LED lamp until the starting material disappeared. The crudes were purified by *i*) a filtration on a 5 mm layer of silica gel using CH₂Cl₂ as eluent or *ii*) an extraction with H₂O/Et₂O. The filtered solutions or the combined dried organic layers were concentrated under reduced pressure to dryness at 0°C to give the desired products (**27d-e**, **27g**). The reaction conducted on compound **27a** gave a complex crude.

Ethyl 2-((5''r,7''r)-2-fluoro-7-methyl-10H-dispiro[acridine-9,3'-[1,2]dioxetane-4',2''-adamantan]-10-yl)acetate (27d)

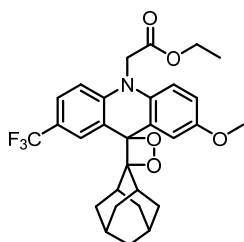


17 mg (0.04 mmol). Yield: 79%. Yellow solid. ¹H-NMR (CDCl₃, 400 MHz): δ 0.63 (t, 2H, J = 12 Hz), 1.15-2.12 (m, 10H), 2.42 (s, 2H), 2.48 (s, 3 H), 4.27 (q, 2H, J = 8.00 Hz), 4.59 (s, 2H), 6.66-6.79 (m, 2H), 7.01-7.12 (m, 1H), 7.14-7.20 (m, 1H), 7.88-7.95 (m, 1H), 7.95-8.01 (m, 1H). ¹³C-NMR (CDCl₃, 100.6 MHz): δ 14.3, 20.7, 27.5, 29.8, 36.4,

3.1 Synthesis

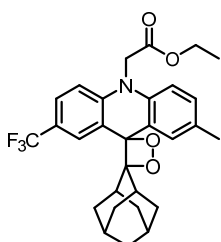
39.4, 47.1, 48.8, 62.4, 112.5, 112.7, 114.2, 116.3 (x2), 121.8, 122.2, 122.5, 127.4, 131.9, 135.9, 138.9, 140.4, 156.6, 159.1, 168.3. ^{19}F -NMR (CDCl_3 , 376 MHz): -79.27.

Ethyl 2-((5''r,7''r)-2-methoxy-7-(trifluoromethyl)-10H-dispiro[acridine-9,3'-[1,2]dioxetane-4',2''-adamantan]-10-yl)acetate (27e)



9 mg (0.02 mmol). Yield: 45%. Yellow solid. ^1H -NMR (CDCl_3 , 400 MHz): δ 0.56 (d, 2H, $J = 13.4$ Hz), 1.15-2.17 (m, 10H), 2.35 (s, 1H), 2.55 (s, 1H), 3.90 (s, 3H), 4.32 (q, 2H, $J = 7.04$ Hz), 4.64 (s, 2H), 6.73-6.91 (m, 2H), 6.94-7.02 (dd, 1H, $J_1 = 2.94$, $J_2 = 8.86$), 7.55-7.64 (m, 1H), 7.73-7.80 (m, 1H), 8.43-8.49 (m, 1H). ^{13}C -NMR (CDCl_3 , 100.6 MHz): δ 14.3, 25.5, 25.7, 31.7, 31.8, 32.9, 33.0, 36.4, 48.8, 56.0, 62.0, 98.0, 107.3, 111.9, 112.5, 113.4, 115.1, 116.4, 125.2, 128.5, 129.2, 131.1, 137.4, 148.2, 151.8, 168.9. ^{19}F -NMR (CDCl_3 , 376 MHz): -61.71

Ethyl 2-((5''r,7''r)-2-methyl-7-(trifluoromethyl)-10H-dispiro[acridine-9,3'-[1,2]dioxetane-4',2''-adamantan]-10-yl)acetate (27g)

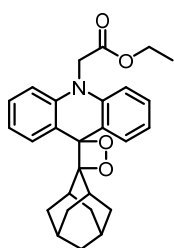


21 mg (0.04 mmol). Yield: 93%. Yellow solid. ^1H -NMR (CDCl_3 , 400 MHz): δ 0.59 (t, 2H, $J = 14.3$ Hz), 1.18 (d, 2H, $J = 12.1$ Hz), 1.28 (t, 3H, $J = 7.09$ Hz), 1.36-1.86 (m, 8H), 2.15 (s, 1H), 2.31 (s, 1H), 2.44 (s, 3H), 4.28 (q, 2H, $J = 7.07$ Hz), 4.65 (s, 2H), 6.71-6.78 (m, 1H), 6.84-6.90 (m, 1H), 7.18-7.23 (m, 1H), 7.56-7.63 (m, 1H), 7.99-8.03 (m, 1H), 8.45-8.50 (m, 1H). ^{13}C -NMR (CDCl_3 , 100.6 MHz): δ 14.3, 20.9, 25.5, 25.7, 31.7, 31.8, 33.0 (x3), 36.0, 36.1, 48.5, 86.7, 97.8, 112.0, 112.1, 121.2, 121.8, 125.9, 126.2, 128.7, 130.3, 131.5, 136.5, 141.9, 168.8. ^{19}F -NMR (CDCl_3 , 376 MHz): -61.79.

Continuous flow set-up for the optimization of photooxygenation step: Corning reactor

A syringe pump from Syrris ltd equipped with Asia red syringes (2.5 mL/5.0 mL, flow rate range= 50 μL -10 mL min^{-1}) was used to convey the feed solution of olefin **36** and MB into the Corning[®] Advanced-Flow[™] Lab Photo Reactor manufactured by Corning SAS (1 fluidic module, 2.6 mL internal volume). The gas flow rate was controlled with a Bronkhorst[®] F210C[™] mass flow controller (MFC). A Zaiput Flow Technologies[®] dome-type back-pressure regulator (BPR) was inserted downstream and connected to a cylinder of compressed nitrogen (set point: 5.6 barg). The reactor was maintained at reaction temperature with a LAUDA Integral XT 280 thermostat while LAUDA[®] Proline RP 845[™] thermostat was used for the thermoregulation of the mesofluidic reaction glass module and the LED illumination setup at 15 °C using silicone oil as coolant. LED panels were mounted on both sides of the fluidic module (40 mm from the centre of the reaction path). Each LED panel was equipped with multiple wavelengths (20 LEDs for 6 wavelengths) with wireless intensity control.

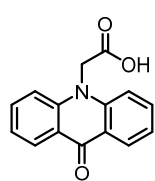
Ethyl 2-(9-((5r,7r)-adamantan-2-ylidene)acridin-10(9H)-yl)acetate (**3**)



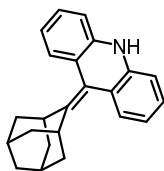
20 mg (0.05 mmol). Yield: 97%. Yellow solid. ¹H-NMR (CDCl₃, 400 MHz): δ 0.62 (d, 2H, J = 12.4 Hz), 1.15 (d, 2H, J = 12.4 Hz), 1.27 (t, 3H, J = 7.1 Hz), 1.37-2.07 (m, 8H), 2.28 (s, 2H), 4.28 (q, 2H, J = 7.08 Hz), 4.65 (s, 2H), 6.81-6.83 (m, 2H), 7.18-7.22 (m, 2H), 7.35-7.39 (m, 2H), 8.20-8.22 (m, 2H). ¹³C-NMR (CDCl₃, 100.6 MHz): δ 14.2, 17.4, 25.4, 25.6, 26.9, 31.7, 32.8, 32.9, 36.1, 39.2, 48.4, 61.6, 86.8, 97.8, 111.8, 121.0, 121.6, 128.4, 129.1, 139.1, 169.2.

Development of a new molecular probe based on TCL phenomenon

Compound **39** was synthesized following a classical alkaline hydrolysis procedure from the corresponding ester derivative **26**.¹⁶⁶ A solution of NaOH (10 mL, 0.5 M) was added to a suspension of **26** (1.78 mmol, 1 equiv.) in EtOH (33 mL, 0.05 M). The solution was stirred at r.t. overnight. The crude was poured into cold water and acidified until pH= 4-5 using HCl 6N. The water solution was extracted with EtOAc, and the combined organic layers were washed with H₂O, brine and dried over anhydrous Na₂SO₄. After evaporated the solvent, the crude was use for the next step without any further purification.

2-(9-oxoacridin-10(9H)-yl)acetic acid (39)

444 mg (1.75 mmol). Yield: > 98%. Yellow solid. ¹H-NMR (CDCl₃, 400 MHz): δ 5.31 (s, 2H), 7.27-7.37 (m, 2H), 7.62-7.68 (m, 2H), 7.74-7.83 (m, 2H), 8.31-8.37 (m, 2H). ¹³C-NMR (CDCl₃, 100.6 MHz): δ 48.1, 116.3, 122.1, 122.2, 127.2, 134.8, 142.7, 170.6, 177.3.

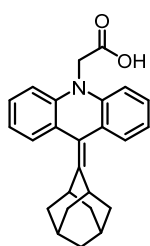
9-((1r,3r,5r,7r)-adamantan-2-ylidene)-9,10-dihydroacridine (41)

Compound **41** was submitted at general McMurry procedure reported in literature starting from the commercial 9(10*H*)-acridanone **40**.^{25a} 138 mg (0.4405 mmol). Yield: 43%. Pale yellow solid. ¹H-NMR (CDCl₃, 400 MHz): δ 1.50-2.11 (m, 12H), 3.50 (brs, 2 H), 6.81-6.87 (m, 2H), 6.88-7.00 (m, 2H), 7.07-7.13 (m, 2H), 7.20-7.26 (m, 2H). ¹³C-NMR (CDCl₃, 100.6 MHz): δ 27.2, 31.8, 37.9, 38.8, 113.9, 120.4, 123.2, 126.4, 127.8, 142.8, 144.3.

General procedure for hydrolysis of intermediate **37**.¹⁶⁷

To a suspension of starting material **36** (1 equiv.) in EtOH absolute (1.1 mL, 0.23 M), an aqueous solution of NaOH 15 % (w/w) (383 μ L) was added dropwise and the suspension was heated at reflux for 10 minutes. After the complete dissolution of starting material (yellow solution), the mixture was cooled at 0 °C and HCl 3 N was added until pH= 4. The mixture was extracted with EtOAc. The combined organic phases were washed with H₂O, brine, dried over anhydrous Na₂SO₄, and concentrated under reduced pressure. The desired product proved to be unstable. The crude was used for the next step without any further purification.

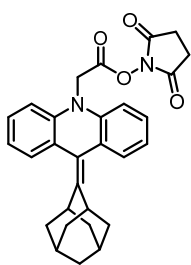
2-(9-((5*r*,7*r*)-adamantan-2-ylidene)acridin-10(9*H*)-yl)acetic acid (**37**).¹⁶⁸



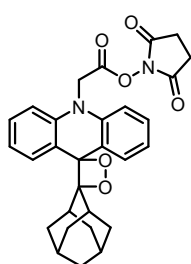
93 mg (0.25 mmol). White/brownish solid. ¹H-NMR (DMSO-d₆, 400 MHz): δ 1.13-2.23 (m, 12H), 5.39 (s, 2H), 6.91 (d, 2H, J = 7.00 Hz), 7.01 (t, 2H, J = 7.00 Hz), 7.08-7.15 (m, 4H).

General procedure for Succinimide Coupling (**43** and **50**)¹⁷⁰

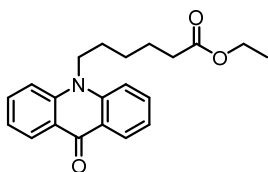
Corresponding acid derivative **37** and/or **49** (1 equiv.) and 1-hydroxybenzotriazole hydrate (1.5 equiv.) dissolved in anhydrous DMF (0.02 M) were treated with *N*-methyl morpholine (3.5 equiv.) and *N*-hydroxysuccinimide (1.3 equiv.) followed by TBTU (1.5 equiv.) addition. The mixture was stirred overnight at r.t.. After the complete disappearance of starting material, the crudes were washed with a solution of LiCl 5% and extracted with EtOAc. The combined organic phases were washed with H₂O, brine and dried over anhydrous Na₂SO₄. The crudes were concentrated under reduced pressure and purified by automated flash chromatography to give the desired products **43** and **50**.

2,5-dioxopyrrolidin-1-yl 2-(9-((5*r*,7*r*)-adamantan-2-ylidene)acridin-10(9*H*)-yl)acetate (43)

50 mg (0.11 mmol). Overall yield: 40% (after two steps). White/pale yellow solid. ¹H-NMR (CDCl₃, 400 MHz): δ 1.50-2.20 (m, 12H), 2.74 (s, 4 H), 3.44 (s, 2H), 5.00 (s, 2H), 6.88-6.94 (m, 2H), 7.01-7.08 (m, 2H), 7.19-7.27 (m, 4H). ¹³C-NMR (CDCl₃, 100.6 MHz): δ 15.7, 25.9, 32.6, 37.5, 40.6, 46.6, 66.3, 112.9, 120.1, 121.6, 126.9 (x2), 127.9, 142.9, 145.7, 165.7, 169.3 (x2).

2,5-dioxopyrrolidin-1-yl 2-((5''*r*,7''*r*)-10H-dispiro[acridine-9,3'-[1,2]dioxetane-4',2''-adamantan]-10-yl)acetate (44)

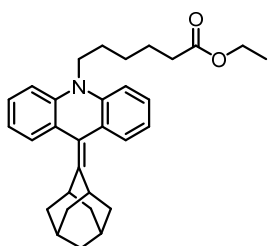
Compound **44** was synthesized according to the photooxygenation procedure.¹¹⁰ 18 mg (0.04 mmol). Yield: 87%. Pale yellow solid. ¹H-NMR (CDCl₃, 400 MHz): δ 0.65 (d, 2H, J = 12 Hz), 1.18-1.54 (m, 10H), 2.32 (s, 2H), 2.89 (s, 4H), 5.05 (s, 2H), 6.97-7.01 (m, 2H), 7.27-7.32 (m, 2H), 7.44-7.51 (m, 2H), 8.23-8.28 (m, 2H).

Ethyl 6-(9-oxoacridin-10(9*H*)-yl)hexanoate (47)

Compound **47** was synthesized according to alkylation procedure using ethyl 6-bromohexanoate as alkylation agent starting from the commercial 9(10*H*)-acridone **40**.^{25c} 1.6 g (4.76 mmol). Yield: 62%. Yellow solid. ¹H-NMR (CDCl₃, 400 MHz): δ 1.16 (t, 3H, J = 7.09 Hz), 1.38-1.49 (m, 2H), 1.58-1.69 (m, 2H), 1.69-1.79 (m, 2H), 2.24 (t, 3H, J = 7.24 Hz), 4.04 (q, 2H, J = 7.23 Hz), 4.07-4.11 (m, 4 H), 7.05-7.12 (m, 2H), 7.23-7.29 (m, 2H), 7.48-7.56 (m,

2H), 8.35-8.41 (m, 2H). $^{13}\text{C-NMR}$ (CDCl_3 , 100.6 MHz): δ 14.4, 24.7, 26.4, 26.9, 34.1, 45.9, 60.4, 114.6, 121.1, 122.3, 127.7, 133.9, 141.6, 173.4, 177.8.

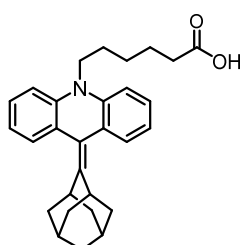
Ethyl 6-(9-((5r,7r)-adamantan-2-ylidene)acridin-10(9H)-yl)hexanoate (48)



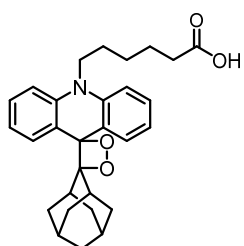
Compound **48** was synthesized according to McMurry procedure starting from **47**.^{25a} 580 mg (1.27 mmol). Yield: 63%. Colorless oil. $^1\text{H-NMR}$ (CDCl_3 , 400 MHz): δ 1.25 (t, 3H, $J = 7.08$ Hz), 1.36-1.47 (m, 2H), 1.60-1.69 (m, 2H), 1.80-1.88 (m, 2H), 1.86-2.23 (m, 10 H), 2.27 (t, 3H, $J = 7.40$ Hz), 3.45 (s, 2H), 3.96 (t, 2H, $J = 6.95$), 4.12 (q, 2H, $J = 7.13$ Hz), 6.93-7.04 (m, 4H), 7.15-7.25 (m, 4H). $^{13}\text{C-NMR}$ (CDCl_3 , 100.6 MHz): δ 14.4, 24.8, 26.3, 26.6, 32.3, 34.4, 37.3, 45.2, 60.4, 60.5, 113.1, 120.0, 120.8, 126.3, 126.9, 127.5, 143.7, 143.0, 173.7.

General procedure for hydrolysis of intermediate 48.

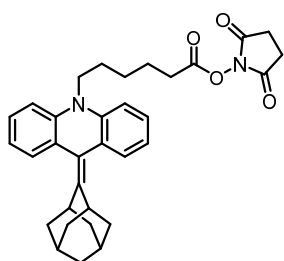
To a suspension of corresponding ester derivative **48** in EtOH absolute (8 mL, 0.02 M), an aqueous solution of LiOH (1.5 equiv.) was added and the suspension was stirred overnight at r.t.. After the complete disappearance of starting material, the mixture was diluted with H_2O and extracted with CH_2Cl_2 . The water phase was acidified with HCl 3 N until pH= 3 and extracted with CH_2Cl_2 . The organic phase was washed with H_2O , brine, dried over anhydrous Na_2SO_4 , and concentrated under reduced pressure. The crude was used for the next step without any further purification.

6-(9-((5*r*,7*r*)-adamantan-2-ylidene)acridin-10(9*H*)-yl)hexanoic acid (49)

68 mg (0.16 mmol). Yield: > 98%. Pale yellow solid. ¹H-NMR (CDCl₃, 400 MHz): δ 1.35-1.46 (m, 2H), 1.60-1.69 (m, 2H), 1.80-1.86 (m, 2H), 1.83-2.26 (m, 8H), 2.31 (t, 2H, J = 7.34 Hz), 3.41 (s, 2H), 3.96 (t, 2H, J = 6.72 Hz), 6.91-7.02 (m, 4H), 7.14-7.23 (m, 4H). ¹³C-NMR (CDCl₃, 100.6 MHz): δ 24.5, 26.2, 26.5, 32.3, 34.0, 37.2, 45.3, 113.2, 120.1, 120.7, 126.2, 127.0, 127.5, 143.6, 144.2, 179.6.

6-((5'*r*,7''*r*)-10*H*-dispiro[acridine-9,3'-[1,2]dioxetane-4',2''-adamantan]-10-yl)hexanoic acid (45)

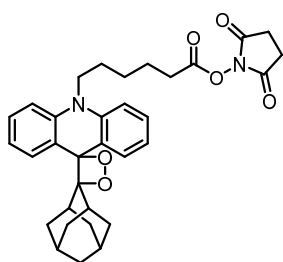
Compound **45** was synthesized according to the photooxygenation procedure starting from **49**.¹¹⁰ 13 mg (0.03 mmol). Yield: 59%. Pale yellow solid. ¹H-NMR (CDCl₃, 400 MHz): δ 0.58 (d, 2H, J = 12.7), 1.46-1.56 (m, 2H), 1.58-1.67 (m, 2H), 1.80-1.86 (m, 2H), 1.86-2.26 (m, 10H), 2.44 (t, 2H, J = 7.34 Hz), 2.55 (s, 2H), 3.96 (t, 2H, J = 8.11), 7.00-7.05 (m, 2H), 7.50-7.78 (m, 2H), 8.17-8.23 (dd, 2H, J₁ = 1.59, J₂ = 7.72 Hz), 8.56-8.62 (dd, 2H, J₁ = 1.64, J₂ = 8.03 Hz).

2,5-dioxopyrrolidin-1-yl 6-(9-((5*r*,7*r*)-adamantan-2-ylidene)acridin-10(9*H*)-yl)hexanoate (50)

Compound **50** was synthesized according to succinimide coupling procedure starting from **49**.¹⁷⁰ 99 mg (0.19 mmol). Yield: 81%. Pale yellow solid. ¹H-NMR (CDCl₃, 400 MHz): δ 1.47-1.57 (m, 2H), 1.73-1.81 (m, 2H), 1.80-1.88 (m, 2H), 1.86-2.35 (m, 10H), 2.57 (t, 3H, J = 8.00 Hz), 2.78 (s, 4H), 3.44 (s, 2H),

3.97 (t, 2H, J = 4.00), 6.93-7.05 (m, 4H), 7.15-7.25 (m, 4H). ¹³C-NMR (CDCl₃, 100.6 MHz): δ 24.7, 56.0, 26.3, 26.4, 31.3, 37.5, 45.4, 113.2, 119.7, 121.0, 126.9, 127.2, 127.3, 143.6, 144.2, 168.9, 169.6 (x2).

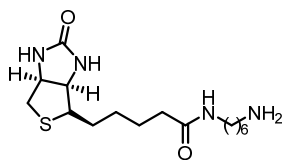
2,5-dioxopyrrolidin-1-yl 6-((5''r,7''r)-10H-dispiro[acridine-9,3'-[1,2]dioxetane-4',2''-adamantan]-10-yl)hexanoate (46)



Compound **46** was synthesized according to photooxygenation procedure starting from **50**.¹¹⁰ 17 mg (0.03 mmol). Yield: 81%. Pale yellow solid. ¹H-NMR (CDCl₃, 400 MHz): δ 0.59 (d, 2H, J = 12.74), 1.09-2.10 (m, 16H), 2.25 (s, 2H), 2.68 (t, 2H, J = 7.14 Hz), 2.86 (s, 4H), 3.98 (t, 2H, J = 7.98), 7.00-7.06 (m, 2 H), 7.11-7.19 (m, 2H), 7.35-7.43 (m, 2H), 8.17-8.23 (dd, 2H, J₁ = 1.03, J₂ = 7.69 Hz).

General procedure for the synthesis of bt-hexanediamine adduct (53).¹⁷⁶

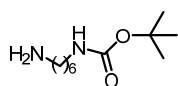
D-bt (**52**, 1.23 mmol, 1 equiv.) and *N,N'*-disuccinimidyl carbonate (DSC, 1.40 mmol, 1.14 equiv.) were dissolved in anhydrous DMF (10 mL, 0.12 M), and Et₃N (300 μL, 4.1 M) was added. The solution was stirred at r.t. for 6 hours, after that a solution of 1,6-hexanediamine (11.6 mmol, 9.4 equiv.) in anhydrous DMF was added. The mixture was stirred at r.t. overnight. The precipitate thus formed was filtrated, washed with Et₂O and CH₂Cl₂, and dried in vacuo. The crude was used for the next step without any further purification.

N-(6-aminohexyl)-5-((3aR,4S,6aS)-2-oxohexahydro-1H-thieno[3,4-d]imidazol-4-yl)pentanamide (53)

421 mg (1.23 mmol). Yield: > 98%. White solid. ¹H-NMR (DMSO-d₆, 400 MHz): δ 1.20-1.60 (m, 14H), 2.02 (t, 2H, J = 7.29 Hz), 2.56 (d, 1H, J = 12.57 Hz), 2.80 (dd, 1H, J₁ = 5.03, J₂ = 12.42 Hz), 2.96-3.02 (m, 2H), 3.06-3.09 (m, 1H), 4.08-4.14 (m, 1H), 4.26-4.31 (m, 1H), 6.35 (brs, 1 H), 6.42 (brs, 1H), 7.71 (brs, 1H). ¹³C-NMR (DMSO-d₆, 100.6 MHz): δ 26.0, 26.7, 28.6 (x2), 28.8, 29.7, 35.8, 38.9, 40.5, 56.0, 59.8, 61.7, 163.3, 172.4.

General procedure for mono-BOC protection (55).¹⁷⁸

Under nitrogen atmosphere, a solution of di-tert-butyl dicarbonate (Boc₂O, 1.78 mmol, 0.2 equiv.) in CHCl₃ (9 mL, 1 M) was added dropwise to a solution of 1,6-hexanediamine (8.88 mmol, 1 equiv.) in CHCl₃ (45 mL, 0.2 M) at 0 °C. The reaction was stirred at r.t. overnight. The crude was concentrated and purified through automated flash chromatography.

Tert-butyl (6-aminohexyl)carbamate (55)

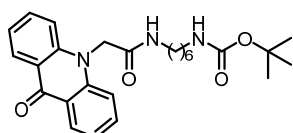
132 mg (0.61 mmol). Yield: 44%. Yellow semisolid. ¹H-NMR (CDCl₃, 400 MHz): δ 1.07 (s, 2H), 1.23-1.30 (m, 4H), 1.33-1.43 (m, 13H), 2.61 (t, 2H, 4.50), 3.03 (m, 2H), 4.77 (brs, 1H). ¹³C-NMR (CDCl₃, 100.6 MHz): δ 26.5, 27.1, 28.2, 30.7, 33.3, 40.3, 41.8, 78.5, 155.9.

General procedure for coupling using COMU (56).¹⁷⁹

Under nitrogen atmosphere, COMU coupling reagent (0.82 mmol, 1 equiv.) was added to a solution of the acid **39** (0.82 mmol, 1 equiv.), *N,N*-diisopropylethylamine (DIPEA, 1.65 mmol, 2 equiv.) and mono-*N*-Boc

hexanediamine **55** (0.82 mmol, 1 equiv.) in anhydrous DMF (13 mL, 0.06 M) at 0 °C. The solution was stirred at 0 °C for 1 hour and then at r.t. overnight. The crude was washed with a solution of LiCl 5% (w/v) and extracted with EtOAc. The combined organic layers were washed with H₂O, brine, dried over Na₂SO₄, and evaporated under vacuum. The crude was purified by automated flash chromatography.

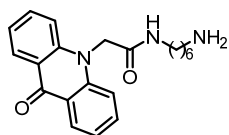
Tert-butyl (6-(2-(9-oxoacridin-10(9H)-yl)acetamido)hexyl)carbamate (56)



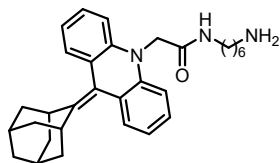
332 mg (0.73 mmol). Yield: 91%. Yellow solid. ¹H-NMR (CDCl₃, 400 MHz): δ 1.17-1.24 (m, 4H), 1.31-1.40 (m, 11H), 1.43-1.51 (m, 2H), 2.94 (q, 2H, J = 6.31 Hz), 3.29 (q, 2H, J = 6.35 Hz), 4.58 (s, 1H), 4.83 (s, 2H), 6.93-7.04 (m, 2H), 7.20-7.28 (m, 2H), 7.39-7.46 (m, 1H), 7.53-7.62 (m, 2H), 7.83-7.90 (m, 2H). ¹³C-NMR (CDCl₃, 100.6 MHz): δ 26.0, 26.2, 28.3, 29.1, 29.9, 39.4, 40.1, 50.6, 78.9, 114.5, 121.8 (x2), 127.0, 134.1, 142.1, 156.1, 167.3, 177.8.

General procedure for BOC deprotection (57).

Under nitrogen atmosphere, trifluoroacetic acid (TFA, 12 mmol, 18 equiv.) was added to a solution of **56** (0.65 mmol, 1 equiv.) in anhydrous CH₂Cl₂ (12 mL, 0.05 M) at 0 °C. The reaction was stirred at r.t. for 3 hours. The crude was neutralized with NaHCO_{3(ss)} until pH= 8. The basic aqueous solution was extracted with CH₂Cl₂. The combined organic layers were washed with H₂O, brine, dried over anhydrous Na₂SO₄, and evaporated under vacuum. The crude was used for the next step without a further purification.

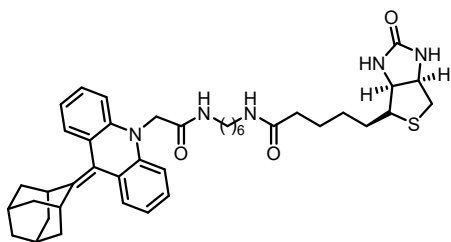
N-(6-aminohexyl)-2-(9-oxoacridin-10(9H)-yl)acetamide (57)

152 mg (0.43 mmol). Yield: 66%. Yellow solid. ¹H-NMR (CD₃OD, 400 MHz) δ 1.15-1.30 (m, 4H), 1.30-1.45 (m, 2H), 1.45-1.52 (m, 2H), 2.58 (t, 2H, J = 7.12 Hz), 3.20 (t, 2H, 6.96 Hz), 5.02 (s, 2H), 7.15-7.24 (m, 2H), 7.39-7.45 (m, 2H), 7.62-7.70 (m, 2H), 8.21-8.29 (dd, 2H, J₁ = 1.57, J₂ = 8.05). ¹³C-NMR (CD₃OD, 100.6 MHz): δ 26.1, 26.3, 28.9, 31.8, 39.1, 40.8, 49.1, 115.1, 121.5, 121.7, 126.6, 134.1, 142.5, 168.2, 178.3.

2-(9-((1r,3r,5r,7r)-adamantan-2-ylidene)acridin-10(9H)-yl)-N-(6-aminohexyl)acetamide (58)

Compound **58** was synthesized following the McMurry procedure and quenched under basic conditions.^{25a} The crude was used without any further purification. ¹H-NMR (CDCl₃, 400 MHz): δ 0.98-1.08 (m, 2H), 1.12-1.22 (m, 2H), 1.28-1.35 (m, 5H), 1.37-1.55 (m, 4H), 1.89 (s, 3H), 1.94-2.29 (m, 4H), 2.60 (t, 2H, J = 7.2 Hz), 3.19 (q, 2H, J = 6.8 Hz), 3.44 (s, 2H), 4.57 (s, 2H), 5.93 (s, 1H), 6.93 (d, 2H, J = 8.2), 7.05 (td, 2H, J₁ = 7.6, J₂ = 1.2 Hz), 7.19 (td, 2H, J₁ = 7.6, J₂ = 1.2 Hz, 2H), 7.28-7.24 (m, 2H). ¹³C-NMR (CDCl₃, 100 MHz) δ 26.3 (x2), 29.2, 32.2, 33.3, 36.9, 39.1, 41.9, 50.4, 112.4, 119.7, 121.1, 126.4, 126.7, 127.4, 142.7, 145.5, 168.5.

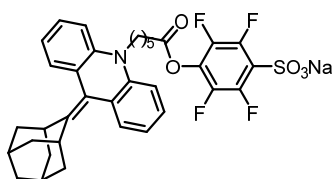
N-(6-(2-(9-((1*r*,3*r*,5*r*,7*r*)-adamantan-2-ylidene)acridin-10(9*H*)-yl)acetamido)hexyl)-5-((3*a*S,4*R*,6*a*R)-2-oxohexahydro-1*H*-thieno[3,4-*d*]imidazol-4-yl)pentanamide (54)



Compound **54** was synthesized following the general coupling procedure between D-bt **52** and the corresponding McMurry derivative **58** using COMU as coupling agent.¹⁷⁹ 63 mg (0.10 mmol). Overall yield: 28%

(after two steps). Yellow solid. ¹H-NMR (CDCl₃, 400 MHz): δ 1.04-1.23 (m, 4H), 1.25-1.50 (m, 10H), 1.59-1.79 (m, 6H), 1.89 (s, 3H), 2.17-2.23 (m, 5H), 2.73 (d, 1H, J = 12.89 Hz), 2.90 (dd, 1H, J₁ = 4.86, J₂ = 12.79 Hz), 3.12-3.22 (m, 5H), 3.44 (s, 2H), 4.31 (dd, 1H, J₁ = 4.42, J₂ = 7.81 Hz), 4.50 (dd, 1H, J₁ = 5.13, J₂ = 7.73 Hz), 4.58 (s, 2H), 5.46 (s, 1H), 5.95-6.10 (m, 2H), 6.18 (s, 1H), 6.90-6.94 (m, 2H), 7.02-7.08 (m, 2H), 7.17-7.23 (m, 2H), 7.23-7.28 (m, 2H). ¹³C-NMR (CDCl₃, 100.6 MHz): δ 25.6, 26.0, 26.1, 28.0, 28.1, 29.2, 29.3, 29.7, 30.9, 32.3, 35.9, 36.9, 39.0, 39.2, 40.5, 53.4, 55.4, 60.1, 61.8, 112.5, 119.7, 121.2, 126.6, 126.8, 127.5, 142.8, 145.7, 163.3, 168.8, 172.9.

Sodium 4-((6-(9-((1*r*,3*r*,5*r*,7*r*)-adamantan-2-ylidene)acridin-10(9*H*)-yl)hexanoyloxy)-2,3,5,6-tetrafluorobenzenesulfonate (66)



Compound **66** was synthesized following the general coupling procedure between 4-sulfo-2,3,5,6-tetrafluorophenol sodium salt (STP) and the corresponding McMurry long chain acid derivative **49**.¹⁷⁹ 74 mg (0.11 mmol). Oil. Yield: 47 %. ¹H-NMR (DMSO-*d*₆, 400 MHz): δ 1.28-2.25 (m, 20H), 2.69 (t, 2H, 6.82 Hz), 3.32 (brs, 2H), 3.96-3.90 (m, 2H), 6.92-7.00 (m, 2H), 7.09-7.22 (m, 6H). ¹³C-NMR (DMSO-*d*₆, 100.6 MHz):

3.2 Computational details

δ 24.2, 25.7, 27.2, 27.4, 28.1, 32.0, 32.9, 34.0, 35.9, 36.8, 38.9, 44.6, 46.7, 113.7, 116.5, 120.2, 120.6, 121.3, 121.6, 124.7, 124.8, 124.9, 125.9, 126.8, 127.2, 128.4, 134.8, 139.0, 139.2, 141.5, 141.7, 141.8, 142.1, 143.3, 143.4, 144.5, 169.8, 174.7, 177.3. ^{19}F -NMR (DMSO- d_6 , 376 MHz): -71.43, -69.54.

3.2 Computational details

Conformational Search

MMFF conformational searches were performed with the Spartan suite of programs, using the keywords SEARCHMETHOD=SYSTEMATIC, FINDBOATS and KEEPALL. All the conformers contained in an 8 kcal/mol window were reoptimized at the B3LYP/6-31G(d) DFT level and confirmed as true minima by frequency analysis. DFT calculations were performed with Gaussian 16.¹⁸² Structural and electronic descriptors were taken from the lowest energy conformation obtained at the DFT level after Boltzmann analysis. The computation details (Gibbs energies of conformers and PCA/LDA analysis) are reported in the *Supporting Info* of Moroni *et al.*¹¹⁰

3.3 Analytical measurements

TCL device

A compact imaging system, controlled by a laptop computer, was built by employing a portable battery-operated CCD camera (model MZ-2PRO, MagZero, Pordenone, Italy) equipped with a thermoelectrically cooled monochrome CCD image sensor. The camera was coupled with an objective (low distortion wide angle lenses 1/3 in 1.28 mm, fl.8) obtained from Edmund Optics

(Barrington, NJ) and connected to a light-tight dark box. The inner surface of the dark box top cover was equipped with a flat heating element ($20 \times 20 \text{ mm}^2$), comprising a serpentine nickel/chrome thin-film resistance (79.5Ω) encased in kapton, and clamps to hold $20 \times 20 \text{ mm}^2$ glass slides in contact with the heater. The heater was powered by the CCD battery and, with the use of a manually regulated resistor, the appropriate voltage was applied to reach the required temperature (e.g., 4.5 V for a 120-140 °C temperature). Thanks to its light reflecting properties, the metal heater also increased the fraction of emitted photons that could reach the CCD sensor. Images, acquired employing 1-min integration time, were recorded in the Flexible Image Transport System (FITS) format and analyzed with the WinLight 32 software version 2.91 (Berthold Technologies GmbH & Co. KG, Bad Wildbad, Germany). For reference, a research-grade luminograph (NightOWLLB 981, Berthold Technologies GmbH & Co. KG) equipped with a back-illuminated, thermoelectrically cooled CCD camera was also employed. In this case, microscope glass slides glued to a $50 \times 70 \text{ mm}^2$ flat heating element were employed as a solid support. The temperature of the support was varied by applying a suitable current and monitored by a copper/constantan thermocouple. Image integration times varied from 5 to 30 seconds (for evaluation of TCL decay kinetics) to 5 minutes (for stability measurements).

TCL Measurements

TCL and fluorescence spectra were recorded using a Varian Eclipse spectrofluorimeter (Varian Inc., Palo Alto, CA). TCL imaging experiments were performed using a LB-980 Night Owl low-light luminograph (Berthold Technologies, Bad Wildbad, Germany). Image integration times varied from 5 seconds (for evaluation of the TCL decay kinetics) to 5 minutes (for assessment of the detectability by TCL imaging). TCL images were acquired and analyzed

to measure the TCL signals using the image analysis software (WinLight 32) provided with the instrument. For TCL imaging measurements, microscope glass slides glued to a flat heating element or high resistivity (70-100 Ω) indium-tin oxide (ITO)-coated microscope glass slides (SPI Supplies/Structure Probe Inc., West Chester, PA) were used as solid supports. In the latter case, heating was provided by a suitable electrical current flowing through the ITO coating. The temperature of the support was controlled by varying the applied current and monitored by a copper/constantan thermocouple. Samples were deposited on the supports as CH_3CN solutions either with a micropipette or using a manual microarrayer (Glass Slide Microarrayer, V&P Scientific Inc., San Diego, CA). The manual microarrayer deposited arrays of spots of about 10 nL with diameters in the range of 500-800 μm depending on the nature of the surface. The spots were left to dry before the TCL measurement.

Estimation of TCL efficiency

The chemiluminescence luminol- H_2O_2 reaction was conducted by adding 0.1 mL of a solution containing hydrogen peroxide (H_2O_2) (1.0×10^{-2} M) in distilled H_2O to 10 μL of a solution containing luminol (3.0×10^{-3} M) and horseradish peroxidase (HRP, 1.0×10^{-4} mg mL^{-1}). For TCL measurements, 10 μL of a 3.0×10^{-3} M solution of each tested TCL compound (**27d**, **27e** and **27g**, **Table 12**) was heated at 120 $^\circ\text{C}$, upon solvent evaporation. In both cases, photon emission was measured using the CCD detector until complete luminescence decay. Each measurement was performed in triplicate. The AUC was calculated and employed to estimate the Φ_{TCL} , as a relative value with respect to luminol Φ_{CL} (1.24) reported in literature.¹⁵⁴

$$\Phi_{\text{TCL}}(\text{dioxetane}) = \frac{[\text{AUC}(\text{dioxetane})]}{[\text{AUC}(\text{luminol})]} \times \Phi_{\text{CL}}(\text{luminol})$$

Table 12. Estimated values of TCL efficiency (Φ_{TCL})

Compound	R ₁	R ₂	TCL efficiency
27d	F	CH ₃	0.01
27e	CF ₃	OCH ₃	0.16
27g	CF ₃	CH ₃	0.36

Synthesis and characterization of PluS NPs

Chemicals. All reagents and solvents were used as received without further purifications: non-ionic triblock surfactant Pluronic PF127, TEOS (99.99%), TMSCl ($\geq 98\%$), AcOH ($\geq 99.7\%$), Prodan P (*N,N*-Dimethyl-6-propionyl-2-naphthylamine, $\geq 98.0\%$), and Nile Red NR ($\geq 98.0\%$) were purchased from Aldrich. Reagent grade NaCl was purchased from Fluka. A MilliQ Millipore system was used for the purification of water (resistivity $<18 \text{ M}\Omega$).

Synthesis. PluS NPs have been synthesized by using methods reported in literature.^{157,183} Briefly, TEOS (180 μL , 0.8 mmol) was added to an acidic aqueous solution (AcOH, 1M) of Pluronic F127 (100 mg) and NaCl (67 mg) under magnetic stirring, and its hydrolysis and condensation was allowed to proceed for 3 hours. TMSCl (10 μL , 0.08 mmol) was then added and the solution was stirred overnight. The resulting Plus NPs dispersion was purified *via* dialysis for at least 4 days, using RC membrane (cut of 12 KDa) against water. The dispersion in the membrane was recovered and diluted to 10 ml, yielding a final PluS NPs concentration of 10 μM .¹⁸⁴

Dimensional characterization of doped PluS NPs

The morphology of PluS NPs was characterized with DLS analysis and TEM microscopy to verify the formation of core-shell silica NPs and their dimension. The size distribution of the doped PluS NPs in H₂O is represented in **Figure 34**,

while **Table 13** reports the size and the PDI values of the distribution (**3** and **27g**, respectively).

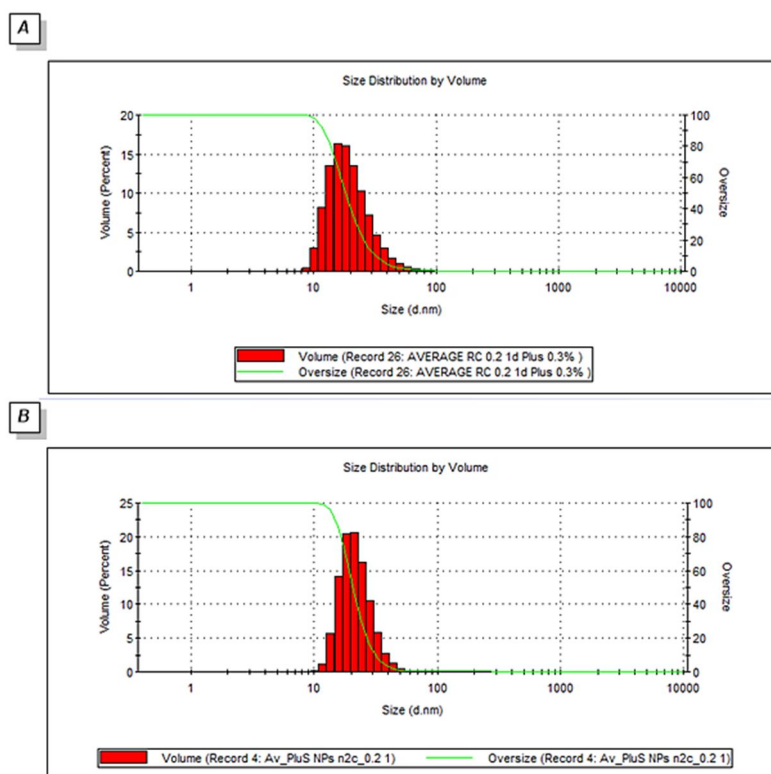


Figure 34. Size distribution by Volume-Histogram and oversize curve of **3** (A) and **27g**-doped PluS NPs (B).

Table 13. Z-Average and PDI values for **1-PluS NPs_0.3%** and **4g-PluS NPs_0.2%** in H₂O.

	Size (d. nm)	PDI ^a
1-PluS NPs_0.3%	20.6	0.345
27g-PluS NPs_0.2%	22.1	0.276

^a Polydispersity index.

Representative Dynamic Light Scattering (DLS) results and Transmission Electron Microscopy (TEM) image used for image analysis are shown in **Figure 35**.

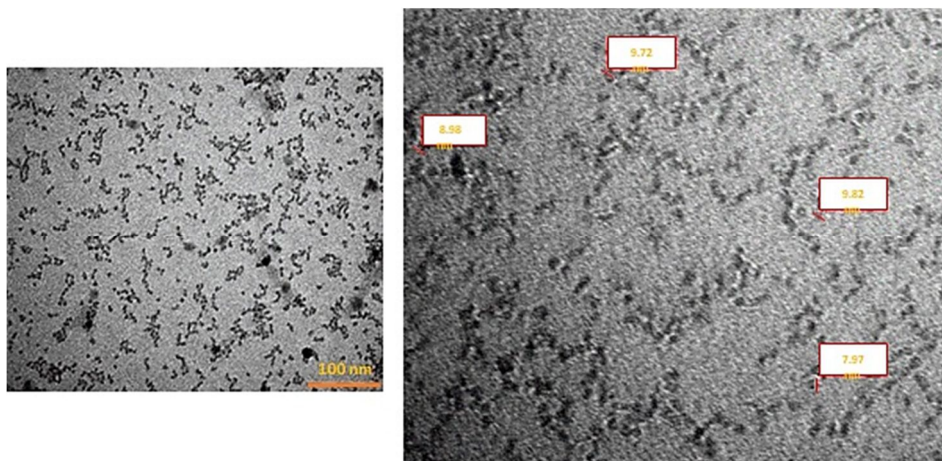


Figure 35. TEM images and diameter distribution of core-shell silica nanoparticles doped with **3**.

DLS measurements and TEM showed uniform characteristics for the synthesized samples in terms of hydrodynamic diameter and of silica core diameter distributions. At the same time, we can observe the presence of black spots probably corresponding to NPs clusters (**Figure 35**).

References and Notes

-
1. Selected publications on CL: a) Roda, A., Mirasoli, M., Michelini, E., Di Fusco, M., Zangheri, M., Cevenini, L., Roda, B., Simoni, P. Progress in chemical luminescence-based biosensors: A critical review. *Biosens. Bioelectron.* **2016**, *76*, 164-179. DOI: [10.1016/j.bios.2015.06.017](https://doi.org/10.1016/j.bios.2015.06.017). b) Mirasoli, M., Guardigli, M., Michelini, E., Roda, A. Recent advancements in chemical luminescence-based lab-on-chip and microfluidic platforms for bioanalysis. *J. Pharm. Biomed.* **2014**, *87*, 36-52. DOI: [10.1016/j.jpba.2013.07.008](https://doi.org/10.1016/j.jpba.2013.07.008). c) Roda, A., Michelini, E., Cevenini, L., Calabria, D., Calabretta, M. M., Simoni, P. Integrating bio-chemiluminescence detection on smartphones: mobile chemistry platform for point-of-need analysis. *Anal. Chem.* **2014**; *86* (15), 7299-7304. DOI: [10.1021/ac502137s](https://doi.org/10.1021/ac502137s). d) Roda, A., Guardigli, M., Pasini, P., Mirasoli, M., Musiani, M. Bio- and chemiluminescence imaging in analytical chemistry. *Anal. Chim. Acta*, **2005**, *541* (1-2), 25-35. DOI: [10.1016/j.aca.2004.11.083](https://doi.org/10.1016/j.aca.2004.11.083). e) Roda, A., Pasini, P., Mirasoli, M., Michelini, E., Guardigli, M. Biotechnological applications of bioluminescence and chemiluminescence. *Trends Biotechnol.* **2004**, *22* (6), 295-303. DOI: [10.1016/j.tibtech.2004.03.011](https://doi.org/10.1016/j.tibtech.2004.03.011). f) Roda, A., Guardigli, M., Michelini, E., Mirasoli M., Pasini, P. Peer reviewed: advances in analytical bioluminescence and chemiluminescence. *Anal. Chem.* **2003**, *75* (21), 462A-470A. DOI: [10.1021/ac031398v](https://doi.org/10.1021/ac031398v).
 2. Selected publications on PL: a) Photoluminescence: advances in research and applications. (Marsden, E. Ed.) *Nova Science Publishers, Inc.*, **2018**, pp. 219. b) Moura, H. S. R. P., Mol, A. R., Sampaio, T. R., Fonseca, A. Image-based luminescence detection for quantitative determinations in continuous flow analysis microsystems. *Anal. Methods*, **2018**, *10* (46), 5571-5576. DOI: [10.1039/C8AY01973H](https://doi.org/10.1039/C8AY01973H). c) Kulmala, S., Suomi, J. Current status of modern analytical luminescence methods. *Anal. Chim. Acta*, **2003**, *500* (1-2), 21-69. DOI: [10.1016/j.aca.2003.09.004](https://doi.org/10.1016/j.aca.2003.09.004).
 3. Wiedemann, E. "Über fluoreszenz und phosphoreszenz. *Ann. Phys.* **1888**, *34*, 446-463. DOI: [10.1002/andp.18882700703](https://doi.org/10.1002/andp.18882700703).

4. Fereja, T. H., Hymete, A., Gunasekaran, T. A recent review on chemiluminescence reaction, principle and application on pharmaceutical analysis. *ISRN Spectrosc.* **2013**, 5-6, 1-12. DOI: [10.1155/2013/230858](https://doi.org/10.1155/2013/230858).
5. a) Reviews in fluorescence 2016. (Geddes, C. D. Ed.), *Springer International*, **2017**, pp. 360. DOI: [10.1007/978-3-319-48260-6](https://doi.org/10.1007/978-3-319-48260-6). b) Gong, X., Cai, J., Zhang, B., Zhao, Q., Piao, J., Peng, W., Gao, W., Zhou, D., Zhao, M., Chang, J. A review of fluorescent signal-based lateral flow immunochromatographic strips. *J. Mater. Chem. B*, **2017**, 5 (26), 5079-5091. DOI: [10.1039/C7TB01049D](https://doi.org/10.1039/C7TB01049D). c) Wolfbeis, O. S. An overview of nanoparticles commonly used in fluorescent bioimaging. *Chem. Soc. Rev.* **2015**, 44 (14), 4743-4768. DOI: [10.1039/C4CS00392F](https://doi.org/10.1039/C4CS00392F). d) Strianese, M., Staiano, M., Ruggiero, G., Labella, T., Pellecchia, C., D'Auria, S. Fluorescence-based biosensors. *Methods Mol. Biol.* **2012**, 875, 193-216. DOI: [10.1007/978-1-61779-806-1_9](https://doi.org/10.1007/978-1-61779-806-1_9). e) Godlewski, M., Turowska, A., Jedynek, P., Martinez, D., Nevalainen, H. Fluorescence applications in biotechnology and life sciences. (Goldys, E. M. Ed.), *Wiley-Blackwell*, **2009**, pp. 99-116.
6. Waters, J. C. Accuracy and precision in quantitative fluorescence microscopy. *J. Cell. Biol.* **2009**, 185 (7), 1135-1148. DOI: [10.1083/jcb.200903097](https://doi.org/10.1083/jcb.200903097).
7. Dodeigne, C., Thunus, L., Lejeune, R. Chemiluminescence as diagnostic tool. A review. *Talanta*, **2000**, 51 (3), 415-439. DOI: [10.1016/s0039-9140\(99\)00294-5](https://doi.org/10.1016/s0039-9140(99)00294-5).
8. Selected reviews on CL applications: a) Lara, F. J., Airado-Rodriguez, D., Moreno-Gonzalez, D., Huertas-Perez, J. F., Garcia-Campana, A. M. Applications of capillary electrophoresis with chemiluminescence detection in clinical, environmental and food analysis. A review. *Anal. Chim. Acta*, **2016**, 913, 22-40. DOI: [10.1016/j.aca.2016.01.046](https://doi.org/10.1016/j.aca.2016.01.046). b) Liu, Y. X., Huang, X. Y., Ren, J. C. Recent advances in chemiluminescence detection coupled with capillary electrophoresis and microchip capillary electrophoresis. *Electrophoresis*, **2016**, 37 (1), 2-18. DOI: [10.1002/elps.201500314](https://doi.org/10.1002/elps.201500314). c) Huertas-Pérez, F. J., Moreno-Gonzalez, D., Airado-Rodriguez, D., Lara, F. J., Garcia-Campana, A. M. Advances in the application of chemiluminescence detection in liquid chromatography. *Trends Anal. Chem.* **2016**, 75, 35-48. DOI: [10.1016/j.trac.2015.07.004](https://doi.org/10.1016/j.trac.2015.07.004). d) Li, N., Su, X., Lu, Y. Nanomaterial-based biosensors using dual transducing elements for solution phase detection. *Analyst*, **2015**, 140 (9), 2916-2943. DOI: [10.1039/C4AN02376E](https://doi.org/10.1039/C4AN02376E). e) Dong, Y., Cai, J., You, X., Chi, Y.

Sensing applications of luminescent carbon based dots. *Analyst*, **2015**, *140* (22), 7468-7486. DOI: [10.1039/C5AN01487E](https://doi.org/10.1039/C5AN01487E). f) Seidel, M., Niessner, R. Chemiluminescence microarrays in analytical chemistry: a critical review. *Anal. Bioanal. Chem.* **2014**, *406* (23), 5589-5612. DOI: [10.1007/s00216-014-7968-4](https://doi.org/10.1007/s00216-014-7968-4). g) Iranifam, M. Analytical applications of chemiluminescence methods for cancer detection and therapy. *Trends Anal. Chem.* **2014**, *59*, 56-183. DOI: [10.1016/j.trac.2014.03.010](https://doi.org/10.1016/j.trac.2014.03.010). h) Park, J. Y., Kricka, L. J. Prospects for the commercialization of chemiluminescence-based point-of-care and on-site testing devices. *Anal. Bioanal. Chem.* **2014**, *406* (23), 5631-5637. DOI: [10.1007/s00216-014-7697-8](https://doi.org/10.1007/s00216-014-7697-8).

9. Selected reviews on BL applications: a) Xu, T. T., Close, D., Handagama, D. W., Marr, E., Sayler, G., Ripp, S. The expanding toolbox of in vivo bioluminescent imaging. *Front. Oncol.* **2016**, *6* (4), 150-157. DOI: [10.3389/fonc.2016.00150](https://doi.org/10.3389/fonc.2016.00150). b) Romieu, A. "AND" luminescent "reactive" molecular logic gates: a gateway to multi-analyte bioimaging and biosensing. *Org. Biomol. Chem.* **2015**, *13* (5), 1294-1306. DOI: [10.1039/C4OB02076F](https://doi.org/10.1039/C4OB02076F). c) Coleman, S. M., McGregor, A. A bright future for bioluminescent imaging in viral research. *Future Virol.* **2015**, *10* (2), 169-183. DOI: [10.2217/fvl.14.96](https://doi.org/10.2217/fvl.14.96). d) Wu, N., Rathnayaka, T., Kuroda, Y. Bacterial expression and re-engineering of gaussia princeps luciferase and its use as a reporter protein. *Biochim. Biophys. Acta*, **2015**, *1854* (10A), 1392-1399. DOI: [10.1016/j.bbapap.2015.05.008](https://doi.org/10.1016/j.bbapap.2015.05.008). e) Lomakina, G. Y., Modestova, Y. A., Ugarova, N. N. Bioluminescence assay for cell viability. *Biochemistry (Moscow)*, **2015**, *80* (6), 701-713. DOI: [10.1134/S0006297915060061](https://doi.org/10.1134/S0006297915060061). f) Hattori, M., Ozawa, T. Bioluminescent tools for the analysis of G-protein-coupled receptor and arrestin interactions. *RSC Adv.* **2015**, *5* (17), 12655-12663. DOI: [10.1039/C4RA14979C](https://doi.org/10.1039/C4RA14979C). g) Markova, S. V., Vysotski, E. S. Coelenterazine-dependent luciferases. *Biochemistry (Moscow)*, **2015**, *80* (6), 714-732. DOI: [10.1134/S0006297915060073](https://doi.org/10.1134/S0006297915060073). h) Coutant, E. P., Janin, Y. L. Synthetic routes to coelenterazine and other imidazo[1,2-a]pyrazin-3-one luciferins: essential tools for bioluminescence-based investigations. *Chem. Eur. J.* **2015**, *21* (48), 17158-17171. DOI: [10.1002/chem.201501531](https://doi.org/10.1002/chem.201501531). i) Roda, A., Guardigli, M., Michelini, E., Mirasoli, M. Bioluminescence in analytical chemistry and in vivo imaging. *Trends Anal. Chem.* **2009**, *28* (3), 307-322. DOI: [10.1016/j.trac.2008.11.015](https://doi.org/10.1016/j.trac.2008.11.015).

-
10. Selected reviews on ECL applications: a) Hesari, M., Mahdi, Z. Review-electrogenerated chemiluminescence: light years ahead. *J. Electrochem. Soc.* **2016**, *163* (4), H3116-H3131. DOI: [10.1149/2.0161604jes](https://doi.org/10.1149/2.0161604jes). b) Doeven, E. H., Barbante, G. J., Hogan, C. F., Francis, P. S. Potential-resolved electrogenerated chemiluminescence for the selective detection of multiple luminophores. *ChemPlusChem*, **2015**, *80* (3), 456-470. DOI: [10.1002/cplu.201402407](https://doi.org/10.1002/cplu.201402407). c) Kirschbaum, S. E. K., Baeumner, A. J. A review of electrochemiluminescence (ECL) in and for microfluidic analytical devices. *Anal. Bioanal. Chem.* **2015**, *407* (14), 3911-3926. DOI: [10.1007/s00216-015-8557-x](https://doi.org/10.1007/s00216-015-8557-x). d) Zhao, W. -W., Wang, J., Zhu, Y. -C., Xu, J. -J., Chen, H. -Y. Quantum dots: electrochemiluminescent and photoelectrochemical bioanalysis. *Anal. Chem.* **2015**, *87* (19), 9520-9531. DOI [10.1021/acs.analchem.5b00497](https://doi.org/10.1021/acs.analchem.5b00497). e) Liu, Z., Qi, W., Xu, G. Recent advances in electrochemiluminescence. *Chem. Soc. Rev.* **2015**, *44* (10), 3117-3142. DOI: [10.1039/C5CS00086F](https://doi.org/10.1039/C5CS00086F). f) Zhou, H., Liu, J., Zhang, S. Quantum dot-based photoelectric conversion for biosensing applications. *Trends Anal. Chem.* **2015**, *67*, 56-73. DOI: [10.1016/j.trac.2014.12.007](https://doi.org/10.1016/j.trac.2014.12.007). g) Ding, C., Zhang, W., Wang, W., Chen, Y., Li, X. Amplification strategies using electrochemiluminescence biosensors for the detection of DNA, bioactive molecules and cancer biomarkers. *Trends Anal. Chem.* **2015**, *65*, 137-150. DOI: [10.1016/j.trac.2014.10.015](https://doi.org/10.1016/j.trac.2014.10.015). h) Bertoncetto, P., Stewart, A. J., Dennany, L. Analytical applications of nanomaterials in electrogenerated chemiluminescence. *Anal. Bioanal. Chem.* **2014**, *406* (23), 5573-5587. DOI: [10.1007/s00216-014-7946-x](https://doi.org/10.1007/s00216-014-7946-x). i) Xu, Y. H., Liu, J. Q., Gao, C. L., Wang, E. K. Applications of carbon quantum dots in electrochemiluminescence: a mini review. *Electrochem. Commun.* **2014**, *48*, 151-154. DOI: [10.1016/j.elecom.2014.08.032](https://doi.org/10.1016/j.elecom.2014.08.032). j) Zhang, S., Ding, Y., Wei, H. Ruthenium polypyridine complexes combined with oligonucleotides for bioanalysis: a review. *Molecules*, **2014**, *19* (8), 11933-11987. DOI: [10.3390/molecules190811933](https://doi.org/10.3390/molecules190811933).
11. Selected reviews on TCL applications: a) Gilbert, M., Zakharova, V., Ramenda, A., Jebsen, C., Schulze, B., Wilhelm, C. Thermochemiluminescence as a fast method to detect and characterize hydroperoxide moieties in novel 3-hydroperoxyisothiazole 1,1-dioxides. *Tetrahedron*, **2012**, *68* (33), 6765-6771. DOI: [10.1016/j.tet.2012.05.100](https://doi.org/10.1016/j.tet.2012.05.100). b) Kong, H., Wang, H., Zhang, S., Zhang, X. A thermochemiluminescence array for recognition of protein subtypes and their denatured shapes. *Analyst*, **2011**, *136* (18), 3643-

-
3648. DOI: [10.1039/c1an15382j](https://doi.org/10.1039/c1an15382j). c) Wiener-Megnazi, Z., Shiloh, H., Avraham, L., Lahav-Baratz, S., Koifman, M., Reznick, A. Z., Auslender, R., Dirnfeld, M. Oxidative parameters of embryo culture media may predict treatment outcome in vitro fertilization: a novel applicable tool for improving embryo selection. *Fertil. Steril.* **2011**, *95* (3), 979-984. DOI: [10.1016/j.fertnstert.2010.10.019](https://doi.org/10.1016/j.fertnstert.2010.10.019). d) Kong, H., Liu, D., Zhang, S., Zhang, X. Protein sensing and cell discrimination using a sensor array based on nanomaterial-assisted chemiluminescence. *Anal. Chem.* **2011**, *83* (6), 1867-1870. DOI: [10.1021/ac200076c](https://doi.org/10.1021/ac200076c). e) Amir, O., Yamin, C., Sagiv, M., Eynon, N., Shnizer, S., Kagan, T., Reznick, A. Z., Sagiv, M., Amir, R. E. Acute incremental exercise to maximal performance does not cause alterations in serum oxidant levels of healthy young individuals. *J. Sports Med. Phys. Fitness*, **2009**, *49* (1), 105-111. f) Amir, O., Paz, H., Rogowski, O., Barshai, M., Sagiv, M., Shnizer, S., Reznick, A. Z., Amir, R. E. Serum oxidative stress level correlates with clinical parameters in chronic systolic heart failure patients. *Clin. Cardiol.* **2009**, *32* (4), 199-203. DOI: [10.1002/clc.20317](https://doi.org/10.1002/clc.20317). g) Sukhotnik, I., Brod, V., Lurie, M., Rahat, M. A., Shnizer, S., Lahat, N., Mogilner, J. G., Bitterman, H. The effect of 100% oxygen on intestinal preservation and recovery following ischemia-reperfusion injury in rats. *Crit. Care Med.* **2009**, *37* (3), 1054-1061. DOI: [10.1097/CCM.0b013e31819d0f5c](https://doi.org/10.1097/CCM.0b013e31819d0f5c). h) Wiener-Megnazi, Z., Vardi, L., Lissak, A., Shnizer, S., Reznick, A. Z., Ishai, D., Lahav-Baratz, S., Shiloh, H., Koifman, M., Dirnfeld, M. Oxidative stress indices in follicular fluid as measured by the thermochemiluminescence assay correlate with outcome parameters in vitro fertilization. *Fertil. Steril.* **2004**, *82* (3), 1171-1176. DOI: [10.1016/j.fertnstert.2004.06.013](https://doi.org/10.1016/j.fertnstert.2004.06.013). i) Shnizer, S., Kagan, T., Lanir, A., Maor, I., Reznick, A. A. Modifications and oxidation of lipids and proteins in human serum detected by thermochemiluminescence. *Luminescence*, **2003**, *18* (2), 90-96. DOI: [10.1002/bio.699](https://doi.org/10.1002/bio.699). j) Shnizer, S., Resnik, A., Lanir, A., Piuk, V. Method and apparatus for measuring lipid peroxidation in biological fluids and suspensions of tissues. Patent, **1999**, *WO9919728A1*. k) Kiel, J. L., Alls, J. L., Holwitt, E. A., Stribling, L. J. V., Parker, J. E. Thermochemiluminescence as a technique for radio frequency radiation dosimetry. *Bioelectrochem. Bioenerg.* **1998**, *47* (2), 253-257. DOI: [10.1016/S0302-4598\(98\)00196-2](https://doi.org/10.1016/S0302-4598(98)00196-2).

-
12. Roda, A., Cui, H., Lu, C. Highlights of analytical chemical luminescence and cataluminescence. *Anal. Bioanal. Chem.* **2016**, *408* (30), 8727-8729. DOI: [10.1007/s00216-016-0032-9](https://doi.org/10.1007/s00216-016-0032-9).
13. Roda, A., Guardigli, M. Analytical chemiluminescence and bioluminescence: latest achievements and new horizons. *Anal. Bioanal. Chem.* **2012**, *402* (1), 69-76. DOI: [10.1007/s00216-011-5455-8](https://doi.org/10.1007/s00216-011-5455-8).
14. Michelini, E., Cevenini, L., Mezzanotte, L., Ablamsky, D., Southworth, T., Branchini, B. R., Roda, A. Combining intracellular and secreted bioluminescent reporter proteins for multicolor cell-based assays. *Photochem. Photobiol. Sci.* **2008**, *7* (2), 212-217. DOI: [10.1039/B714251J](https://doi.org/10.1039/B714251J).
15. a) Luider, T. M., Hummelen, J. C., Koek, J. N., Oudman, D., Wynberg, H. Luminescence immunoassay and molecular applications. (van Dyke, K., van Dyke, R. Eds.), *CRC Press*, Boca Raton, **1990**, *Chapter 15*, pp. 217-231. b) Luider, T., Hummelen, J. C., Koek, J. N., Wynberg, H. Thermochemiluminescent cyclodextrin complexes. Patent, **1988**, *EP261719A2*. c) Hummelen, J. C., Luider, T. M., Wynberg, H. Stable 1,2-dioxetanes as labels for thermochemiluminescent immunoassay. *Methods Enzymol.* **1986**, *133*, 531-557. DOI: [10.1016/0076-6879\(86\)33088-x](https://doi.org/10.1016/0076-6879(86)33088-x). d) Hummelen, J. C., Wynberg, H. Chemiluminescent labelled organic reagents and their use in analysis of organic compounds. Patent, **1985**, *WO8504958A1*.
16. Wieringa, J. H., Starting, J., Wynberg, H., Adam W. Adamantylideneadamantane peroxide, a stable 1,2-dioxetane. *Tetrahedron Lett.* **1972**, *13*, 169-172. DOI: [10.1016/S0040-4039\(01\)84269-6](https://doi.org/10.1016/S0040-4039(01)84269-6).
17. a) Ciscato, L. F. M. L., Bartoloni, F. H., Weiss, D., Beckert, R., Baader, W. J. Experimental evidence of the occurrence of intramolecular electron transfer in catalyzed 1,2-dioxetane decomposition. *J. Org. Chem.* **2010**, *75* (19), 6574-6580. DOI: [10.1021/jo1013405](https://doi.org/10.1021/jo1013405). b) Adam, W., Encarnacion, L. A. A., Zinner, K. Thermal stability of spiro[adamantane-[1,2]dioxetanes]. *Chem. Ber.* **1983**, *116*, 839-846. DOI: [10.1002/cber.19831160302](https://doi.org/10.1002/cber.19831160302). c) Lee, C., Singer, L. A. Structural effects on the intramolecular electron transfer induced decomposition of a series of 1,2-dioxetanes derived from 9-alkylidene-10-methylacridans. *J. Am. Chem. Soc.* **1980**, *102* (11), 3823-3829. DOI: [10.1021/ja00531a026](https://doi.org/10.1021/ja00531a026). d) McCapra, F., Beheshti, I., Burford, A., Hann, R. A.,

-
- Zaklika, K. A. Singlet excited states from dioxetan decomposition. *J. Chem. Soc. Chem. Commun.* **1977**, *24*, 944-946. DOI: [10.1039/C39770000944](https://doi.org/10.1039/C39770000944). e) Lechtken, P., Reissenweber, G., Grubmüller, P. Die bedeutung von konformation und substitution auf die stabilität und anregungsausbeute bei der thermolyse von alkylsubstituierten 1,2-dioxetanen. *Tetrahedron Lett.* **1977**, *18 (33)*, 2881-2884. DOI: [10.1016/S0040-4039\(01\)83100-2](https://doi.org/10.1016/S0040-4039(01)83100-2). f) Wieringa, J. H., Wynberg, H., Starting, J. The geminal 1,1'-biadamantyl group as a stabilizer of reactive functions: 1,1'-biadamantyldiazomethane, 1,1'-biadamanthylemethylen-iminoxyl and 1,1'-biadamanthylemethylen-iminyl. *Tetrahedron*, **1974**, *30 (17)*, 3053-3058. DOI: [10.1016/S0040-4020\(01\)97552-0](https://doi.org/10.1016/S0040-4020(01)97552-0).
18. Hirano, T., Matsuhashi, C. A stable chemiluminophore, adamantylideneadamantane 1,2-dioxetane: from fundamental properties to utilities in mechanochemistry and soft crystal science. *J. Photochem. Photobiol. C: Photochem. Rev.* **2022**, *51*, 100483. DOI: [10.1016/j.jphotochemrev.2022.100483](https://doi.org/10.1016/j.jphotochemrev.2022.100483).
19. a) Syed Mohamed, A., Padma Malar, E. J. Density functional theory investigation on the mechanism of chemiluminescent decomposition in adamantylideneadamantane-1,2-dioxetane (BAAD) and monoadamantylidene-1,2-dioxetane (MAD). *J. Comput. Methods Mol. Des.* **2021**, *11 (4)*, 1-9 www.scholarsresearchlibrary.com. b) Hummelen, J. C., Luider, T. M., Wynberg, H. Functionalized adamantylideneadamantane 1,2-dioxetanes: investigations on stable and inherently chemiluminescent compounds as a tool for clinical analysis. *Pure Appl. Chem.* **1987**, *59 (5)*, 639-650. DOI: [10.1351/pac198759050639](https://doi.org/10.1351/pac198759050639).
20. Schuster, G. B., Turro, N. J., Steinmetzer, H. -C., Schaap, A. P., Faler, G., Adam, W., Liu, J. C. Adamantylideneadamantane-1,2-dioxetane. An investigation of the chemiluminescence and decomposition kinetics of an unusually stable 1,2-dioxetane. *J. Am. Chem. Soc.* **1975**, *97 (24)*, 7110-7118. DOI: [10.1021/ja00857a024](https://doi.org/10.1021/ja00857a024).
21. a) O'Sullivan, M. P., Testa, A. C. Fluorescence of aliphatic ketones. *J. Am. Chem. Soc.* **1970**, *92 (20)*, 5842-5844. DOI: [10.1021/ja00723a005](https://doi.org/10.1021/ja00723a005). b) Hara, K., Schuster, G. B., Drickamer, H. The effect of pressure on the fluorescence and absorption of adamantanone. *Chem. Phys. Lett.* **1977**, *47 (3)*, 462-465. DOI: [10.1016/0009-2614\(77\)85016-1](https://doi.org/10.1016/0009-2614(77)85016-1).

-
22. Luider, T. M., Hummelen, J. C., Oudman, D., Wynberg, H. Thermochemiluminescence immunoassay for hCG. *EPRINTS-BOOK-TITLE*, University of Groningen, Stratingh Institute for Chemistry. **1990**, *Chapter 15*, pp. 217-231.
23. Hummelen, J. C., Luider, T. M., Wynberg, H. Thermochemiluminescence immunoassays. *EPRINTS-BOOK-TITLE*, University of Groningen, Stratingh Institute for Chemistry, **1988**, *Chapter 14*, pp. 191-208.
24. Selected reviews on 1,2-dioxetanes: a) Pradal, A. Four-membered rings with two oxygen atoms. Comprehensive heterocyclic chemistry IV. A review of literature 2008-2021. (Black, D., Cossy, J., Stevens, C. Eds.), *Elsevier*, **2022**, *Vol. 2*, pp. 507-537. DOI: [10.1016/B978-0-12-818655-8.00152-9](https://doi.org/10.1016/B978-0-12-818655-8.00152-9). b) Taylor, D. Four-membered rings with two oxygen atoms. Comprehensive heterocyclic chemistry III. (Katritzky, A., Ramsden, C., Scriven, E., Taylor, R. Eds.), **2008**, *Vol. 2*, pp. 775-794. DOI: [10.1016/B978-008044992-0.00216-9](https://doi.org/10.1016/B978-008044992-0.00216-9). c) Adam, W., Trofimov, A. V. The chemistry of peroxides. (Rappoport, Z. Ed.), *Wiley*, New York, **2006**, *Vol. 2*, pp. 1171-1209. d) Saha-Moeller, C. R., Adam, W. Four-membered rings, with all fused systems containing four-membered rings. Comprehensive heterocyclic chemistry II. A review of the literature 1982-1995: the structure, reactions, synthesis, and uses of heterocyclic compounds. (Katritzky, A. R., Rees, C. W., Scriven, E. F. V. Eds.), *Pergamon*, New York, **1996**, pp. 1041-1082. e) Adam, W., Heil, M., Mosandl, T., Saha-Moeller, C. R. Dioxetanes and α -peroxy lactones, four membered ring cyclic peroxides. Organic peroxides. (Ando, W. Ed.), *Wiley*, Chichester, **1992**, *24 (31)*, pp. 221-254. DOI: [10.1002/chin.199331315](https://doi.org/10.1002/chin.199331315). f) Adam, W. The chemistry of heterocycle compounds. Small ring heterocycles. (Hassner, A. Ed.), *Wiley*, New York, **1986**, pp. 351-429. g) Adam, W. The chemistry of peroxide. (Patai, S. Ed.), *Wiley*, New York, **1983**, pp. 829-920. h) Bartlett, P. D., Landis, M. E. The 1,2-dioxetanes. Singlet oxygen. (Wasserman, H. H., Murray, R. W. Eds.), *Academic Press*, New York, **1979**, pp. 243-286.
25. a) Andronico, L. A., Quintavalla, A., Lombardo, M., Mirasoli, M., Guardigli, M., Trombini, C., Roda, A. Synthesis of 1,2-dioxetanes as thermochemiluminescent labels for ultrasensitive bioassays: rational prediction of olefin photooxygenation outcome by using a chemometric approach. *Chem. Eur. J.* **2016**, *22 (50)*, 18156-18168. DOI: [10.1002/chem.201603765](https://doi.org/10.1002/chem.201603765). b) Di Fusco, M., Quintavalla, A., Trombini, C., Lombardo,

-
- M., Roda, A., Guardigli, M., Mirasoli, M. Preparation and characterization of thermochemiluminescent acridine-containing 1,2-dioxetanes as promising ultrasensitive labels in bioanalysis. *J. Org. Chem.* **2013**, *78* (22), 11238-11246. DOI: [10.1021/jo401683r](https://doi.org/10.1021/jo401683r). c) Roda, A., Di Fusco, M., Quintavalla, A., Guardigli, M., Mirasoli, M., Lombardo, M., Trombini, C. Dioxetane-doped silica nanoparticles as ultrasensitive reagentless thermochemiluminescent labels for bioanalytics. *Anal. Chem.* **2012**, *84* (22), 9913-9919. DOI: [10.1021/ac302306u](https://doi.org/10.1021/ac302306u).
26. Di Fusco, M., Quintavalla, A., Lombardo, M., Guardigli, M., Mirasoli, M., Trombini, C., Roda, A. Organically modified silica nanoparticles doped with new acridine-1,2-dioxetane analogues as thermochemiluminescence reagentless labels for ultrasensitive immunoassays. *Anal. Bioanal. Chem.* **2015**, *407* (6), 1567-1576. DOI: [10.1007/s00216-014-8406-3](https://doi.org/10.1007/s00216-014-8406-3).
27. Andronico, L. A., Chen, L., Mirasoli, M., Guardigli, M., Quintavalla, A., Lombardo, M., Trombini, C., Chiu, D. T., Roda, A. Thermochemiluminescent semiconducting polymer dots as sensitive nanoprobe for reagentless immunoassay. *Nanoscale*, **2018**, *10*, 14012-14021. DOI: [10.1039/C8NR03092H](https://doi.org/10.1039/C8NR03092H).
28. Di Fusco, M., Guardigli, M., Lombardo, M., Mirasoli, M., Quintavalla, A., Roda, A., Trombini, C. Method for the production of thermochemiluminescent silica nanoparticles and their use as markers in bioanalytic methods. Patent, **2016**, *EP13765518B1*.
29. Zaklika, K. A., Burns, P. A., Schaap, A. P. Enhanced chemiluminescence from the silica gel catalyzed decomposition of a 1,2-dioxetane. *J. Am. Chem. Soc.* **1978**, *100* (1), 318-320. DOI: [10.1021/ja00469a072](https://doi.org/10.1021/ja00469a072).
30. Adam, W., Heil, M. Reaction of 1,2-dioxetanes with heteroatom nucleophiles: adduct formation by nucleophilic attack at the peroxide bond. *J. Am. Chem. Soc.* **1992**, *114* (14), 5591-5598. DOI: [10.1021/ja00040a017](https://doi.org/10.1021/ja00040a017).
31. Roda, A., Zangheri, M., Calabria, D., Mirasoli, M., Caliceti, C., Quintavalla, A., Lombardo, M., Trombini, C., Simoni, P. A simple smartphone-based thermochemiluminescent immunosensor for valproic acid detection using 1,2-dioxetane analogue-doped nanoparticles as a label. *Sens. Actuators B- Chem.* **2019**, *279*, 327-333. DOI: [10.1016/j.snb.2018.10.012](https://doi.org/10.1016/j.snb.2018.10.012).

32. a) Albrecht, H. O. Über die chemilumineszenz des aminophthalsäurehydrazids. *Zeitschrift für Physikalische Chemie*, **2017**, *136U (1)*, 321-330. DOI: [10.1515/zpch-1928-13625](https://doi.org/10.1515/zpch-1928-13625). b) Merényi, G., Lind, J., Eriksen, T. E. Luminol chemiluminescence: chemistry, excitation, emitter. *J. Biolumin. Chemilumin.* **1990**, *5 (1)*, 53-56, DOI: [10.1002/bio.1170050111](https://doi.org/10.1002/bio.1170050111).
33. Gleu, K., Petsch, W. Die chemilumineszenz der dimethyl-diacridyliumsalze. *Angew. Chem.* **1935**, *48*, 57-59. DOI: [10.1002/ange.19350480302](https://doi.org/10.1002/ange.19350480302).
34. a) Hori, K., Charbonneau, H., Hart, R. C., Cormier, M. J. Structure of native renilla reinformis luciferin. *PNAS*, **1977**, *74 (10)*, 4285-4287. DOI: [10.1073/pnas.74.10.4285](https://doi.org/10.1073/pnas.74.10.4285). b) Shimomura, O., Johnson, F. H. Chemical nature of bioluminescence systems in coelenterates. *PNAS*, **1975**, *72*, 1546-1549. DOI: [10.1073/pnas.72.4.1546](https://doi.org/10.1073/pnas.72.4.1546). c) Rauhut, M. M., Bollyky, L. J., Roberts, B. G., Loy, M., Whitman, R. H., Iannotta, A. V., Semsel, A. M., Clarke, R. A. Chemiluminescence from reactions of electronegatively substituted aryl oxalates with hydrogen peroxide and fluorescent compounds. *J. Am. Chem. Soc.* **1967**, *89*, 6515-6522. DOI: [10.1021/ja01001a025](https://doi.org/10.1021/ja01001a025).
35. a) Stanley, P. E. Bioluminescence and chemiluminescence: instruments and applications. *J. Biolumin. Chemilumin.* (van Dyke, K. Ed.) *CRC Press*, Inc., Boca Raton, Florida, **1986**, *1 (1)*, pp. 45-46. DOI: [10.1002/bio.1170010109](https://doi.org/10.1002/bio.1170010109). b) Roswell, D. F., White, E. H. The chemiluminescence of luminol and related hydrazides. *Methods Enzymol.* **1978**, *57*, 409-423, DOI: [10.1016/0076-6879\(78\)57038-9](https://doi.org/10.1016/0076-6879(78)57038-9). c) Brundrett, R. B., White, E. H. Synthesis and chemiluminescence of derivatives of luminol and isoluminol. *J. Am. Chem. Soc.* **1974**, *96 (24)*, 7497-7502. DOI: [10.1021/ja00831a018](https://doi.org/10.1021/ja00831a018).
- 36 Nakazono, M., Oshikawa, Y., Nakamura, M., Kubota, H., Nanbu, S. Strongly chemiluminescent acridinium esters under neutral conditions: synthesis, properties, determination, and theoretical study. *J. Org. Chem.* **2017**, *82 (5)*, 2450-2461. DOI: [10.1021/acs.joc.6b02748](https://doi.org/10.1021/acs.joc.6b02748).
- 37 a) Vysotski, E. S., Lee, J. Ca²⁺ regulated photoproteins: structural insight into the bioluminescence mechanism. *Acc. Chem. Res.* **2004**, *37 (6)*, 405-415. DOI: [10.1021/ar0400037](https://doi.org/10.1021/ar0400037). b) Shimomura, O., Teranishi, K. Light-emitters involved in the luminescence of coelenterazine. *Luminescence*, **2000**, *15 (1)*, 51-58. DOI: [10.1002/\(SICI\)1522-7243\(200001/02\)15:1<51::AID-BIO555>3.0.CO;2-J](https://doi.org/10.1002/(SICI)1522-7243(200001/02)15:1<51::AID-BIO555>3.0.CO;2-J). c) Chokshi,

-
- H. P., Barbush, M., Carlson, R. G., Givens, R. S., Kuwana, T., Schowen, R. L. Oxalate/hydrogen peroxide chemiluminescence reaction. A ^{19}F NMR probe of the reaction mechanism. *Biomed. Chromatogr.* **1990**, *4*, 96-99. DOI: [10.1002/bmc.1130040304](https://doi.org/10.1002/bmc.1130040304). d) Orlovic, M., Schowen, R. L., Givens, R. S., Alvarez, F., Matuszewski, B. Parekh, N. A simplified model for the dynamics of chemiluminescence in the oxalate-hydrogen peroxide system: toward a reaction mechanism. *J. Org. Chem.* **1989**, *54* (15), 3606-3610. DOI: [10.1021/jo00276a021](https://doi.org/10.1021/jo00276a021). e) Catherall, C. L. R., Palmer, T. F., Cundall, R. B. Chemiluminescence from reactions of bis(pentachlorophenyl)oxalate, hydrogen peroxide and fluorescent compounds. Kinetics and mechanism. *J. Chem. Soc., Faraday Trans. 2*, **1984**, *80*, 823-836. DOI: [10.1039/F29848000823](https://doi.org/10.1039/F29848000823). f) Hastings, J. Chemistry and control of luminescence in marine organisms. *Bull. Mar. Sci.* **1983**, *33* (44), 818-828.
38. a) Li, J., Chen, L., Du, L., Li, M. Cage the firefly luciferin! - a strategy for developing bioluminescent probes. *Chem. Soc. Rev.* **2013**, *42* (2), 662-676. DOI: [10.1039/C2CS35249D](https://doi.org/10.1039/C2CS35249D). b) Matsumoto, M. Advanced chemistry of dioxetane-based chemiluminescent substrates originating from bioluminescence. *J. Photochem. Photobiol. C: Photochem. Rev.* **2004**, *5* (1), 27-53. DOI: [10.1016/j.jphotochemrev.2004.02.001](https://doi.org/10.1016/j.jphotochemrev.2004.02.001). c) Steinberg, S. M., Poziomek, E. J., Engelmann, W. H., Rogers, K. R. A review of environmental applications of bioluminescence measurements. *Chemosphere*, **1995**, *30* (11), 2155-2197. DOI: [10.1016/0045-6535\(95\)00087-O](https://doi.org/10.1016/0045-6535(95)00087-O).
39. a) Marques, S. M., Esteves da Silva, J. C. G. Firefly bioluminescence: A mechanistic approach of luciferase catalyzed reactions. *IUBMB Life*, **2009**, *61*, 6-17. DOI: [10.1002/iub.134](https://doi.org/10.1002/iub.134). b) Fraga, H. Firefly luminescence: a historical perspective and recent developments. *Photochem. Photobiol. Sci.* **2008**, *7* (2), 146-158. DOI: [10.1039/B719181B](https://doi.org/10.1039/B719181B).
40. a) Clough, J. M., Creton, C., Craig, S. L., Sijbesma, R. P. Covalent bond scission in the Mullins effect of a filled elastomer: real-time visualization with mechanoluminescence. *Adv. Funct. Mat.* **2016**, *26* (48), 9063-9074. DOI: [10.1002/adfm.201602490](https://doi.org/10.1002/adfm.201602490). b) Chen, Y., Spiering, A. J. H., Karthikeyan, S., Peters, G. W. M., Meijer, E. W., Sijbesma, R. P. Mechanically induced chemiluminescence from

-
- polymers incorporating a 1,2-dioxetane unit in the main chain. *Nat. Chem.* **2012**, *4* (7), 559-562. DOI: [10.1038/nchem.1358](https://doi.org/10.1038/nchem.1358).
41. a) Hummelen, J. C., Luider, T. M., Oudman, D., Koek, J. N., Wynberg, H. 1,2-Dioxetanes: luminescent and nonluminescent decomposition, chemistry, and potential applications. *EPRINTS-BOOK-TITLE*, University of Groningen, Stratingh Institute for Chemistry, **1991**, *Chapter 18*, pp. 17. b) Kopecky, K. R. Synthesis of 1,2-dioxetanes. Chemical and biological generation of excited states. (Adam, W., Cilento, G. Eds.), **1982**, pp. 85-114. DOI: [10.1016/B978-0-12-044080-1.50008-0](https://doi.org/10.1016/B978-0-12-044080-1.50008-0). c) Turro, N. J., Lechtken, P. Thermal and photochemical generation of electronically excited organic molecules: tetramethyl-1,2-dioxetane and naphthvalene. *Pure Appl. Chem.* **1973**, *33* (2-3), 363-388. DOI: [10.1351/pac197333020363](https://doi.org/10.1351/pac197333020363).
42. Kopecky, K. R., Filby, J. E., Mumford, C., Lockwood, P. A., Ding, J. -Y. Preparation and thermolysis of some 1,2-dioxetanes. *Can. J. Chem.* **1975**, *53* (8), 1103-1122. DOI: [10.1139/v75-154](https://doi.org/10.1139/v75-154).
43. Kopecky, K. R., Mumford, C. Luminescence in the thermal decomposition of 3,3,4-trimethyl-1,2-dioxetane. *Can. J. Chem.* **1969**, *47* (4), 709-711. DOI: [10.1139/v69-114](https://doi.org/10.1139/v69-114).
44. White, E. H., Wildes, P. D., Wiecko, J., Doshan, H., Wei, C. C. Chemically produced excited states. Energy transfer, photochemical reactions, and light emission. *J. Am. Chem. Soc.* **1973**, *95* (21), 7050-7058. DOI: [10.1021/ja00802a028](https://doi.org/10.1021/ja00802a028).
45. Adam, W., Baader, W. J. Effects of methylation on the thermal stability and chemiluminescence properties of 1,2-dioxetanes. *J. Am. Chem. Soc.* **1985**, *107* (2), 410-416. DOI: [10.1021/ja00288a022](https://doi.org/10.1021/ja00288a022).
46. Richardson, W. H., Montgomery, F. C., Yelvington, M. B., O'Neal, H. E. Kinetics of the thermal decomposition of 3,3-diphenyl- and 3,3-dibenzyl-1,2-dioxetane. Consideration of stepwise and concerted mechanisms. *J. Am. Chem. Soc.* **1974**, *96* (24), 7525-7532. DOI: [10.1021/ja00831a022](https://doi.org/10.1021/ja00831a022).
47. Kopecky, K. R., Lockwood, P. A., Rico Gomez, R., Ding, J. -Y. Thermolysis of the tricyclic 1,2-dioxetanes 3,4:3,4-dipropano-, 3,4-pentano-3,4-propano-, and 3,4-butano-3,4-propano-1,2-dioxetane. *Can. J. Chem.* **1981**, *59*, 851-858. DOI: [10.1139/v81-123](https://doi.org/10.1139/v81-123).

-
48. a) Baader, W. J., Bastos, E. L. Product subclass 2: four-membered cyclic peroxides (1,2-dioxetanes and 1,2-dioxetanones). Science of synthesis: Houben-Weyl methods of molecular transformations. (Berkessel, A. Ed.), *Georg Thieme Verlag KG*, Stuttgart, **2008**, pp. 323-344. DOI: [10.1055/sos-SD-038-00347](https://doi.org/10.1055/sos-SD-038-00347). b) Baader, W. J., Stevani, C. V., Bastos, E. L. Chemiluminescence of organic peroxides. Patai's chemistry of functional groups. (Rappaport, Z. Ed.), *Wiley*, Chichester, **2006**, *16* (2), pp. 1211-1278. DOI: [10.1002/9780470682531.pat0362](https://doi.org/10.1002/9780470682531.pat0362).
49. Lippold, T., Neudörfl, J. G., Griesbeck, A. New acridone- and (thio)xanthone-derived 1,1-donor-acceptor-substituted alkenes: pH-dependent fluorescence and unusual photooxygenation properties. *Molecules*, **2021**, *26* (11), 3305. DOI: [10.3390/molecules26113305](https://doi.org/10.3390/molecules26113305).
50. Richard, J. -A. Singlet oxygen. *Synlett*, **2009**, *4* (7), 1187-1188. DOI: [10.1055/s-0028-1088111](https://doi.org/10.1055/s-0028-1088111).
51. Mazur, S. Foote C. S. Chemistry of singlet oxygen. IX. Stable dioxetane from photooxygenation of tetramethoxyethylene. *J. Am. Chem. Soc.* **1970**, *92* (10), 3225-3226. DOI: [10.1021/ja00713a073](https://doi.org/10.1021/ja00713a073).
52. Foote, C. S., Wexler, S., Ando, W., Higgins, R. Chemistry of singlet oxygen. IV. Oxygenations with hypochlorite-hydrogen peroxide. *J. Am. Chem. Soc.* **1968**, *90* (4), 975-981. DOI: [10.1021/ja01006a023](https://doi.org/10.1021/ja01006a023).
53. Gollnick, K., Schenck, G. O. Oxygen as dienophile. 1,4-Cycloaddition reactions: the Diels-Alder reaction in heterocyclic syntheses. (Hamer, J. Ed.) *Academic Press Inc.*, New York, **1967**, *Vol. 10*, pp. 255.
54. a) Wu, W., An, F., Geng, Z., Zhang, R., Jiang, Z. Novel and versatile photosensitized oxygenation reaction of α -cedrene. *Lett. Org. Chem.* **2013**, *10* (3), 223-227. DOI: [10.2174/1570178611310030015](https://doi.org/10.2174/1570178611310030015). b) Ohkubo, K., Nanjo, T., Fukuzumi, S. Efficient photocatalytic oxygenation of aromatic alkene to 1,2-dioxetane with oxygen via electron transfer. *Org. Lett.* **2005**, *7* (19), 4265-4268. DOI: [10.1021/ol051696+](https://doi.org/10.1021/ol051696+). c) Poon, T., Sivaguru, J., Franz, R., Jockusch, S., Martinez, C., Washington, I., Adam, W., Inoue, Y., Turro, N. J. Temperature and solvent control of the stereoselectivity in the reactions of singlet oxygen with oxazolidinone-substituted enecarbamates. *J. Am. Chem. Soc.* **2004**, *126* (34), 10498-10499. DOI: [10.1021/ja048438c](https://doi.org/10.1021/ja048438c). d) Kojima, M., Nakajoh, M.,

- Matsubara, C., Hashimoto, S. Photooxygenation of aromatic alkenes in zeolite nanocavities. *J. Chem. Soc., Perkin Trans. 2*, **2002**, *11*, 1894-1901. DOI: [10.1039/B205672K](https://doi.org/10.1039/B205672K). e) Adam, W., Bosio, S. G., Turro, N. J. Control of the mode selectivity (ene reaction versus [2+2] cycloaddition) in the photooxygenation of ene carbamates: directing effect of an alkenylic nitrogen functionality. *J. Am. Chem. Soc.* **2002**, *124* (47), 8814-8815. DOI: [10.1021/ja028407m](https://doi.org/10.1021/ja028407m). f) Adam, W., Saha-Moeller, C. R., Schambony, S. B. A highly diastereoselective dioxetane formation by the hydroxy-directed [2+2] cycloaddition of singlet oxygen to a chiral allylic alcohol. *J. Am. Chem. Soc.* **1999**, *121* (9), 1834-1838. DOI: [10.1021/ja9835077](https://doi.org/10.1021/ja9835077). g) Matsumoto, M., Kitano, Y., Kobayashi, H., Ikawa, H. Singlet oxygenation of 1-aminomethyl-1-tert-butyl-2-methoxy-2-(3-methoxy-phenyl) ethylenes: marked effect of allylic nitrogen on the reaction pathways and chemoselectivity. *Tetrahedron Lett.* **1996**, *37* (45), 8191-8194. DOI: [10.1016/0040-4039\(96\)01858-8](https://doi.org/10.1016/0040-4039(96)01858-8). h) Matsumoto, M., Kobayashi, H., Matsubara, J., Watanabe, N., Yamashita, S., Oguma, D., Kitano, Y., Ikawa, H. Effect of allylic oxygen on the reaction pathways of singlet oxygenation: selective formation of 1,2-dioxetanes from 1-alkoxymethyl-2-aryl-1-tert-butyl-2-methoxyethylenes. *Tetrahedron Lett.* **1996**, *37* (3), 397-400. DOI: [10.1016/0040-4039\(95\)02185-X](https://doi.org/10.1016/0040-4039(95)02185-X). i) Yoshioka, Y., Yamada, S., Kawakami, T., Nishino, M., Yamaguchi, K., Saito, I. Ab initio molecular orbital studies of singlet oxygen reactions of olefins, enol ethers, and enamines. *Bull. Chem. Soc. Jpn.* **1996**, *69* (10), 2683-2699. DOI: [10.1246/bcsj.69.2683](https://doi.org/10.1246/bcsj.69.2683). j) Clennan, E. L., Nagraba, K. Additions of singlet oxygen to alkoxy-substituted dienes. The mechanism of the singlet oxygen 1,2-cycloaddition reaction. *J. Am. Chem. Soc.* **1988**, *110* (13), 4312-4318. DOI: [10.1021/ja00221a034](https://doi.org/10.1021/ja00221a034). k) Yamaguchi, K., Yabushita, S., Fueno, T., Houk, K. N. Mechanism of photooxygenation reactions. Computational evidence against the diradical mechanism of singlet oxygen ene reactions. *J. Am. Chem. Soc.* **1981**, *103* (17), 5043-5046. DOI: [10.1021/ja00407a013](https://doi.org/10.1021/ja00407a013).
55. Sagadevan, A., Hwang, K. C. Su, M. -D. Singlet oxygen-mediated selective C-H bond hydroperoxidation of ethereal hydrocarbons. *Nat Commun.* **2017**, *8* (1), 1812. DOI: [10.1038/s41467-017-01906-5](https://doi.org/10.1038/s41467-017-01906-5).

-
56. Singlet oxygen: applications in biosciences and nanosciences. (Nonell, S., Flors, C. Eds.), *Royal Society of Chemistry*, Cambridge, **2016**, Vol. 2, pp. 374. DOI: [10.1039/9781782626992](https://doi.org/10.1039/9781782626992).
57. Matsumoto, M., Watanabe, N., Shiono, T., Suganuma, H., Matsubara, J. Chemiluminescence of spiro[1,2-dioxetane-3,1'-dihydroisobenzofuran]s, spiro[1,2-dioxetane-3,1'-isochroman]s and a spiro[1,2-dioxetane-3,1'-(2-benzoxepane)]. *Tetrahedron Lett.* **1997**, 38 (33), 5825-5828. DOI: [10.1016/S0040-4039\(97\)01332-4](https://doi.org/10.1016/S0040-4039(97)01332-4).
58. Matsumoto, M., Ishihara, T., Watanabe, N., Hiroshima, T. Synthesis of thermally stable 1,2-dioxetanes bearing a phenylethenyl or a phenylethynyl moiety and their base-induced decomposition. *Tetrahedron Lett.* **1999**, 40 (24), 4571-4574. DOI: [10.1016/S0040-4039\(99\)00793-5](https://doi.org/10.1016/S0040-4039(99)00793-5).
59. Einaga, H., Nojima, M., Abe, M. Photooxygenation ($^1\text{O}_2$) of silyl enol ethers derived from indan-1-ones: competitive formation of tricyclic 3-siloxy-1,2-dioxetane and α -silylperoxy ketone. *J. Chem. Soc., Perkin Trans. 1*, **1999**, 31 (3), 2507-2512. DOI: [10.1039/A903516H](https://doi.org/10.1039/A903516H).
60. Matsumoto, M., Hiroshima, T., Chiba, S., Isobe, R., Watanabe, N., Kobayashi, H. Synthesis of 3-ethoxy-4,4-diisopropyl-1,2-dioxetanes bearing a benzo(b)furan-2-yl or a benzo(b)thiophen-2-yl group: CIEEL-active dioxetanes emitting red light. *Luminescence*, **1999**, 14, 345-348. DOI: [10.1002/\(SICI\)1522-7243\(199911/12\)14:6<345::AID-BIO559>3.0.CO;2-T](https://doi.org/10.1002/(SICI)1522-7243(199911/12)14:6<345::AID-BIO559>3.0.CO;2-T).
61. Roeschlaub, C. A., Sammes, P. G. Use of the Wadsworth-Emmons reaction for preparing hindered vinyl ethers and related 1,2-dioxetanes. *J. Chem. Soc., Perkin Trans 1*, **2000**, 14, 2243-2248. DOI: [10.1039/B002101F](https://doi.org/10.1039/B002101F).
62. Matsumoto, M., Ito, Y., Matsubara, J., Sakuma, T., Mizoguchi, Y., Watanabe, N. Base-induced chemiluminescent decomposition of stereoisomeric 5-tert-butyl-1-(3-tert-butyl-dimethylsiloxy)phenyl-4,4-dimethyl-3-phenyl-2,6,7-trioxabicyclo[3.2.0]hepta and their related dioxetanes. *Tetrahedron Lett.* **2001**, 42 (12), 2349-2352. DOI: [10.1016/S0040-4039\(01\)00171-X](https://doi.org/10.1016/S0040-4039(01)00171-X).
63. Matsumoto, M., Murayama, J., Nishiyama, M., Mizoguchi, Y., Sakuma, T., Watanabe, N. Synthesis of 1-(3-tert-butyl-dimethylsiloxy)phenyl-5,5-dimethyl-2,7,8-trioxabicyclo[4.2.0]octanes: new dioxetanes giving high chemiexcitation yields in

thermolysis and in fluoride-induced CIEEL-decay 'jointly worked'. *Tetrahedron Lett.* **2002**, *43* (8), 1523-1527. DOI: [10.1016/S0040-4039\(02\)00052-7](https://doi.org/10.1016/S0040-4039(02)00052-7).

64. Watanabe, N., Nagashima, Y., Yamazaki, T., Matsumoto, M. Fluoride-induced chemiluminescent decomposition of dioxetanes bearing a siloxyaryl moiety to produce an alkyl aryl ketone as an emitter. *Tetrahedron*, **2003**, *59* (26), 4811-4819. DOI: [10.1016/S0040-4020\(03\)00727-0](https://doi.org/10.1016/S0040-4020(03)00727-0).

65. Matsumoto, M., Hamaoka, K., Takashima, Y., Yokokawa, M., Yamada, K., Watanabe, N., Ijuin, H. K. Chemiluminescence in molecular recognition: base-induced decomposition of optically active dioxetanes bearing a bisnaphthol moiety with a complex of optically active crown ether-potassium tert-butoxide. *J. Chem. Soc., Chem. Commun.* **2005**, *6*, 808-810. DOI: [10.1039/B414001J](https://doi.org/10.1039/B414001J).

66. Watanabe, N., Sano, Y., Suzuki, H., Tanimura, M., Ijuin, H. K., Matsumoto, M. Synthesis of thermally stable acylamino-substituted bicyclic dioxetanes and their base-induced chemiluminescent decomposition. *J. Org. Chem.* **2010**, *75* (17), 5920-5926. DOI: [10.1021/jo101114b](https://doi.org/10.1021/jo101114b).

67. Watanabe, N., Kikuchi, M., Maniwa, Y., Ijuin, H. K., Matsumoto, M. Synthesis of sulfanyl-, sulfinyl-, and sulfonyl-substituted bicyclic dioxetanes and their base-induced chemiluminescence. *J. Org. Chem.* **2010**, *75* (3), 879-884. DOI: [10.1021/jo902477n](https://doi.org/10.1021/jo902477n).

68. Ciscato, L. F. M. L., Weiss, D., Beckert, R., Baader, W. J. Fenchyl substituted 1,2-dioxetanes as an alternative to adamantyl derivatives for bioanalytical applications. *J. Photochem. Photobiol. A Chem.* **2011**, *218* (1), 41-47. DOI: [10.1016/j.jphotochem.2010.12.001](https://doi.org/10.1016/j.jphotochem.2010.12.001).

69. Koči, J., Grandclaude, V., Massonneau, M., Richard, J. -A., Romieu, A., Renard, P. -Y. A novel and unusually long-lived chemiluminophore based on the 7-hydroxycoumarin scaffold. *Chem. Commun.* **2011**, *47*, 6713-6715. DOI: [10.1039/C1CC11919B](https://doi.org/10.1039/C1CC11919B).

70. Watanabe, N., Kino, H., Watanabe, S., Ijuin, H. K., Yamada, M., Matsumoto, M. Synthesis of bicyclic dioxetanes tethering a fluororescer through an ω -carbamoyl-substituted linker and their high-performance chemiluminescence in an aqueous system. *Tetrahedron*, **2012**, *68* (30), 6079-6087. DOI: [10.1016/j.tet.2012.04.078](https://doi.org/10.1016/j.tet.2012.04.078).

-
71. Silva, A. F., Oliveira Jr, V. X., Silva, L. S., Pinheiro, A. A. S., Ciscato, L. F. M. L. Antiplasmodial activity of alkyl-substituted 1,2-dioxetanes against *Plasmodium falciparum*. *Bioorg. Med. Chem. Lett.* **2016**, *26* (20), 5007-5008. DOI: [10.1016/j.bmcl.2016.08.096](https://doi.org/10.1016/j.bmcl.2016.08.096).
72. Hisamatsu, Y., Fukiage, T., Honma, K., Balia, A. G., Umezawa, N., Kato, N., Higuchi, T. Effect of the o-acetamido group on pH-dependent light emission of a 3-hydroxyphenyl-substituted dioxetane luminophore. *Org. Lett.* **2019**, *21* (5), 1258-1262. DOI: [10.1021/acs.orglett.8b03913](https://doi.org/10.1021/acs.orglett.8b03913).
73. Kotani, H., Ohkubo, K., Fukuzumi, S. Photocatalytic oxygenation of anthracenes and olefins with dioxygen via selective radical coupling using 9-mesityl-10-methylacridinium ion as an effective electron-transfer photocatalyst. *J. Am. Chem. Soc.* **2004**, *126* (49), 15999-16006. DOI: [10.1021/ja048353b](https://doi.org/10.1021/ja048353b).
74. Adam, W., Kazakov, D. V., Kazakov, V. P. Singlet-oxygen chemiluminescence in peroxide reactions. *Chem. Rev.* **2005**, *105* (9), 3371-3387. DOI: [10.1021/cr0300035](https://doi.org/10.1021/cr0300035).
75. a) Posner, G. H., Weitzberg, M., Nelson, W. M., Murr, B. L., Seliger, H. H. 1,2-Dioxetanes from vinyl aromatics. *J. Am. Chem. Soc.* **1987**, *109* (1), 278-279. DOI: [10.1021/ja00235a045](https://doi.org/10.1021/ja00235a045). b) Lee, K. -W., Singer, L. A., Legg, K. D. Chemiluminescence from the reaction of singlet oxygen with 10,10'-dimethyl-9,9'-biacridylidene. A reactive 1,2-dioxetane. *J. Org. Chem.* **1976**, *41* (16), 2685-2688. DOI: [10.1021/jo00878a005](https://doi.org/10.1021/jo00878a005). c) Schaap, A. P., Bartlett, P. D. Direct reaction of triphenyl phosphite ozonide with cis- and trans-diethoxyethylenes. *J. Am. Chem. Soc.* **1970**, *92* (20), 6055-6057. DOI: [10.1021/ja00723a041](https://doi.org/10.1021/ja00723a041). d) Murray, R. W., Kaplan, M. L. Singlet oxygen sources in ozone chemistry. Chemical oxygenations using the adducts between phosphite esters and ozone. *J. Am. Chem. Soc.* **1969**, *91* (19), 5358-5364. DOI: [10.1021/ja01047a027](https://doi.org/10.1021/ja01047a027).
76. Posner, G. H., Oh, C. H., Milhous, W. K. Olefin oxidative cleavage and dioxetane formation using triethylsilyl hydrotrioxide: applications to preparation of potent antimalarial 1,2,4-trioxanes. *Tetrahedron Lett.* **1991**, *32* (34), 4235-4238. DOI: [10.1016/S0040-4039\(00\)92136-1](https://doi.org/10.1016/S0040-4039(00)92136-1).
77. Corey, E. J., Mehrotra, M. M., Khan, A. U. Generation of $^1\Delta_g$ O₂ from triethylsilane and ozone. *J. Am. Chem. Soc.* **1986**, *108* (9), 2472-2473. DOI: [10.1021/ja00269a070](https://doi.org/10.1021/ja00269a070).

-
78. Bastos, E. L., Ciscato, L. F. M. L., Weiss, D., Beckert, R., Baader, W. J. Comparison of convenient alternative synthetic approaches to 4-[(3-tert-butyltrimethylsilyloxy)phenyl]-4-methoxyspiro[1,2-dioxetane-3,2'-adamantane]. *Synthesis*, **2006**, *11*, 1781-1786. DOI: [10.1055/s-2006-942357](https://doi.org/10.1055/s-2006-942357).
79. Pierlot, C., Nardello, V., Schrive, J., Mabilille, C., Barbillat, J., Sombret, B., Aubry, J. -M. Calcium peroxide diperoxohydrate as a storable chemical generator of singlet oxygen for organic synthesis. *J. Org. Chem.* **2002**, *67* (8), 2418-2423. DOI: [10.1021/jo010766x](https://doi.org/10.1021/jo010766x).
80. Elsherbini, M., Allemann, R. -K., Wirth, T. "Dark" singlet oxygen made easy. *Chem. Eur. J.* **2019**, *25* (54), 12486-12490. DOI: [10.1002/chem.201903505](https://doi.org/10.1002/chem.201903505).
81. Aubry, J. -M., Bouttemy, S. Preparative oxidation of organic compounds in microemulsions with singlet oxygen generated chemically by the sodium molybdate/hydrogen peroxide system. *J. Am. Chem. Soc.* **1997**, *119* (23), 5286-5294. DOI: [10.1021/ja9644079](https://doi.org/10.1021/ja9644079).
82. Stephenson, L. M., Zielinski, M. B. Transfer of oxygen (O₂) from triphenyl phosphite ozonide to alkyl-substituted olefins. *J. Am. Chem. Soc.* **1982**, *104* (21), 5819-5820. DOI: [10.1021/ja00385a059](https://doi.org/10.1021/ja00385a059).
83. Richard, J. -A., Jean, L., Schenkels, C., Massonneau, M., Romieu, A., Renard, P. -Y. Self-cleavable chemiluminescent probes suitable for protease sensing. *Org. Biomol. Chem.* **2009**, *7*, 2941-2957. DOI: [10.1039/b905725k](https://doi.org/10.1039/b905725k).
84. Sabelle, S., Renard, P. -Y., Pecorella, K., De Suzzoni-Dézard, S., Créminon, C., Grassi, J., Mioskowski, C. Design and synthesis of chemiluminescent probes for the detection of cholinesterase activity. *J. Am. Chem. Soc.* **2002**, *124* (17), 4874-4880. DOI: [10.1021/ja0171299](https://doi.org/10.1021/ja0171299).
85. a) Khalitova, L. R., Grabovskii, S. A., Cerkovnik, N. N. K. Formation of singlet oxygen during thermal degradation of hydrotrioxides of triorganosilanes. *High Energy Chem.* **2019**, *53* (6), 435-437. DOI: [10.1134/S0018143919060109](https://doi.org/10.1134/S0018143919060109). b) Cerkovnik, J., Plesnicar, B. Recent advances in the chemistry of hydrogen trioxide (HOOOH). *Chem. Rev.* **2013**, *113* (10), 7930-7951. DOI: [10.1021/cr300512s](https://doi.org/10.1021/cr300512s). c) Cerkovnik, J., Tuttle, T., Kraka, E., Lendero, N., Plesničar, B., Cremer, D. The ozonation of silanes and germanes: an experimental and theoretical investigation. *J. Am. Chem. Soc.* **2006**, *128* (12), 4090-

-
4100. DOI: [10.1021/ja058065v](https://doi.org/10.1021/ja058065v). d) Sary, F. E., Emge, D. E., Murray, R. W. Ozonization of organic substrates. Hydrotrioxide formation and decomposition to give singlet oxygen. *J. Am. Chem. Soc.* **1976**, *98* (7), 1880-1884. DOI: [10.1021/ja00423a039](https://doi.org/10.1021/ja00423a039).
86. a) Saito, I., Nagata, R., Nakagawa, H., Moriyama, H., Matsuura, T., Inoue, K. New singlet oxygen source and trapping reagent for peroxide intermediates. *Free Radic. Res. Commun.* **1987**, *2* (4-6), 327-336. DOI: [10.3109/10715768709065299](https://doi.org/10.3109/10715768709065299). b) Jefford, C. W., Rimbault, C. G. Characterization of a dioxetane deriving from norbornene and evidence for its zwitterionic peroxide precursor. *J. Am. Chem. Soc.* **1978**, *100* (1), 295-296. DOI: [10.1021/ja00469a057](https://doi.org/10.1021/ja00469a057). c) Eriksen, J., Foote, C. S., Parker, T. L. Photosensitized oxygenation of alkenes and sulfides via a non-singlet-oxygen mechanism. *J. Am. Chem. Soc.* **1977**, *99* (19), 6455-6456. DOI: [10.1021/ja00461a055](https://doi.org/10.1021/ja00461a055).
87. a) Aubry, J. -M., Cazin, B., Duprat, F. Chemical sources of singlet oxygen. 3. Peroxidation of water-soluble singlet oxygen carriers with the hydrogen peroxide-molybdate system. *J. Org. Chem.* **1989**, *54* (3), 726-728. DOI: [10.1021/jo00264a046](https://doi.org/10.1021/jo00264a046). b) Aubry, J. -M., Cazin, B. Chemical sources of singlet oxygen. 2. Quantitative generation of singlet oxygen from hydrogen peroxide disproportionation catalyzed by molybdate ions. *Inorg. Chem.* **1988**, *27* (12), 2013-2014. DOI: [10.1021/ic00285a001](https://doi.org/10.1021/ic00285a001). c) Aubry, J. -M. Search for singlet oxygen in the decomposition of hydrogen peroxide by mineral compounds in aqueous solutions. *J. Am. Chem. Soc.* **1985**, *107* (21), 5844-5849. DOI: [10.1021/ja00307a002](https://doi.org/10.1021/ja00307a002).
88. You, Y. Chemical tools for the generation and detection of singlet oxygen. *Org. Biomol. Chem.* **2018**, *16* (22), 4044-4060. DOI: [10.1039/C8OB00504D](https://doi.org/10.1039/C8OB00504D).
89. Nardello, V., Bogaert, S., Alsters, P. L., Aubry, J. -M. Singlet oxygen generation from H₂O₂/MoO₄²⁻: peroxidation of hydrophobic substrates in pure organic solvents. *Tetrahedron Lett.* **2002**, *43* (48), 8731-8734. DOI: [10.1016/S0040-4039\(02\)02108-1](https://doi.org/10.1016/S0040-4039(02)02108-1).
90. Nardello, V., Marko, J., Vermeersch, G., Aubry, J. -M. ⁹⁰Mo NMR and kinetic studies of peroxomolybdic intermediates involved in the catalytic disproportionation of hydrogen peroxide by molybdate ions. *Inorg. Chem.* **1995**, *34*, 4950-4957. DOI: [10.1021/ic00124a007](https://doi.org/10.1021/ic00124a007).
91. Yu, L., Ren, L., Yi, R., Guo, R. Cerium (IV) ammonium nitrate-mediated oxidation of monoaryl-substituted methylenecyclobutanes: a convenient method for the

synthesis of spirocyclobutyl-1,2-dioxethanes. *Synt. Commun.* **2011**, *41* (27), 2530-2538. DOI: [10.1080/00397911.2010.505705](https://doi.org/10.1080/00397911.2010.505705).

92. Farahani, P., Roca-Sanjuán, D., Zapata, F., Lindh, R. Revisiting the nonadiabatic process in 1,2-dioxetane. *J. Chem. Theory Comput.* **2013**, *9* (12), 5404-5411. DOI: [10.1021/ct4007844](https://doi.org/10.1021/ct4007844).

93. a) Kearns, D. R. Physical and chemical properties of singlet molecular oxygen. *Chem. Rev.* **1971**, *71* (4), 395-427. DOI: [10.1021/cr60272a004](https://doi.org/10.1021/cr60272a004). b) McCapra, F. The chemiluminescence of organic compounds. *Pure Appl. Chem.* **1970**, *24* (3), 611-630. DOI: [10.1351/pac197024030611](https://doi.org/10.1351/pac197024030611). c) Kearns, D. R. Selection rules for singlet-oxygen reactions. Concerted addition reactions. *J. Am. Chem. Soc.* **1969**, *91* (24), 6554-6563. DOI: [10.1021/ja01052a003](https://doi.org/10.1021/ja01052a003). d) McCapra, F. An application of the theory of electrocyclic reactions to bioluminescence. *Chem. Commun.* **1968**, *3*, 155-156. DOI: [10.1039/C19680000155](https://doi.org/10.1039/C19680000155).

94. a) Turro, N. J., Devaquet, A. Chemiexcitation mechanisms. Role of symmetry and spin-orbit-coupling in diradicals. *J. Am. Chem. Soc.* **1975**, *97* (13), 3859-3862. DOI: [10.1021/ja00846a075](https://doi.org/10.1021/ja00846a075). b) Turro, N. J., Lechtken, P. Molecular photochemistry. LXII. Thermal generation of organic molecules in electronically excited states. Evidence for a spin forbidden, diabatic pericyclic reaction. *J. Am. Chem. Soc.* **1973**, *95* (1), 264-266. DOI: [10.1021/ja00782a059](https://doi.org/10.1021/ja00782a059).

95. (a) Richardson, W. H., O'Neal, H. E. Thermochemistry and estimated activation parameters for the thermal decomposition of 1,2-dioxetanedione, 4-tert-butyl-1,2-dioxetan-3-one, and 4,4-dimethyl-1,2-dioxetan-3-one. *J. Am. Chem. Soc.* **1972**, *94* (25), 8665-8668. DOI: [10.1021/ja00780a002](https://doi.org/10.1021/ja00780a002). b) O'Neal, H. E., Richardson, W. H. Additions and corrections - the thermochemistry of 1,2-dioxetane and its methylated derivatives. An estimate of activation parameters. *J. Am. Chem. Soc.* **1971**, *93* (7), 1828-1828. DOI: [10.1021/ja00736a602](https://doi.org/10.1021/ja00736a602). c) O'Neal, H. E., Richardson, W. H. Thermochemistry of 1,2-dioxetane and its methylated derivatives. Estimate of activation parameters. *J. Am. Chem. Soc.* **1970**, *92* (22), 6553-6557. DOI: [10.1021/ja00725a029](https://doi.org/10.1021/ja00725a029).

96. Harding, L. B., Goddard III, W. A. Intermediates in the chemiluminescent reaction of singlet oxygen with ethylene. Ab initio studies. *J. Am. Chem. Soc.* **1977**, *99* (13), 4520-4523. DOI: [10.1021/ja00455a061](https://doi.org/10.1021/ja00455a061).

-
97. Dewar, M. J. S., Kirschner, S. MINDO/3 study of the thermolysis of dioxetane. Role of the triplet state. *J. Am. Chem. Soc.* **1974**, *96* (24), 7578-7579. DOI: [10.1021/ja00831a046](https://doi.org/10.1021/ja00831a046).
98. Dewar, M. J. S., Kirschner, S., Kollmar, H. W. Cryptochemiluminescence in the rearrangements of dewar benzenes. Requirements for pericyclic reaction to be chemiluminescent. *J. Am. Chem. Soc.* **1974**, *96* (24), 7579-7581. DOI: [10.1021/ja00831a047](https://doi.org/10.1021/ja00831a047).
99. a) Schmidt, S. P., Vincent, M. A., Dykstra, C. E., Schuster, G. B. Chemiluminescence of dioxetanone investigated by self-consistent-field theory. *J. Am. Chem. Soc.* **1981**, *103* (5), 1292-1293. DOI: [10.1021/ja00395a084](https://doi.org/10.1021/ja00395a084). b) Barnett, G. Decomposition mechanism of 1,2-dioxetane. *Can. J. Chem.* **1974**, *52*, 3837-3843. DOI: [10.1139/v74-574](https://doi.org/10.1139/v74-574). c) Evleth, E. M., Feler, G. CNDO CI calculations of the 1,2-dioxetane to two formaldehydes conversion. *Chem. Phys. Lett.* **1973**, *22* (3), 499-502. DOI: [10.1016/0009-2614\(73\)87016-2](https://doi.org/10.1016/0009-2614(73)87016-2).
100. Wilsey, S., Bernardi, F., Olivucci, M., Robb, M. A., Murphy, S., Adam, W. The thermal decomposition of 1,2-dioxetane revisited. *J. Phys. Chem. A*, **1999**, *103* (11), 1669-1677. DOI: [10.1021/jp9848086](https://doi.org/10.1021/jp9848086).
101. Murphy, S., Adam, W. The elusive 1,4-dioxy biradical: revised mechanism for the formation of diol from 3,3-dimethyldioxetane in cyclohexadiene. *J. Am. Chem. Soc.* **1996**, *118* (51), 12916-12921. DOI: [10.1021/ja9540886](https://doi.org/10.1021/ja9540886).
102. De Vico, L., Liu, Y. -J., Krogh, J. W., Lindh, R. Chemiluminescence of 1,2-dioxetane. Reaction mechanism uncovered. *J. Chem. Phys. A*, **2007**, *111* (32), 8013-8019. DOI: [10.1021/jp074063g](https://doi.org/10.1021/jp074063g).
103. Vacher, M., Brakestad, A., Karlsson, H. O., Galván, I. F., Lindh, R. Dynamical insights into the decomposition of 1,2-dioxetane. *J. Chem. Theory Comput.* **2017**, *13* (6), 2448-2457. DOI: [10.1021/acs.jctc.7b00198](https://doi.org/10.1021/acs.jctc.7b00198).
104. Schaap, A. P., Gagnon, S. D. Chemiluminescence from a phenoxide-substituted 1,2-dioxetane: a model for firefly bioluminescence. *J. Am. Chem. Soc.* **1982**, *104* (12), 3504-3506. DOI: [10.1021/ja00376a044](https://doi.org/10.1021/ja00376a044).
105. a) Hoshiya, N., Fukuda, N., Maeda, H., Watanabe, N., Matsumoto, M. Synthesis and fluoride-induced chemiluminescent decomposition of bicyclic dioxetanes substituted

- with a 2-hydroxynaphthyl group. *Tetrahedron*, **2006**, *62* (24), 5808-5820. DOI: [10.1016/j.tet.2006.03.082](https://doi.org/10.1016/j.tet.2006.03.082). b) Bronstein, I., Edwards, B., Sparks, A. Improved chemiluminescent 1,2-dioxetanes. Patent, **1994**, *WO9426726*. c) Edwards, B., Sparks, A., Voyta, J. C., Bronstein, I. Unusual luminescent properties of odd- and even-substituted naphthyl-derivatized dioxetanes. *J. Biolumin. Chemilumin.* **1990**, *5* (1), 1-4. DOI: [10.1002/bio.1170050102](https://doi.org/10.1002/bio.1170050102). d) Bronstein, I., Edwards, B., Voyta, J. C. 1,2 Dioxetanes: novel chemiluminescent enzyme substrates. applications to immunoassays. *J. Biolumin. Chemilumin.* **1989**, *4* (1), 99-111. DOI: [10.1002/bio.1170040116](https://doi.org/10.1002/bio.1170040116). e) Schaap, A. P., Handley, R. S., Giri, B. P. Chemical and enzymatic triggering of 1,2-dioxetanes. 1: aryl esterase-catalyzed chemiluminescence from a naphthyl acetate-substituted dioxetane. *Tetrahedron Lett.* **1987**, *28* (9), 935-938. DOI: [10.1016/S0040-4039\(00\)95878-7](https://doi.org/10.1016/S0040-4039(00)95878-7). f) Schaap, A. P., Chen, T. S., Handley, R. S., DeSilva, R., Giri, B. P. Chemical and enzymatic triggering of 1,2-dioxetanes. 2: fluoride-induced chemiluminescence from tert-butyl dimethylsilyloxy-substituted dioxetanes. *Tetrahedron Lett.* **1987**, *28* (11), 1155-1158. DOI: [10.1016/S0040-4039\(00\)95313-9](https://doi.org/10.1016/S0040-4039(00)95313-9). g) Schaap, A. P., Sandison, M. D., Handley, R. S. Chemical and enzymatic triggering of 1,2-dioxetanes. 3: alkaline phosphatase-catalyzed chemiluminescence from an aryl phosphate-substituted dioxetane. *Tetrahedron Lett.* **1987**, *28* (11), 1159-1162. DOI: [10.1016/S0040-4039\(00\)95314-0](https://doi.org/10.1016/S0040-4039(00)95314-0).
106. a) Hananya, N., Shabat, D. Recent advances and challenges in luminescent imaging: bright outlook for chemiluminescence of dioxetanes in water. *ACS Cent. Sci.* **2019**, *5* (6), 949-959. DOI: [10.1021/acscentsci.9b00372](https://doi.org/10.1021/acscentsci.9b00372). b) Gnaim, S., Green, O., Shabat, D. The emergence of aqueous chemiluminescence: new promising class of phenoxy 1,2-dioxetane luminophores. *Chem. Commun.* **2018**, *54* (17), 2073-2085. DOI: [10.1039/C8CC00428E](https://doi.org/10.1039/C8CC00428E). c) Green, O., Eilon, T., Hananya, N., Gutkin, S., Bauer, C. R., Shabat, D. Opening a gateway for chemiluminescence cell imaging: distinctive methodology for design of bright chemiluminescent dioxetane probes. *ACS Cent. Sci.* **2017**, *3* (4), 349-358. DOI: [10.1021/acscentsci.7b00058](https://doi.org/10.1021/acscentsci.7b00058).
107. a) Schuster, G. B., Schmidt, S. P. Chemiluminescence of organic compounds. *Adv. Phys. Org. Chem.* **1982**, *18*, 187-238. DOI: [10.1016/S0065-3160\(08\)60140-9](https://doi.org/10.1016/S0065-3160(08)60140-9). b) Schmidt, S. P., Schuster, G. B. Chemiluminescence of dimethyldioxetanone. Unimolecular generation of excited singlet and triplet acetone. Chemically initiated

-
- electron-exchange luminescence, the primary light generating reaction. *J. Am. Chem. Soc.* **1980**, *102* (1), 306-314. DOI: [10.1021/ja00521a049](https://doi.org/10.1021/ja00521a049). c) Schmidt, S. P., Schuster, G. B. Anomalous metalloporphyrin and chlorophyll an activated chemiluminescence of dimethyldioxetanone. Chemically initiated electron-exchange luminescence. *J. Am. Chem. Soc.* **1980**, *102* (23), 7100-7103. DOI: [10.1021/ja00543a036](https://doi.org/10.1021/ja00543a036). d) Schuster, G. B. Chemiluminescence of organic peroxides. Conversion of ground-state reactants to excited-state products by the chemically initiated electron-exchange luminescence mechanism. *Acc. Chem. Res.* **1979**, *12* (10), 366-373. DOI: [10.1021/ar50142a003](https://doi.org/10.1021/ar50142a003). e) Schmidt, S. P., Schuster, G. B. Dioxetanone chemiluminescence by the chemically initiated electron exchange pathway. Efficient generation of excited singlet states. *J. Am. Chem. Soc.* **1978**, *100* (6), 1966-1968. DOI: [10.1021/ja00474a074](https://doi.org/10.1021/ja00474a074). f) Koo, J. A., Schmidt, S. P., Schuster, G. B. Bioluminescence of the firefly: key steps in the formation of the electronically excited state for model systems. *PNAS*, **1978**, *75* (1), 30-33. DOI: [10.1073/pnas.75.1.30](https://doi.org/10.1073/pnas.75.1.30). g) Koo, J. -Y., Schuster, G. B. Chemically initiated electron exchange luminescence. A new chemiluminescent reaction path for organic peroxides. *J. Am. Chem. Soc.* **1977**, *99*, 6107-6109. DOI: [10.1021/ja00460a050](https://doi.org/10.1021/ja00460a050).
108. Teng, X., Jin, M., Ding, C., Lu, C. Rapid screening method for thermal conductivity property of thermal insulation materials by thermochemiluminescent probe. *Chem. Commun.* **2020**, *56* (84), 12781-12784. DOI: [10.1039/D0CC04654J](https://doi.org/10.1039/D0CC04654J).
109. Imanishi, T., Ueda, Y., Tainaka, R., Miyashita, K. Synthesis and chemiluminescent property of the novel 1,2-dioxetanes containing an acridane-10-acetate moiety as the luminophore and trigger unit. *Tetrahedron Lett.* **1997**, *38* (5), 841-844. DOI: [10.1016/S0040-4039\(96\)02463-X](https://doi.org/10.1016/S0040-4039(96)02463-X).
110. Moroni, G., Calabria, D., Quintavalla, A., Lombardo, M., Mirasoli, M., Roda, A., Gioiello, A. Thermochemiluminescence-based sensitive probes: synthesis and photophysical characterization of acridine-containing 1,2-dioxetanes focusing on fluorophore push-pull effects. *ChemPhotoChem*, **2021**, *5*, 1-11. DOI: [10.1002/cptc.202100152](https://doi.org/10.1002/cptc.202100152).
111. Orda-Zgadzaj, M. M., Abraham, W. Photoswitchable macrocycles incorporating acridane moieties. *Synthesis*, **2007**, *21*, 3345-3356. DOI: [10.1055/s-2007-990829](https://doi.org/10.1055/s-2007-990829).

-
112. Oh, S. J., Hwang, S. J., Jung, J., Yu, K., Kim, J., Choi, J. Y., Hartzell, H. C., Roh, E. J., Lee, C. J. MONNA, a potent and selective blocker for transmembrane protein with unknown function 16/anoctamin-1. *Mol. Pharmacol.* **2013**, *84* (5), 726-735. DOI: [10.1124/mol.113.087502](https://doi.org/10.1124/mol.113.087502).
113. Csuk, R., Barthel, A., Raschke, C. Convenient access to substituted acridines by a Buchwald-Hartwig amination. *Tetrahedron*, **2004**, *60* (27), 5737-5750. DOI: [10.1016/j.tet.2004.05.013](https://doi.org/10.1016/j.tet.2004.05.013).
114. Dodean, R. A., Kancharla, P., Li, Y., Melendez, V., Read, L., Bane, C. E., Vesely, B., Kreishman-Deitrick, M., Black, C., Li, Q., Sciotti, L. J., Olmeda, R., Luong, T. L., Gaona, H., Potter, B., Sousa, J., Marcsisin, S., Caridha, D., Xie, L., Vuong, C., Zeng, Q., Zhang, J., Zhang, P., Lin, H., Butler, K., Roncal, N., Gaynor-Ohnstad, L., Leed, S. E., Nolan, C., Huezo, S. J., Rasmussen, S. A., Stephens, M. T., Tan, J. C., Cooper, R. A., Smilkstein, M. J., Pou, S., Winter, R. W., Riscoe, M. K., Kelly, J. K. Discovery and structural optimization of acridones as broad-spectrum antimalarials. *J. Med. Chem.* **2019**, *62* (7), 3475-3502. DOI: [10.1021/acs.jmedchem.8b01961](https://doi.org/10.1021/acs.jmedchem.8b01961).
115. <https://thalesnano.com/products-and-services/h-cube-pro/>.
116. Rurack, K. Fluorescence quantum yields: methods of determination and standards. Standardization and quality assurance in fluorescence measurements I. (Resch-Genger, U. Ed.), *Springer*, Berlin, Heidelberg, **2008**, pp. 101-145. DOI: [10.1007/4243_2008_019](https://doi.org/10.1007/4243_2008_019).
117. Chen, M. -C., Chen, D. -G., Chou, P. -T. Fluorescent chromophores containing the nitro group: relatively unexplored emissive properties. *ChemPlusChem* **2021**, *86* (1), 11-27. DOI: [10.1002/cplu.202000592](https://doi.org/10.1002/cplu.202000592).
118. Zhang, X. F. The effect of phenyl substitution on the fluorescence characteristics of fluorescein derivatives via intramolecular photoinduced electron transfer. *Photochem. Photobiol. Sci.* **2010**, *9* (9), 1261-1268. DOI: [10.1039/c0pp00184h](https://doi.org/10.1039/c0pp00184h).
119. Rettig, W., Klock, A. Intramolecular fluorescence quenching in aminocoumarines. Identification of an excited state with full charge separation. *Can. J. Chem.* **1985**, *63* (7), 1649-1653. DOI: [10.1139/V85-277](https://doi.org/10.1139/V85-277).
120. a) Robiette, R. *Comprehensive organic synthesis II.* (Knochel, P., Molander, G. A. Eds.), **2014**, *5*, pp. 85-128. b) Adam, W., Prein, M. The Schenck Ene reaction:

diastereoselective oxyfunctionalization with singlet oxygen in synthetic applications. *Angew. Chem.* **1996**, *35* (5), 477-494. DOI: [10.1002/anie.199604771](https://doi.org/10.1002/anie.199604771).

121. Griesbeck, A. G. Handbook of synthetic photochemistry. (Fagnoni, M., Albini, A. Eds.), *Wiley VCH*, Weinheim, **2009**, pp. 464. DOI: [10.1002/anie.201003164](https://doi.org/10.1002/anie.201003164).

122. Wasserman, H. H., DeSimone, R. W., Chia, X. R. X., Banwell, M. G. Singlet oxygen. Encyclopedia of reagents for organic synthesis. (Charette, A. Ed.), *John Wiley & Sons*, Ltd, **2013**, pp. 11. DOI: [10.1002/047084289X.rs035](https://doi.org/10.1002/047084289X.rs035).

123. Lu, T., Chen, F. Multiwfn: A multifunctional wavefunction analyzer. *J. Comp. Chem.* **2012**, *33* (5), 580-592. DOI: [10.1002/jcc.22885](https://doi.org/10.1002/jcc.22885).

124. Gasteiger, J., Marsili, M. Iterative partial equalization of orbital electronegativity—a rapid access to atomic charges. *Tetrahedron*, **1980**, *36* (22), 3219-3228. DOI: [10.1016/0040-4020\(80\)80168-2](https://doi.org/10.1016/0040-4020(80)80168-2).

125. Hirshfeld, F. L. Bonded-atom fragments for describing molecular charge densities. *Theoret. Chim. Acta*, **1977**, *44*, 129-138. DOI: [10.1007/BF00549096](https://doi.org/10.1007/BF00549096).

126. a) Yue, L., Yu, L., Xu, C., Zhu, C., Liu, Y. Quantum yields of singlet and triplet chemiexcitation of dimethyl 1,2-dioxetane: ab initio nonadiabatic molecular dynamic simulations. *Phys. Chem. Chem. Phys.* **2020**, *22*, 11440-11451. DOI: [10.1039/D0CP00811G](https://doi.org/10.1039/D0CP00811G). b) Sevin, F., McKee, M. L. Reactions of 1,3-cyclohexadiene with singlet oxygen. A theoretical study. *J. Am. Chem. Soc.* **2001**, *123*, 4591-4600. DOI: [10.1021/ja010138x](https://doi.org/10.1021/ja010138x).

127. a) Xie, J., Zhao, D. Continuous-flow photochemistry: an expanding horizon of sustainable technology. *Chin. Chem. Lett.* **2020**, *31* (9), 2395-2400. DOI: [10.1016/j.ccllet.2020.03.022](https://doi.org/10.1016/j.ccllet.2020.03.022). b) Rehm, T. H. Reactor technology concepts for flow photochemistry. *ChemPhotoChem*, **2019**, *4* (4), 235-254. DOI: [10.1002/cptc.201900247](https://doi.org/10.1002/cptc.201900247). c) Radjagobalou, R., Blanco, J. -F., Dechy-Cabaret, O., Oelgemoller, M., Loubiere, K. Photooxygenation in an advanced led-driven flow reactor module: Experimental investigations and modelling. *Chem. Eng. Process.: Process Intensif.* **2018**, *130*, 214-228. DOI: [10.1016/j.cep.2018.05.015](https://doi.org/10.1016/j.cep.2018.05.015).

128. a) Di Filippo, M., Bracken, C., Baumann, M. Continuous flow photochemistry for the preparation of bioactive molecules. *Molecules*, **2020**; *25* (2), 356-369. DOI: [10.3390/molecules25020356](https://doi.org/10.3390/molecules25020356). b) Cambié, D., Noël, T. Solar photochemistry in flow. *Top.*

Curr. Chem. **2018**, *376* (6), 45. DOI: [10.1007/s41061-018-0223-2](https://doi.org/10.1007/s41061-018-0223-2). c) Sambiagio, C., Noël, T. Flow photochemistry: shine some light on those tubes! *Trends Chem.* **2020**, *2* (2), 92-106. DOI: [10.1016/j.trechm.2019.09.003](https://doi.org/10.1016/j.trechm.2019.09.003). d) Noël, T. A personal perspective on the future of flow photochemistry. *J. Flow Chem.* **2017**, *7*, 87-93. DOI: [10.1556/1846.2017.00022](https://doi.org/10.1556/1846.2017.00022). e) Cambié, D., Bottecchia, C., Straathof, N. J. W., Hessel, V., Noël, T. Applications of continuous-flow photochemistry in organic synthesis, material science, and water treatment. *Chem. Rev.* **2016**, *116* (17), 10276-10341. DOI: [10.1021/acs.chemrev.5b00707](https://doi.org/10.1021/acs.chemrev.5b00707). f) Knowles, J. P., Elliott, L. D., Booker-Milburn, K. I. Flow photochemistry: old light through new windows. *Beilstein J. Org. Chem.* **2012**, *8*, 2025-2052. DOI: [10.3762/bjoc.8.229](https://doi.org/10.3762/bjoc.8.229).

129. a) Baker, J. R., Gilbert, J., Paula, S., Zhu, X., Sako, J. A., McCluskey, A. Dichlorophenylacrylonitriles as AhR ligands that display selective breast cancer cytotoxicity in vitro. *Chem. Med. Chem.* **2018**, *13* (14), 1447-1458. DOI: [10.1002/cmdc.201800256](https://doi.org/10.1002/cmdc.201800256). b) Bume, D. D., Harry, S. A., Pitts, C. R., Lectka, T. J. Sensitized aliphatic fluorination directed by terpenoidal enones: a “visible light” approach. *Org. Chem.* **2018**, *83* (3), 1565-1575. DOI: [10.1021/acs.joc.7b02807](https://doi.org/10.1021/acs.joc.7b02807). c) Strauss, F. J., Cantillo, D., Guerra, J., Kappe, C. O. A laboratory-scale continuous flow chlorine generator for organic synthesis. *React. Chem. Eng.* **2016**, *1* (5), 472-476. DOI: [10.1039/C6RE00135A](https://doi.org/10.1039/C6RE00135A). d) Rehm, T. H. Photochemical fluorination reactions - a promising research field for continuous-flow synthesis. *Chem. Eng. Technol.* **2016**, *39* (1), 66-80. DOI: [10.1002/ceat.201500195](https://doi.org/10.1002/ceat.201500195).

130. a) Barthelemy, A. -L., Dagousset, G., Magnier, E. Metal-free visible-light-mediated hydrotrifluoromethylation of unactivated alkenes and alkynes in continuous flow. *Eur. J. Org. Chem.* **2019**, *10*, 1429-1432. DOI: [10.1002/ejoc.201901252](https://doi.org/10.1002/ejoc.201901252). b) Abdiaj, I., Bottecchia, C., Alcazar, J., Noël, T. Visible-light-induced trifluoromethylation of highly functionalized arenes and heteroarenes in continuous flow. *Synthesis*, **2017**, *49* (22), 4978-4985. DOI: [10.1055/s-0036-1588527](https://doi.org/10.1055/s-0036-1588527). c) Beatty, J. W., Douglas, J. J., Cole, K. P., Stephenson, C. R. J. A scalable and operationally simple radical trifluoromethylation. *Nat. Commun.* **2015**, *6* (1), 7919. DOI: [10.1038/ncomms8919](https://doi.org/10.1038/ncomms8919).

131. a) Santoro, S., Ferlin, F., Ackermann, L., Vaccaro, L. C-H functionalization reactions under flow conditions. *Chem. Soc. Rev.* **2019**, *48*, 2767-2782. DOI:

-
- [10.1039/C8CS00211H](https://doi.org/10.1039/C8CS00211H). b) Babra, J. S., Russell, A. T., Smith, C. D., Zhang, Y. Combining C-H functionalisation and flow photochemical heterocyclic metamorphosis (FP-HM) for the synthesis of benzo[1,3]oxazepines. *Tetrahedron*, **2018**, *74* (38), 5351-5357. DOI: [10.1016/j.tet.2018.05.066](https://doi.org/10.1016/j.tet.2018.05.066). c) Cantillo, D., Mateos, C., Rincon, J. A., De Frutos, O., Kappe, C. O. Light-induced C-H arylation of (hetero)arenes by in situ generated diazo anhydrides. *Chem. Eur. J.* **2015**, *21* (37), 12894-12898. DOI: [10.1002/chem.201502357](https://doi.org/10.1002/chem.201502357).
132. a) Kouridaki, A., Huvaere, K. Singlet oxygen oxidations in homogeneous continuous flow using a gas-liquid membrane reactor. *React. Chem. Eng.* **2017**, *2*, 590-597. DOI: [10.1039/C7RE00053G](https://doi.org/10.1039/C7RE00053G). b) Ushakov, D. B., Gilmore, K., Seeberger, P. H. Consecutive oxygen - based oxidations convert amines to α -cyanoepoxides. *Chem. Commun.* **2014**, *50*, 12649-12651. DOI: [10.1039/C4CC04932B](https://doi.org/10.1039/C4CC04932B).
133. a) Gioiello, A., Piccinno, A., Lozza, A. M., Cerra, B. The medicinal chemistry in the era of machines and automation: recent advances in continuous flow technology. *J. Med. Chem.* **2020**, *63* (13), 6624-6647. DOI: [10.1021/acs.jmedchem.9b01956](https://doi.org/10.1021/acs.jmedchem.9b01956). b) Plutschack, M. B., Pieber, B., Gilmore, K., Seeberger, P. H. The hitchhiker's guide to flow chemistry. *Chem. Rev.* **2017**, *117* (18), 11796-11893. DOI: [10.1021/acs.chemrev.7b00183](https://doi.org/10.1021/acs.chemrev.7b00183). c) Ley, S. V., Fitzpatrick, D. E., Ingham, R. J., Myers, R. M. Organic synthesis: march of the machines. *Angew. Chem. Int. Ed.* **2015**, *54* (11), 3449-3464. DOI: [10.1002/anie.201410744](https://doi.org/10.1002/anie.201410744).
134. Buglioni, L., Raymenants, F., Slattery, A., Zondag, S. D. A., Noël, T. Technological innovations in photochemistry for organic synthesis: flow chemistry, high-throughput experimentation, scale-up, and photoelectrochemistry. *Chem. Rev.* **2022**, *122* (2), 2752-2906. DOI: [10.1021/acs.chemrev.1c00332](https://doi.org/10.1021/acs.chemrev.1c00332).
135. Donnelly, K., Baumann, M. Scalability of photochemical reactions in continuous flow mode. *J. Flow Chem.* **2021**, *11* (3), 223-241. DOI: [10.1007/s41981-021-00168-z](https://doi.org/10.1007/s41981-021-00168-z).
136. Bitton, J., Jamison, T. F. The assembly and use of continuous flow systems for chemical synthesis. *Nat. Protoc.* **2017**, *12* (11), 2423-2446. DOI: [10.1038/nprot.2017.102](https://doi.org/10.1038/nprot.2017.102).
137. Lummiss, J. A. M., Morse, P. D., Beingessner, R. L., Jamison, T. F. Towards more efficient, greener syntheses through flow chemistry. *Chem. Rec.* **2017**, *17* (7), 667-680. DOI: [10.1002/tcr.201600139](https://doi.org/10.1002/tcr.201600139).

-
138. Protti, S., Ravelli, D., Fagnoni, M. Design consideration of continuous-flow photoreactors. From engineering principles to chemical applications. Photochemical processes in continuous-flow reactors. (Noël, T. Ed.), **2017**, pp. 36. DOI: [10.1142/9781786342195_0001](https://doi.org/10.1142/9781786342195_0001).
139. Williams, J. D., Nakano, M., Gérardy, R., Rincon, J. A., De Frutos, O., Mateos, C., Monbaliu, J. -C. M., Kappe, C. O. Finding the perfect match: a combined computational and experimental study towards efficient and scalable photosensitized [2+2] cycloadditions in flow. *Org. Process Res. Dev.* **2019**, *23* (1), 78-87. DOI: [10.1021/acs.oprd.8b00375](https://doi.org/10.1021/acs.oprd.8b00375).
140. a) Baumann, M., Baxendale, I. R. The synthesis of active pharmaceutical ingredients (APIs) using continuous flow chemistry. *Beilstein J. Org. Chem.* **2015**, *11*, 1194-1219. DOI: [10.3762/bjoc.11.134](https://doi.org/10.3762/bjoc.11.134). b) Poechlauer, P., Manley, J., Broxterman, R., Gregertsen, B., Ridemark, M. Continuous processing in the manufacture of active pharmaceutical ingredients and finished dosage forms: an industry perspective. *Org. Process Res. Dev.* **2012**, *16* (10), 1586-1590. DOI: [10.1021/op300159y](https://doi.org/10.1021/op300159y).
141. Malet-Sanz, L., Susanne, F. Continuous flow synthesis. A pharma perspective. *J. Med. Chem.* **2012**, *55* (9), 4062-4098. DOI: [10.1021/jm2006029](https://doi.org/10.1021/jm2006029).
142. Gutmann, B.; Cantillo, D.; Kappe, C. O. Continuous-flow technology - a tool for the safe manufacturing of active pharmaceutical ingredients. *Angew. Chem.* **2015**, *54* (23), 6688-6728. DOI: [10.1002/anie.201409318](https://doi.org/10.1002/anie.201409318).
143. Hone, C. A., Roberge, D. M., Kappe, C. O. The use of molecular oxygen in pharmaceutical manufacturing: is flow the way to go? *ChemSusChem*, **2017**, *10* (1), 32-41. DOI: [10.1002/cssc.201601321](https://doi.org/10.1002/cssc.201601321).
144. Elgue, S., Aillet, T., Loubiere, K., Conté, A., Dechy-Cabaret, O., Prat, L. E., Horn, C. R., Lobet, O., Vallon, S. Flow photochemistry: a meso-scale reactor for industrial applications. *Chemistry Today*, **2015**, *33* (5), 58-61.
145. Bayera, P., Jacobi von Wangelin, A. An entirely solvent-free photooxygenation of olefins under continuous flow conditions. *Green Chem.* **2020**, *22*, 2359-2364. DOI: [10.1039/D0GC00436G](https://doi.org/10.1039/D0GC00436G).

-
146. Roibu, A., Van Gerven, T., Kuhn, S. Photon transport and hydrodynamics in gas-liquid flows part 1: characterization of Taylor flow in a photo microreactor. *ChemPhotoChem*, **2020**, *4* (10), 5181-5192. DOI: [10.1002/cptc.202000065](https://doi.org/10.1002/cptc.202000065).
147. Han, S., Kashfipour, M. A., Ramezani, M., Abolhasani, M. Accelerating gas-liquid chemical reactions in flow. *Chem. Commun.* **2020**, *56* (73), 10593-10607. DOI: [10.1039/D0CC03511D](https://doi.org/10.1039/D0CC03511D).
148. Mallia, C. J., Baxendale, I. R. The use of gases in flow synthesis. *Org. Process Res. Dev.* **2016**, *20* (2), 327-360. DOI: [10.1021/acs.oprd.5b00222](https://doi.org/10.1021/acs.oprd.5b00222).
149. Emmanuel, N., Mendoza, C., Winter, M., Horn, C. R., Vizza, A., Dreesen, L., Heinrichs, B., Monbaliu, J. -C. M. Scalable photocatalytic oxidation of methionine under continuous-flow conditions. *Org. Process Res. Dev.* **2017**, *21* (9), 1435-1438. DOI: [10.1021/acs.oprd.7b00212](https://doi.org/10.1021/acs.oprd.7b00212).
150. Corentin, P., Noirbent, G., Bui, T. -T., Péralta, S., Gigmes, D., Nechab, M., Dumur, F. Push-pull chromophores based on the naphthalene scaffold: potential candidates for optoelectronic applications. *Materials*, **2019**, *12* (8), 1342. DOI: [10.3390/ma12081342](https://doi.org/10.3390/ma12081342).
151. Guerrini, M., Calzolari, A., Corni, S. Solid-state effects on the optical excitation of push-pull molecular j-aggregates by first-principles simulations. *ACS omega*, **2018**, *3* (9), 10481-10486. DOI: [10.1021/acsomega.8b01457](https://doi.org/10.1021/acsomega.8b01457).
152. Schramm, S., Karothu, D. P., Lui, N. M., Commins, P., Ahmed, E., Catalano, L., Naumov, P. Thermochemiluminescent peroxide crystals. *Nature commun.* **2019**, *10* (1), 1-8. DOI: [10.1038/s41467-019-08816-8](https://doi.org/10.1038/s41467-019-08816-8).
153. Sun, C. -W., Chen, S. -C., Fang, T. -S. Substituent effects on the decomposition of chemiluminescent tricyclic aromatic dioxetanes. *Luminescence*, **2014**, *29* (5), 445-450. DOI: [10.1002/bio.2568](https://doi.org/10.1002/bio.2568).
154. Lee, J., Seliger, H. H. Quantum yields of the luminol chemiluminescence reaction in aqueous and aprotic solvents. *Photochem. Photobiol.* **1972**, *15* (2), 227-237. DOI: [10.1111/j.1751-1097.1972.tb06241.x](https://doi.org/10.1111/j.1751-1097.1972.tb06241.x).
155. http://www.pi-j.jp/pdf/manual/PhotonMAX_SystemManual.pdf.

-
156. Bonacchi, S., Genovese, D., Juris, R., Montalti, M., Prodi, L., Rampazzo, E., Zaccheroni, N. Luminescent silica nanoparticles: extending the frontiers of brightness. *Angew. Chem.* **2011**, *50* (18), 4056-4066. DOI: [10.1002/anie.201004996](https://doi.org/10.1002/anie.201004996).
157. Genovese, D., Rampazzo, E., Bonacchi, S., Montalti, M., Zaccheroni, N., Prodi, L. Energy transfer processes in dye-doped nanostructures yield cooperative and versatile fluorescent probes. *Nanoscale*, **2014**, *6*, 3022-3036. DOI: [10.1039/C3NR05599J](https://doi.org/10.1039/C3NR05599J).
158. Bermudez, C. D. L. E., Haddadi, E., Rampazzo, E., Petrizza, L., Prodi, L., Genovese, D. Core-shell pluronic-organosilica nanoparticles with controlled polarity and oxygen permeability. *Langmuir*, **2021**, *37* (16), 4802-4809. DOI: [10.1021/acs.langmuir.0c03531](https://doi.org/10.1021/acs.langmuir.0c03531).
159. Palomba, F., Genovese, D., Petrizza, L., Rampazzo, E., Zaccheroni, N., Prodi, L. Mapping heterogeneous polarity in multicompartment nanoparticles. *Sci. Rep.* **2018**, *8*, 17095. DOI: [10.1038/s41598-018-35257-y](https://doi.org/10.1038/s41598-018-35257-y).
160. a) Rasmi, Y., Li, X., Khan, J., Ozer, T., Choi, J. R. Emerging point-of-care biosensors for rapid diagnosis of COVID-19: current progress, challenges, and future prospects. *Anal. Bioanal. Chem.* **2021**, *413* (16), 4137-4159. DOI: [10.1007/s00216-021-03377-6](https://doi.org/10.1007/s00216-021-03377-6). b) Abida, S. A., Muneerbj, A. A., Al-Kadmycd, I. M. S., Sattare, A. A., Beshbishyf, A. M., El-Saber Batihag, G., Hettahi, H. F. Biosensors as a future diagnostic approach for COVID-19. *Life Sci.* **2021**, *273* (7209), 119117. DOI: [10.1016/j.lfs.2021.119117](https://doi.org/10.1016/j.lfs.2021.119117). c) Samson, R., Navale, G. R., Dharne, M. S. Biosensors: frontiers in rapid detection of COVID-19. *Biotech.* **2020**, *10* (9), 385. DOI: [10.1007/s13205-020-02369-0](https://doi.org/10.1007/s13205-020-02369-0). b) Choi, J. R. Development of point-of-care biosensors for COVID-19. *Front. Chem.* **2020**, *8*, 517. DOI: [10.3389/fchem.2020.00517](https://doi.org/10.3389/fchem.2020.00517).
161. Mädler, S., Bich, C., Touboul, D., Zenobi, R. Chemical cross-linking with NHS esters: a systematic study on amino acid reactivities. *J. Mass. Spectrom.* **2009**, *44* (5), 694-706. DOI: [10.1002/jms.1544](https://doi.org/10.1002/jms.1544).
162. Kalkhof, S., Sinz, A. Chances and pitfalls of chemical cross-linking with amine-reactive N-hydroxysuccinimide esters. *Anal. Bioanal. Chem.* **2008**, *392* (1-2), 305-312. DOI: [10.1007/s00216-008-2231-5](https://doi.org/10.1007/s00216-008-2231-5).

-
163. The molecular probes handbook. A guide to fluorescent probes and labeling technologies XI. (Johnson, I., Spence, M. T. Z. Eds.), *Thermofisher Scientific*, **2010**, pp. 1060.
164. Mattson, G., Conklin, E., Desai, S., Nielander, G., Savage, M. D., Morgensen, S. A practical approach to crosslinking. *Mol. Biol. Rep.* **1993**, *17* (3), 167-183. DOI: [10.1007/BF00986726](https://doi.org/10.1007/BF00986726).
165. Grabarek, Z., Gergely, J. Zero-length crosslinking procedure with the use of active esters. *Anal. Biochem.* **1990**, *185* (1), 131-135. DOI: [10.1016/0003-2697\(90\)90267-d](https://doi.org/10.1016/0003-2697(90)90267-d).
166. David-Cordonnier, M. -H., Hildebrand, M. -P., Baldeyrou, B., Lansiaux, A., Keuser, C., Benzschawel, K., Lemster, T., Pindur, U. Design, synthesis and biological evaluation of new oligopyrrole carboxamides linked with tricyclic DNA-intercalators as potential DNA ligands or topoisomerase inhibitors *Eur. J. Med. Chem.* **2007**, *42* (6), 752-771. DOI: [10.1016/j.ejmech.2006.12.039](https://doi.org/10.1016/j.ejmech.2006.12.039).
167. Takeshi, I., Nobuhiro, H., Kazutoshi, S. Acridine derivative. Patent, **1996**, *JP3551984B2*.
168. Keller, M., Pop, N., Hutzler, C., Beck-Sickinger, A. G., Bernhardt, G., Buschauer, A. Guanidine-acylguanidine bioisosteric approach in the design of radioligands: synthesis of a tritium-labeled NG-propionylargininamide ([³H]-UR-MK114) as a highly potent and selective neuropeptide Y Y1 receptor antagonist. *J. Med. Chem.* **2008**, *51* (24), 8168-8172. DOI: [10.1021/jm801018u](https://doi.org/10.1021/jm801018u).
169. Bonnitcha, P. D., Bayly, S. R., Theobald, M. B. M., Betts, H. M., Lewis, J. S., Dilworth, J. R. Nitroimidazole conjugates of bis(thiosemicarbazonato)⁶⁴Cu(II) - potential combination agents for the PET imaging of hypoxia. *J. Inorg. Biochem.* **2010**, *104* (2), 126-135. DOI: [10.1016/j.jinorgbio.2009.10.009](https://doi.org/10.1016/j.jinorgbio.2009.10.009).
170. Clark, R. F., Sorensen, B., Osuma, A. T., Frey, R., Longenecker, K., Doherty, G., Curtin, M. L., Michaekides, M. R., Sweis, R. F., Pliushchev, M. A., Judd, A., Hansen, T. M., Heyman, H. R. NAMPT inhibitors. Patent, **2013**, *WO2013170112A1*.
171. Anthony, J., Richard, S. West, M. Acridone derivatives as labels for fluorescence detection of target materials. Patent, **2002**, *WO2002099424A2*.

-
172. Lakshmipriya, T., Gopinath, S. C., Hashim, U., Tang, T. -H. Signal enhancement in ELISA: biotin-streptavidin technology against gold nanoparticles. *J. Taibah Univ. Med. Sci.* **2016**, *11* (5), 432-438. DOI: [10.1016/j.jtumed.2016.05.010](https://doi.org/10.1016/j.jtumed.2016.05.010).
173. Diamandis, E. P., Christopoulos, T. K. The biotin-(strept)avidin system: principles and applications in biotechnology. *Clin. Chem.* **1991**, *37* (5), 625-636. DOI: [10.1093/clinchem/37.5.625](https://doi.org/10.1093/clinchem/37.5.625).
174. Bioconjugate techniques III. (Hermanson, G. Ed.), *Elsevier Science*, **2010**, pp. 1200.
175. Advanced organic chemistry: part B: reaction and synthesis. (Carey, F. A., Sundberg, R. J. Eds.), *Springer*, **1976**, pp. 1322.
176. Elfeky, S. A., D'Hooge, F., Poncel, L., Chen, W., Perera, S. P., Van den Elsen, J. M. W., James, T. D., Jenkins, A. T. A., Cameron, P. J., Fossey, J. S. A surface plasmon enhanced fluorescence sensor platform. *New J. Chem.* **2009**, *33*, 1466-1469. DOI: [10.1039/B906125H](https://doi.org/10.1039/B906125H).
177. Kottani, R., Valiulin, R. A., Kutateladze, A. G. Direct screening of solution phase combinatorial libraries encoded with externally sensitized photolabile tags. *PNAS*, **2006**, *103* (38), 13917-13921. DOI: [10.1073/pnas.0606380103](https://doi.org/10.1073/pnas.0606380103).
178. Cinelli, M. A., Cordero, B., Dexheimer, T. S., Pommier, Y., Cushman, M. Synthesis and biological evaluation of 14-(aminoalkyl-aminomethyl)aromathecins as topoisomerase I inhibitors: investigating the hypothesis of shared structure-activity relationships. *Bioorg. Med. Chem.* **2009**, *17* (20), 7145-7155. DOI: [10.1016/j.bmc.2009.08.066](https://doi.org/10.1016/j.bmc.2009.08.066).
179. El-Faham, A., Albericio, F. COMU: a third generation of uronium-type coupling reagents. *J. Pept. Sci.* **2010**, *16* (1), 6-9. DOI: [10.1002/psc.1204](https://doi.org/10.1002/psc.1204).
180. Gee, K. R., Archer, E. A., Kang, H. -C. 4-Sulfotetrafluorophenyl (STP) esters: new water-soluble amine-reactive reagents for labeling biomolecules. *Tetrahedron Lett.* **1999**, *40*, 1471-1474. DOI: [10.1016/S0040-4039\(98\)02695-1](https://doi.org/10.1016/S0040-4039(98)02695-1).
181. Staros, J. V., Wright, R. W., Swingle, D. M. Enhancement by N-hydroxysulfosuccinimide of water-soluble carbodiimide-mediated coupling reactions. *Anal. Biochem.* **1986**, *156* (1), 220-222. DOI: [10.1016/0003-2697\(86\)90176-4](https://doi.org/10.1016/0003-2697(86)90176-4).

182. Gaussian 16, Revision A.03, Frisch, M. J., Trucks, G. W., Schlegel, H. B., Scuseria, G. E., Robb, M. A., Cheeseman, J. R., Scalmani, G., Barone, V., Petersson, G. A., Nakatsuji, H., Li, X., Caricato, M., Marenich, A. V., Bloino, J., Janesko, B. G., Gomperts, R., Mennucci, B., Hratchian, H. P., Ortiz, J. V., Izmaylov, A. F., Sonnenberg, J. L., Williams-Young, D., Ding, F., Lipparini, F., Egidi, F., Goings, J., Peng, B., Petrone, A., Henderson, T., Ranasinghe, D., Zakrzewski, V. G., Gao, J., Rega, N., Zheng, G., Liang, W., Hada, M., Ehara, M., Toyota, K., Fukuda, R., Hasegawa, J., Ishida, M., Nakajima, T., Honda, Y., Kitao, O., Nakai, H., Vreven, T., Throssell, K., Montgomery, Jr., J. A., Peralta, J. E., Ogliaro, F., Bearpark, M. J., Heyd, J. J., Brothers, E. N., Kudin, K. N., Staroverov, V. N., Keith, T. A., Kobayashi, R., Normand, J., Raghavachari, K., Rendell, A. P., Burant, J. C., Iyengar, S. S., Tomasi, J., Cossi, M., Millam, J. M., Klene, M., Adamo, C., Cammi, R., Ochterski, J. W., Martin, R. L., Morokuma, K., Farkas, O., Foresman, J. B., Fox, D. J. Gaussian, Inc., Wallingford CT, **2016**.

183 a) Yi, D., Zhang, Q., Liu, Y., Song, J., Tang, Y., Caruso, F., Wang, Y. Synthesis of chemically asymmetric silica nanobottles and their application for cargo loading and as nanoreactors and nanomotors. *Angew. Chemie.* **2016**, *55* (47), 14733-14737. DOI: [10.1002/anie.201607330](https://doi.org/10.1002/anie.201607330). b) Zhao, Z., Fu, J., Dhakal, S., Johnson-Buck, A., Liu, M., Zhang, T., Woodbury, N. W., Liu, Y., Walter, N. G., Yan, H. Nanocaged enzymes with enhanced catalytic activity and increased stability against protease digestion. *Nat. Commun.* **2016**, *7* (1), 1-9. DOI: [10.1038/ncomms10619](https://doi.org/10.1038/ncomms10619). c) Rampazzo, E., Bonacchi, S., Genovese, D., Juris, R., Sgarzi, M., Montalti, M., Prodi, L., Zaccheroni, N., Tomaselli, G., Gentile, S., Satriano, C., Rizzarelli, E. A Versatile strategy for signal amplification based on core/shell silica nanoparticles. *Chem. Eur. J.* **2011**, *17* (48), 13429-13432. DOI: [10.1002/chem.201101851](https://doi.org/10.1002/chem.201101851). d) Demchenko, A. P., Mély, Y., Duportail, G., Klymchenko, A. S. Monitoring biophysical properties of lipid membranes by environment-sensitive fluorescent probes. *Biophys. J.* **2009**, *96*, 3461-3470. DOI: [10.1016/j.bpj.2009.02.012](https://doi.org/10.1016/j.bpj.2009.02.012). e) Zanarini, S., Rampazzo, E., Bonacchi, S., Juris, R., Marcaccio, M., Montalti, M., Paolucci, F., Prodi, L. Iridium doped silica-PEG nanoparticles: enabling electrochemiluminescence of neutral complexes in aqueous media. *J. Am. Chem. Soc.* **2009**, *131* (40), 14208-14209. DOI: [10.1021/ja906666e](https://doi.org/10.1021/ja906666e).

184 Rampazzo, E., Bonacchi, S., Juris, R., Montalti, M., Genovese, D., Zaccheroni, N., Prodi, L., Rambaldi, D. C., Zatonni, A., Reschiglian, P. Energy transfer from silica core-surfactant shell nanoparticles to hosted molecular fluorophores. *J. Phys. Chem. B*, **2010**, *144* (45), 14605-14613. DOI: [10.1021/jp1023444](https://doi.org/10.1021/jp1023444).